Perceptual metrics of light fields

Xia, Ling

Important note
To cite this publication, please use the final published version (if applicable).
Please check the document version above.

Perceptual metrics of light fields

Ling Xia

Perceptual metrics of light fields

Proefschrift

ter verkrijging van de graad van doctor
aan de Technische Universiteit Delft,
op gezag van de Rector Magnificus prof. ir. K.C.A.M. Luyben,
voorzitter van het College voor Promoties,
in het openbaar te verdedigen op
maandag 3 oktober 2016 om 15:00 uur

door

Ling XIA

Master of Engineering in Physical Electronics, Southeast University, China,
geboren te Changzhou, Jiangsu province, China.

Dit proefschrift is goedgekeurd door de promotoren:

Prof. dr. S.C. Pont en Prof. dr. I.E.J. Heynderickx

Samenstelling promotiecommissie:

Rector Magnificus,	voorzitter
Prof. dr. S.C. Pont,	Technische Universiteit Delft, promotor
Prof. dr. I.E.J. Heynderickx,	Technische Universiteit Eindhoven, promotor

Onafhankelijke leden:

Prof. dr. H. de Ridder,	Technische Universiteit Delft
Prof. dr. ir. P.M. Bluyssen,	Technische Universiteit Delft
Prof. dr. S.F. te Pas,	Universiteit Utrecht
Prof. dr. R.W. Fleming,	Justus-Liebig-Universität Gießen
Dr. I.M.L.C. Vogels,	Technische Universiteit Eindhoven

To everyone accompanying me in my age 25-28.

SUMMARY

The lighting profession is developing from its first and second stage to the third stage. While in the first and second stage lighting professionals mainly focused on providing light for visibility, in the third stage they aim at human visual experience of the actual resulting light and the potential of illumination to interact with its surroundings. Ignoring the spectral characteristics of the light, the distribution of light in a space greatly influences the appearance and experience of the space and objects in it. Designers use layered approaches to compose the light, of which the main elements correspond with physical decompositions of the light field. Psychophysics research using pictures has shown human beings' potential sensitivity to these properties of the light field. This thesis supports bridging the gap between the second stage and third stage of the lighting profession by investigating human perception of (combinations or mixtures of) these elements, their interactions with each other and the environment, and their measurement in real scenes.

In order to do so, we developed an experimental setup based on the generic notion of a "probe object" with which we can intuitively measure human beings' sensitivity to variations of light properties in real scenes. To find a less ambiguous "probe object" a smooth sphere and a rough sphere were compared. This test indeed showed that the rough sphere was a better "probe object" than the smooth sphere, in the sense that it shows less perceptual interactions between light characteristics. In the novel experimental setup, the method of adjustment was implemented to measure human beings' ability of inferring the three basic light field properties (i.e. light density, light direction and diffuseness). In order to determine the feasibility of adjusting three light field properties simultaneously in lighting design or lighting perception research, we compared the independent and simultaneous estimations of the three light field properties. The results showed that the simultaneous adjustment method using an optically mixed scene and rough spherical white probe was an efficient way to measure observers' sensitivity for light field characteristics in real scenes. However, the veridicality of the estimated light flow was found to be influenced by the scene layout and content. This result indicates that light, material, shape and space perception interact and should be studied in an integrated manner.

Besides investigating observers' subjective perception of light, we also studied the objective description, measurement and visualization of the light field. We noticed that unlike the light density and direction, the light diffuseness lacked a unified definition related to the physical light distribution in the space. Thus, we did a theoretical and empirical review of four diffuseness metrics, which led to a novel proposal of a diffuseness metric D_{xia}. D_{xia} reframes Cuttle's "strength of light flow" in a spherical harmonic (SH) description of the light field. Together with the light density and direction, it forms a

global integrated description of the first order properties of the SH light field structure. Additionally, a way to simultaneously describe, measure and visualize the light density, light vector and diffuseness (variations) of the light field was introduced. To conclude, the methods and results presented in this thesis focus on investigating human perception of light in real scenes and its metrics. The outcomes of this research offer insights and methods to improve human perception based lighting design theories, research and applications and allows making the progression towards the third stage of the lighting profession.

SAMENVATTING

De verlichtingsprofessie ontwikkelt zich van zijn eerste en tweede stadium naar het derde stadium. Terwijl verlichtingsprofessionals zich in het eerste en tweede stadium vooral richtten op het verschaffen van licht voor zichtbaarheid, beogen zij in het derde stadium de menselijke visuele ervaring van het eigenlijke licht en het potentieel van verlichting om te interacteren met de omgeving. We laten spectrale eigenschappen van het licht buiten beschouwing en richten ons op de verdeling van het licht in een ruimte, waarmee het uiterlijke voorkomen en de ervaring van de ruimte en objecten erin sterk beïnvloed wordt. Ontwerpers gebruiken een gelaagde benadering om het licht samen te stellen; de belangrijkste elementen van die gelaagdheid corresponderen met fysische decomposities van het lichtveld. Psychofysisch onderzoek met afbeeldingen heeft de gevoeligheid van mensen voor deze elementen van het lichtveld aangetoond. Dit proefschrift draagt bij aan de overbrugging van het tweede naar het derde stadium van de verlichtingsprofessie door de menselijke perceptie van (combinaties van) deze elementen te onderzoeken, alsmede hun interactie met elkaar en met de omgeving, en de meting ervan in echte scène.

Om dit te doen, ontwikkelden we een experimentele opstelling gebaseerd op het gebruik van een meetobject, waarmee we op intuïtieve wijze de gevoeligheid van de mens voor variaties van lichteigenschappen in echte scénes konden meten. Om een minder ambigu meetobject te vinden, hebben we een gladde bol en een ruwe bol vergeleken. Een eerste experiment toonde aan dat de ruwe bol beter in staat was dan de gladde bol om perceptuele interacties tussen de lichteigenschappen te vermijden. De nieuwe experimentele opstelling werd vervolgens gebruikt om het vermogen van mensen voor het bepalen van de drie basale lichtveld-eigenschappen (dat wil zeggen lichtdichtheid, lichtrichting en diffusie) te meten. Om de haalbaarheid van het tegelijkertijd instellen van de drie lichtveld-eigenschappen in lichtontwerpen of verlichtingsperceptie onderzoek te bepalen, vergeleken we afzonderlijke en gelijktijdige schattingen van de drie lichtveld-eigenschappen. De resultaten lieten zien dat de methode van gelijktijdige instelling met gebruik van een optisch gemengde scéne en een ruw bolvormig wit meetobject een efficiënte manier was om de gevoeligheid van waarnemers te meten. Echter, hoe nauwkeurig het geschatte lichtveld het ware lichtveld weergaf, bleek te worden beïnvloed door de lay-out en inhoud van de scéne. Dit resultaat geeft aan dat licht, materiaal, vorm en ruimte perceptief interacteren en op een geïntegreerde wijze onderzocht moeten worden.

Naast het onderzoek naar subjectieve lichtwaarneming , bestudeerden we ook de objectieve beschrijving, meting en visualisatie van het lichtveld. We ontdekten dat het ontbrak aan een uniforme definitie voor de lichtdiffusie in termen van de fysische lichtverdeling in de ruimte. Daarom hebben we een theoretisch en empirisch onderzoek gedaan naar vier diffusiematen, wat leidde tot een nieuw voorstel voor een maat genoemd D_{xia}. Deze maat definieert Cuttle's "strength of light flow" in een sferisch harmonische

(SH) beschrijving van het lichtveld; samen met de lichtdichtheid en -richting vormt deze maat een globale geïntegreerde beschrijving van de eerste orde eigenschappen van de SH lichtveld-structuur. Ook introduceerden we een manier om tegelijkertijd de lichtdichtheid , lichtrichting en diffusie(-variaties) van het lichtveld te beschrijven, te meten en te visualiseren. Samenvattend, de methoden en resultaten die zijn gepresenteerd in dit proefschrift richten zich op het onderzoeken van de menselijke waarneming van licht in echte scénes en de bijbehorende fysische maten. De uitkomsten van dit onderzoek bieden inzichten en methodes ter verbetering van op menselijke waarneming gebaseerde theorieën voor, onderzoek naar en toepassingen van het ontwerpen van licht, en ondersteunen de progressie naar het derde stadium van de verlichtingsprofessie.

CONTENTS

1

INTRODUCTION

1

Visualization of scenes of a story or of certain moments in our deep memory always includes lighting conditions. For instance, I remember having dinner together with my beloved grandparents (in memory) under a dim incandescent lamp with the yellow light pouring over my grandma's dishes. I will never forget the Chinese New Year celebrations with my parents and sister outside our house with fireworks sparkling on their faces every now and then. During the middle school days, lots of my nights were spent doing homework under a table lamp with my books being brightly illuminated in an otherwise dark room. However, I did not pay much attention to lighting until I visited my uncle's home one day. It hit me like lightning how different I experienced his home to be from mine, because of the use of fluorescent lamps instead of incandescent lamps, which made his home much brighter and whiter and uniformly illuminated. Later, in my home city, the supermarkets, shopping centers and advertising boards sprang up like mushrooms. It struck me that some of them gave good lighting experiences and some less good. Later, studying discomfort glare of LED lighting in the office, I found that besides "good" and "less good", lighting can also be "bad", even resulting in discomfort or visual fatigue.

Figure 1.1: Visualizations of certain moments in my deep memory.

During my PhD project I learned that the pictures in my mind were correlated with the "visual light field". The interplay between lighting, geometries and materials shapes the architectural space and the light field in it (i.e. the light distribution). Human beings are sensitive to the lighting distribution in a space in that they have expectations of how objects will look like under certain lighting conditions, which is called the "visual light field" [40]. But questions still largely unanswered are: what kinds of lighting properties are human beings usually concerned about in common lighting environments? Do lighting schemes and design guidelines meet observers' psychological experience of lighting? Using Elsevier Scopus I analysed the 1200 most relevant publications related to lighting design and the visual light field. This input was used in VOSviewer to make a topical structure of this literature. As shown in Figure 1.2, the work is separated into two clusters. On the one hand, researchers in the light perception domain mainly focus on shape and surface properties under different lighting conditions in pictures and how people can extract light(ing) information or otherwise shape and material information from photographs or synthetic images. On the other hand, researchers in lighting design focus on how to improve the light in buildings and how to increase the lighting efficiency and reduce energy costs. The separation between the clusters indicate that the research

being done in these two fields had little connection - while they could benefit from each other if considered integrally.
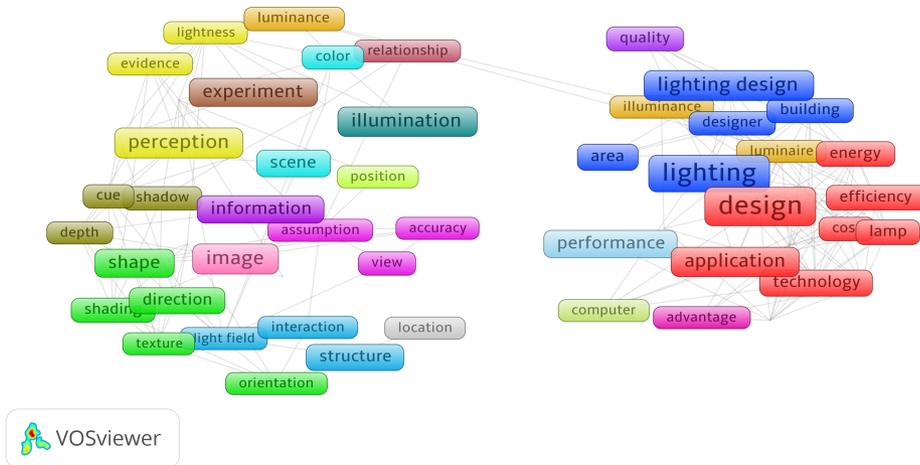
Figure 1.2: Topical structure of lighting related scientific publications analyzed using "VOSviewer". The 1200 most relevant scientific papers were used as input, with 600 linked to "visual light field" (left cluster) and the others linked to "lighting design" (right cluster).

It is undeniable that the primary purpose of artificial lighting for long was visibility, and later the visual performance on specific tasks, while reducing the energy consumption. However, modern designers prefer to see lighting principally in terms of how it influences the appearance of people's surroundings and allows to create various experiences. Thus, a gap between lighting profession and human's experience of lighting exists. The aim of this thesis is to bridge this gap by studying the visual light field and developing perception-based metrics.

The introduction is divided into five parts. In the first part, I give a brief introduction of "what is light". In the second part, I give an overview of the development of methods for interior lighting design, while in the third part, relevant research on human perception of light(ing) is reviewed. This results in the formulation of research questions and the methodologies used to answer these questions, which are described in the fourth part. Finally in the last part, the structure of the thesis is explained.

1.1. What is light?

Light is a kind of medium that makes objects visible without being visible itself in empty space. Our visual system relies on the patterns of light projected on the retina to provide information about the outside world. The photoreceptors in the human eye absorb energy of visible light and thereby initiate the process of seeing [54]. The visible light only

covers a small part of the total electromagnetic spectrum, in the wavelength range 380 nm-780 nm (see Figure 1.3).
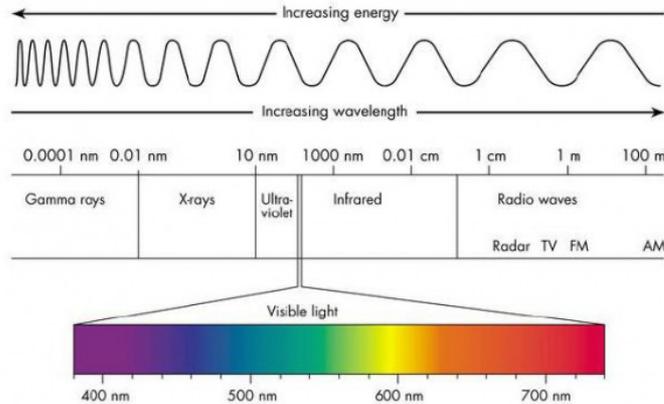
Figure 1.3: The electromagnetic spectrum and the visible light spectrum (from `http:// psychedelic-information-theory.com/em_spectrum`).

Photometry concerns light measurements as experienced by the human visual system. The most frequently used photometric terms are luminous flux, intensity, illuminance and luminance, as shown in Figure 1.4 and described in detail in the following paragraphs.
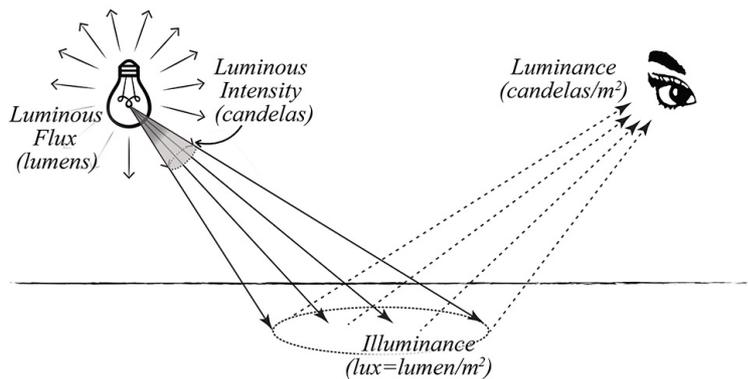
Figure 1.4: Illustration of luminous flux, luminous intensity, illuminance and luminance.

The most fundamental measure of the total power of electromagnetic radiation is the radiant flux (including infrared, ultraviolet, and visible light). Accounting for the sensitivity of the human eyes, scientists use the luminous flux to describe the total amount of light emitted in all directions. The luminous flux is derived from the radiant flux by mul-

tiplying with the relative spectral sensitivity of the human visual system over the wavelength range 380nm to 780nm. The luminous flux is measured in lumens (lm).

Luminous intensity is the amount of luminous flux emitted by the source in a given direction per unit solid angle. The luminaire manufacturers usually use the polar luminous intensity graph to provide a visual representation of the type of light distribution emitted from a luminaire (e.g. wide, narrow, direct, indirect etc.). The unit of measurement of luminous intensity is the candela, which is equivalent to one lumen/steradian.

Illuminance is the luminous flux arriving at a unit area of a surface. The illuminance incident on a surface is the most widely used electric lighting design criterion. The unit of measurement of illuminance is the $lumen/m^2$ or lux.

Luminance is the luminous intensity per unit area of light travelling in a given direction. It describes the amount of light that passes through, is emitted or reflected from a particular area, and falls within a given solid angle. The unit of measurement of luminance is the $candela/m^2$.

In 3D spaces, light rays travel in a straight line until they are reflected, absorbed, or refracted by a surface on its path. Thus, once the light is emitted from its source, it starts a journey, interacting with its surroundings. The interactions between light and scenes result in so-called light fields, a physical concept that was introduced by Gershun in 1936 in a Russian article and published in an English translation three years later [29]. According to Gershun, if color and temporal variations are neglected, the light field is a 5-dimensional function that describes the light traveling in every direction (θ, ϕ) through any point (x, y, z) in space. The focus of this thesis is on the spatial distribution of light and its spectral composition (i.e. color information) will not be discussed here.

1.2. A concise history of lighting design

The lighting profession emerged in 1898 when a meeting of gas engineers in Paris laid the basis for an international system of photometry. The development of the lighting profession can be divided into three stages according to Cuttle [18], which will be treated in the next three sessions.

1.2.1. The first stage of the lighting profession

The first stage of the lighting profession is characterized by the aim of provision of uniform illumination over a horizontal plane. Uniformity is usually defined as the ratio of the minimal illuminance and the area weighted average illuminance:

$$u = E_{min}/E_{average} \qquad (1.1)$$

Because gas lighting was largely used in the 19th century, illumination uniformity was eagerly pursued since the light intensity of a flame burning around a wick varied enormously [32]. Hence, gas engineers tried to develop photometric data in order to improve uniformity in the illuminance. As electric lighting came to dominate lighting practice, the illumination uniformity related studies were switched to focus on uniformity recommendations and acceptable illuminance uniformity for various occasions

[15, 61, 62]. The SLL code suggested that for a room where tasks would have to be done anywhere in the room, the uniformity ratio on the working plane should not be less than 0.7 [54].

1.2.2. The second stage of the lighting profession

With the use of electric lighting as a replacement of gas lighting in the early 20th century, the illumination uniformity on horizontal planes became easier to manipulate. The main reasons were that the emitted light intensity by electric lighting was more uniform than that of gas lighting and that electric lighting had more size and shape variability and was easier and safer to control [6]. The lighting professionals started to focus on the question of how to define the amount of light on the horizontal plane that people needed in order to perform a specific task [4, 21, 26, 27, 55, 56, 66, 67]. Both the Chartered Institution of Building Services Engineers (CIBSE) and the Illuminating Engineering Society of North America (IESNA) established illuminance categories based on descriptions of various visual tasks (see Table 1.1). Although the category descriptions given by the two organizations were different, the underlying visual task-performance relations of these descriptions were similar. Generally, it was suggested that in public spaces where reading and visual inspection were only occasionally performed, the illuminance level could be less than 100 lux. The illuminance levels on a working plane were advised to be in between 300 lux to 500 lux, with higher levels recommended for visual tasks involving critical elements of low contrast or small size. For tasks involving visual inspection of very small or very low contrast critical elements, like medical surgical rooms, an illuminance level higher than 1000 lux was suggested. Elderly have reduced levels of retinal illuminance because their crystalline lens becomes thicker and more absorptive. Thus elderly need higher illuminance levels while doing the same tasks [11].

The illumination uniformity proposed in the first stage and the illuminance levels proposed in the second stage of the lighting profession mainly focused on the horizontal illuminance. These two standards are widely used and serve as valuable references for the traditional lighting schemes in the fields of illumination engineering and architectural lighting design. However, office spaces and work procedures have changed a lot over the past 30 years. Desktop computers have replaced paper, pen, printed materials, typewriters, and drafting tables. Computer screens have a self-illuminated screen, and so continuing using illumination levels on the working plane as standards seems improper.

1.2.3. The third stage of the lighting profession

In the meantime, the development of novel and more efficient lighting technologies, such as LED lighting, made lighting planning and control more flexible and people's expectations of lighting became higher. Instead of taking light simply as a provision for visibility, people expect light to serve as a medium that conveys content, both informative and emotional. In this line of thought, Cuttle proposed that the lighting profession should move from its first and second stage to the third stage [18]. The aim of the third stage of lighting is consistent with the definition of "good lighting" by Boyce et al. [9].

1

Table 1.1: The illuminance levels suggested for various visual tasks by CIBSE and IESNA

Characteristic visual tasks (CIBSE 1994)	Illuminance (lux)	Illuminance category (IESNA 2000)
	30	A. public spaces
Confined to movement and causal seeing without perception of detail	50	B: Simple orientation for short visit
Movement and casual seeing with only limited perception of detail	100	C. Working spaces where simple visual tasks are performed
Involving some risk to people, equipment or product	150	
Requiring some perception of detail	200	
Moderately easy: i.e. large detail, high contrast.	300	D. Performance of visual tasks of high contrast and large size
Moderately difficult: i.e. moderate size, may be of low contrast. Color judgement may be required.	500	E. Performance of visual tasks of high contrast and small size, or low contrast and large size
Difficult: details to be seen are small and of low contrast. Color judgments may be important.	750	
Very difficult: very small details which may be of very low contrast. Accurate color judgements required.	1000	F. Performance of visual tasks of low contrast and small size
Extremely difficult: details are extremely small and of low contrast. Optical aids may be of advantage.	1500	
Exceptionally difficult: details to be seen are exceptionally small and of low contrast. Optical aids will be advantage.	2000	
	3000	G. performance of visual tasks near threshold

1

According to Boyce et al., lighting can be simply classified into "bad lighting", "indifferent lighting" and "good lighting". Characteristics of "good lighting" are not only the guarantee of good functional values of the lighting (ensuring visibility and visual comfort characterized as "indifferent lighting"), but also consider human experiences.

Human beings perceive the outside world primarily via the luminance pattern generated by the environment instead of the illuminance distribution on the objects or planes in the environment. The proximal stimulus for the human visual system is thus generated by the actual light in the space, being the result of the interaction of the primary lighting with the geometry and materials of the environment (so called light field or plenoptic function [2]). Thus, caring about human perception of light (the visual effects of lighting) requires lighting professionals to pay attention to the light (luminance) distribution in the space. Encouragingly, the lighting professional standards are making progress towards such an approach [25, 36]. Comparing with the old codes, the SLL codes 2012 suggest to illuminate the task area (which can be horizontal, vertical or inclined) instead of illuminating an entire space at working plane height. The aim of doing this is to provide visual interest, which has been shown to increase occupant concentration and satisfaction within spaces [10] and reduce energy consumption. Furthermore, the new codes point out that the use of high reflectance of room surfaces allows for an increased quantity of reflected light, which thus increases the brightness of a space. In addition, the new codes introduce the cylindrical illuminance and modelling index, which are stated as "a big step forward in recognizing the importance of the visibility of people's faces and objects, within a space [54]".

To design "good lighting" as the third stage of the lighting profession requires, the actual light in the spaces should be considered as light field. Besides that, attention should also be paid to the aesthetic and emotional aspects of lighting related to human being's experience. Therefore, lighting designers should interact with other design professionals, particularly architects and interior designers, aiming at revealing the potential of illumination to interact with its surroundings to create various types of visual experiences. Thus, besides following the numerical criteria of lighting guidelines to eliminate "bad lighting" and to ensure only "indifferent lighting" [53] how do architects and lighting designers play with lighting to achieve "good lighting"? "To play with light is to play with magic" said Richard Kelly, who is widely recognized as one of the pioneers and great contributors in the history of the architectural lighting profession, and the founder of so-called qualitative or perception-based lighting design. Based on his understanding of "light impact", Richard Kelly noted that a feeling for light and lighting starts with visual imagination, just as a painter's talent. He coined three elemental kinds of light effects in the visual perception of lighting design: (1) focal glow or highlight, (2) ambient luminescence or graded washes, and (3) play of brilliants or sharp detail [37]. He defined them as follows. Focal glow makes the target easier to see, draws attention, pulls together diverse parts, sells merchandise and separates the important from the unimportant (see Figure 1.5 (a)). Ambient luminescence is well known as "global, indirect" lighting. It makes a surrounding look safe and reassuring, produces shadow-free illumination and minimizes the importance of all things and people (see Figure 1.5 (b)). Play of brilliants is also known as "light texture" [50]. Play of brilliants stimulates the body and spirit and entertains the eye and charms the senses as with sunlight on a fountain (see Figure 1.5

(c)). Visual beauty is perceived by the interplay of all three kinds of light (see Figure 1.5 (d)). A designer can mix or superpose these three types of light to achieve the desired result, planning what we see and how we respond to the lighting, though one type of lighting is usually dominant.
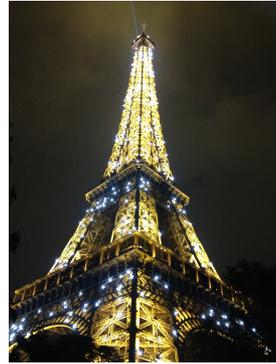
(a) focal glow   (b) ambient luminescence   (c) brilliants

(d) three elements combined

Figure 1.5: The three elemental kinds of light in perception-based lighting design, (a) focal glow, (b) ambient luminescence, and (c) play of brilliants, plus (d) all three elements combined.

Kelly's three types of light effects are consistent with the new direction for general lighting practice proposed much later by Cuttle [19]. Cuttle introduced two criteria for practical lighting installations, being perceived adequacy of illumination (PAI) and illumination hierarchy (HI). He suggested that the third stage has as its objective the provision of acceptably bright surroundings and this can be reflected using PAI. The PAI is corresponding to Kelly's ambient luminescence and known as "ambient light" in computer graphics. The PAI level reflects the perceived brightness of a space and according to Cuttle it can be specified in terms of mean room surface exitance (MRSE), which is a measure of the overall density of reflected (excluding direct) light within a space. Cuttle's IH is corresponding to Kelly's focal glow. IH expresses how the direct flux from the luminaires is distributed to specific targets in spaces and creates visual significance. It

1

is specified in terms of the target/ambient illuminance ratio (TAIR). In addition, Cuttle proposed a design procedure based on MRSE and TAIR. The basic idea is to first fulfill the MRSE considering the brightness requirement of a space and the reflectances of its surfaces, and then to consider TAIR according to which objects or surface areas one wants to highlight with selective lighting. Thus, this proposal also comes down to mixing ambient and focus lighting and is in that regard consistent with Kelly's approach (although the "play of brilliants" is missing in Cuttle's approach). The ratio of ambient and focus components (or "diffuseness") was mentioned to determine the shape and space forming qualities of light [17, 54].

These approaches for lighting design using mixtures of basic light elements can be linked to physical descriptions of light that consist of basic mathematical elements. The physical light field distribution is described by Gershun using a 5-dimensional function of direction and position. He introduced the notion of "density of light" and the notion of "light vector" to describe its two most basic properties [29]. Mury et al. used spherical harmonics decompositions to represent this 5-dimensional function as a combination of components of different mathematical orders [46, 47]. He found that the zeroth order component of such a spherical harmonic decomposition corresponds to Gershun's "density of light" and the first order component corresponds to the "light vector" as defined by Gershun. However, neither Gershun nor Mury defined "diffuseness of light" in their mathematical descriptions of the light field. Moreover, their approaches do not allow straightforward practical application due to the technical complexity of their methods.

In this thesis we investigate the fundamentals of these layered / mixing approaches to describe and design light. How sensitive are human beings to the basic elements of the spatial distribution of a light field in real 3D space? Is there an integral yet practical way to describe and measure these elements of physical light field structures? Can human beings perceive how these basic elements interact with each other and with the environment and objects in it?

1.3. Human perception of lighting properties

Human observers are sensitive to the "(physical) light field" in the sense that they have expectations of how a given object would appear at an arbitrary location in a scene, which was termed as the "visual light field" [40]. The light field in natural scenes is highly complex, containing low and high frequencies due to inter-reflections within scenes. Nonetheless, psychophysical research showed that the human visual system (HVS) is able to distinguish the light density, the primary illumination direction, and the diffuseness, which are basic (low-order) properties of a light field, ignoring color and motion [20, 28, 41, 45, 46, 48–50, 64]. Te Pas and Pont found that observers could not distinguish the difference between illumination of spheres from the Dror database [24] if the global properties of the illumination, such as the average direction and diffuseness, were similar [64]. This suggested that observers primarily used the low order properties of the illumination to distinguish illumination. Thus, we focus only on the three lowest order properties of the illumination (i.e., the intensity, direction and diffuseness) in the rest of this thesis. These properties are consistent with third stage lighting designers' de-

scriptions of the light's shape and space forming qualities; see the examples of how they influence the appearance of a plaster face in Figure 1.6.

(a)	(b)	(c)	(d)

(e)	(f)	(g)
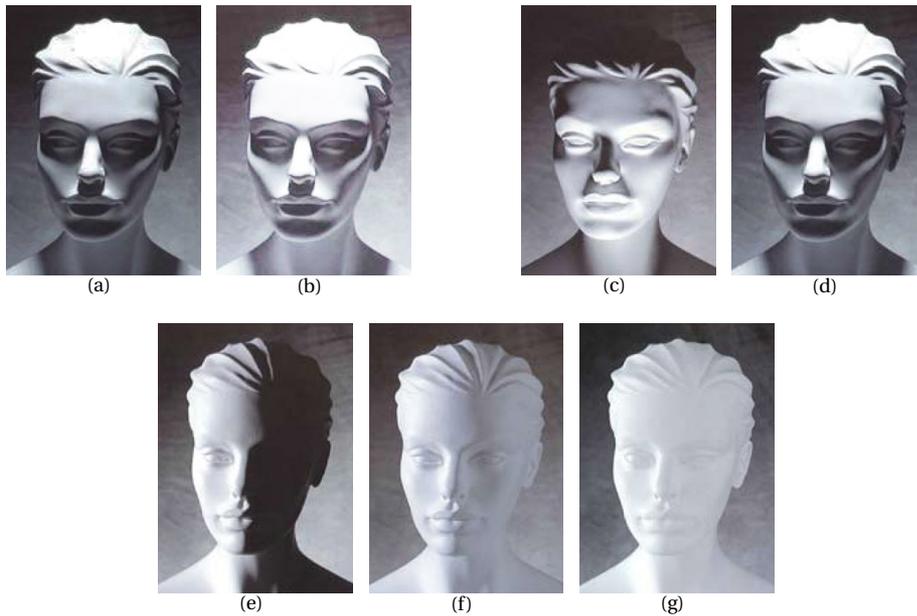
Figure 1.6: A plaster face illuminated by light with different density in (a) and (b), different directions in (c) and (d) and different diffuseness levels in (e), (f) and (g). (photos from:http://www.thornlighting.com)

Research on how well observers can estimate the properties of a light field directly was available. Pentland [49] investigated how well humans could estimate the illumination direction from an image. In his experiment, a paper sheet with a series of disks with varying surface normal was provided to the observers. The observers were asked to select from these disks the one with its surface normal closest to the illumination direction in test pictures of natural objects. The results showed that the observers could estimate both tilt and slant of the illuminant direction. Koenderink et al. [42] did a study on estimating illumination orientation from textures in images. In order to test the perceived illumination in a more genetic and intuitive way, they used a purely visual, appearance-based interface in the form of a rendering of an illuminated hemispherical boss on a plane. The participants were asked to match the illumination direction of this probe to the illumination direction of the textures. They found that participants were generally quite good at estimating the illumination orientation, but not its direction because 180° flips happened quite frequently due to the "convex/concave ambiguity" [14, 33, 52]. Connected with this finding, they confirmed the "light-from-above bias" [34, 52, 58], which predicts a bias toward judging the illumination to be from above rather than from below. Moreover, they found that participants were much worse at estimating the elevation of the illumination than the orientation, as the theory "bas-relief

1

ambiguity" predicts [3]. The lower performance for estimating elevation than for azimuth was confirmed in an experiment done by Pont and Koenderink [51]. In the latter experiment, the observers were asked to match the illumination direction of a probe (i.e. a Lambertian sphere) and that of real rough spherical objects with various surface textures. They varied the diffuseness of the illumination in addition to the illumination direction. The results showed that observers were able to estimate the diffuseness, but with a quite large variance. Furthermore, they found that illumination direction estimates interacted with illumination diffuseness estimates, because more frontal lighting or more diffuse lighting resulted in quite similar changes in object appearance (i.e., "diffuseness-direction ambiguity"). Lighting designers and architects reported this ambiguity for case studies too. In a workshop led by Madsen and Donn [43], white spheres were used as a "light-flow-meter" (light flow is the term used for the set of local average directions of the light throughout a space) to visually assess spatial and form-giving characteristics of daylight. They found that the shading pattern varied with different perspective views and that variations in diffuseness and direction were confounded, complicating precise judgments of light flow using the matte white sphere as a gauge object. Using a scene with penguins facing each other, Koenderink et al.[40] conducted another experiment in which three light field properties (i.e. intensity, direction and diffuseness) could be adjusted simultaneously. They introduced a gauge object into the scene serving as a purely visual "yardstick", which allows the observers to quantify what they see in the scene based on visual "fit". Their results suggested that the observers could estimate a light field filling the entire visual space. Taken together, these studies have shown that for matching experiments on images human observers are able to estimate the illumination orientation in the plane of the image quite well, and the elevation and diffuseness coarsely.

Besides evaluating light field properties directly, studies into surface color and lightness perception often gave indirect evidence of our awareness of the light field [1, 8, 12, 13, 16, 30, 35, 39, 44, 59, 60, 65]. For instance, researchers showed that human observers substantially compensated for changes in test patch orientation when judging surface lightness, whether in computer-rendered scenes [8] or in actual surfaces [5, 57]. Human observers were found to partly discount the perceived orientation of a surface in surface color perception [7, 23]. In another series of studies, instead of changing the orientation of a test surface, the test surface was placed at various locations in a light field [31, 63]. Gilchrist argued that the perceived lightness of a surface is determined by the relationship between the surface and regions that are seen as coplanar. Snyder et al. concluded that all observers significantly discounted the gradient of illumination in depth in all experiments when estimating the lightness of the test patch. Additionally, Doerschner et al. [22] found that the visual system could effectively represent complex lighting models that contain two light sources.

In summary, lighting designers take the low order structure of a light field (i.e., light density, direction and diffuseness) as basic light layers that can be superposed or mixed to arrive at the desired quality of light. The research in the psychophysics domain shows direct and indirect evidence of human being's sensitivity to these lighting properties through a series of experiments, which were mostly performed on the basis of pictures on a computer screen.

1.4. Research questions

In order to achieve good lighting qualities, the lighting profession is developing towards its third stage aiming at revealing the potential of illumination to interact with its surroundings to create various types of visual experiences. Ignoring the spectral characteristics of the light, the distribution of light in a space greatly influences the appearance and experience of the space and objects in it. Designers use layered approaches to compose the light, of which the main elements correspond with physical decompositions of the light field. Psychophysics research using pictures has shown human beings' potential sensitivity to these properties of the light field. This thesis focuses on perception of (combinations or mixtures of) these elements, their interactions with each other and the environment, and their measurement in real scenes. The following 5 main questions have driven the research presented in this thesis.

The first three research questions mainly focus on probing human being's subjective sensitivity for the light density, direction and diffuseness in real scenes. The last two questions focus on the objective description, measurement and visualization of these properties in 3D spaces.

Research Question 1:   Are human beings sensitive to variations of light field properties in real scenes and in what way can their perception be measured intuitively?

Looking at a real scene is different from looking at a picture of it because of the differences in dynamic range, stereo cues, and intra-ocular scattering. Thus, investigating whether human beings are sensitive to variations of light field properties in real scenes is necessary. Furthermore, research based on pictures showed that the method embedding a probe object into the scene and letting the observer judge its "fit" is efficient. The task to judge the visual "fit" quantifies what the observer sees with a purely visual "yardstick". In order to implement this method into real scenes, a novel experimental setup had to be developed.

Research Question 2:   How well can human beings infer light field properties and how can we measure their sensitivity using our real experimental setup?

In order to develop the probing method in perception experiments and for practical lighting interfaces, it is important to find out how well observers are able to infer and adjust the light density, direction and diffuseness in real scenes. More importantly, most of the previous studies focused on observers' estimations of single properties of the light field, with the light direction being studied most intensively. The light intensity, direction and diffuseness influence the appearance of the scenes collectively. The question remains how well human observers can estimate the three lighting properties simultaneously in a real scene. Answering these questions is important to design lighting interfaces for perception research and lighting design and to formulate guidelines for perception based lighting design.

1

Research Question 3:   Can observers' perception of light direction be influenced by scene content and layout in real scenes?

Light makes objects visible without being visible itself in an empty space. As such the appearance of the space and the objects inside it are the main cues for the perception of the lighting. In the experiment conducted to answer Research Question 2, we found that observers' estimated light directions had a significant deviation near a pentagon body and not near a bowling pin in the scene. We noticed that, both in psychophysical research and interior design, it appears to be neglected that objects placed within a 3D space might influence observers' perception of light in that space. There is research showing that light direction estimation can be influenced by materials [38]. However, it is still not clear whether the types of shapes (geometries) and scene layouts affect light direction estimation.

Research Question 4:   Can we find a mathematical way to describe the light diffuseness based on the physical light distribution of light fields?

Light density and direction were well defined by Gershun and Mury et al. and their relationship with the light as such was clarified through a 5-dimensional function of the light field [29] and its spherical harmonics decomposition [46, 47]. However, this is not the case for the light diffuseness. Light diffuseness ranges from fully collimated light (i.e. direct sunlight) via hemispherical diffuseness (i.e. illumination by an overcast sky) to completely diffuse light (i.e. the light in a polar white-out). The light diffuseness can strongly influence the appearance of scenes and objects in it. We found that various practically defined diffuseness metrics exist, but they differ from each other by definition and were implemented in different fields. We investigated how these metrics are related to each other and whether we could find a way to describe the light diffuseness in a theoretically sound and practical way.

Research Question 5:   Can we describe, measure and visualize the complete first order structure of the light field in an integral way?

The light density, the primary illumination direction, and the diffuseness shape the basic (first order) properties of a light field structure and can be perceived by humans. Can we find a method to integrally describe, measure and visualize the global structure of these properties of the light field? Results provide insights into the spatial and form-giving character of light.

1.5. Structure of the thesis

This thesis consists of seven chapters. After introducing the background, the main contributions are presented in Chapters 2-6, answering the research questions formulated in Section 1.4. Each of these chapters addresses one research question, and the corresponding findings and contributions are discussed in each chapter. The work in these chapters is based on the publications listed in Section 1.6. Each chapter is self-contained

and can be read independently. The relationship between the main work described in this thesis and the development of the lighting profession, as well as the general structure of the chapters in this thesis are depicted in Figure 1.7.
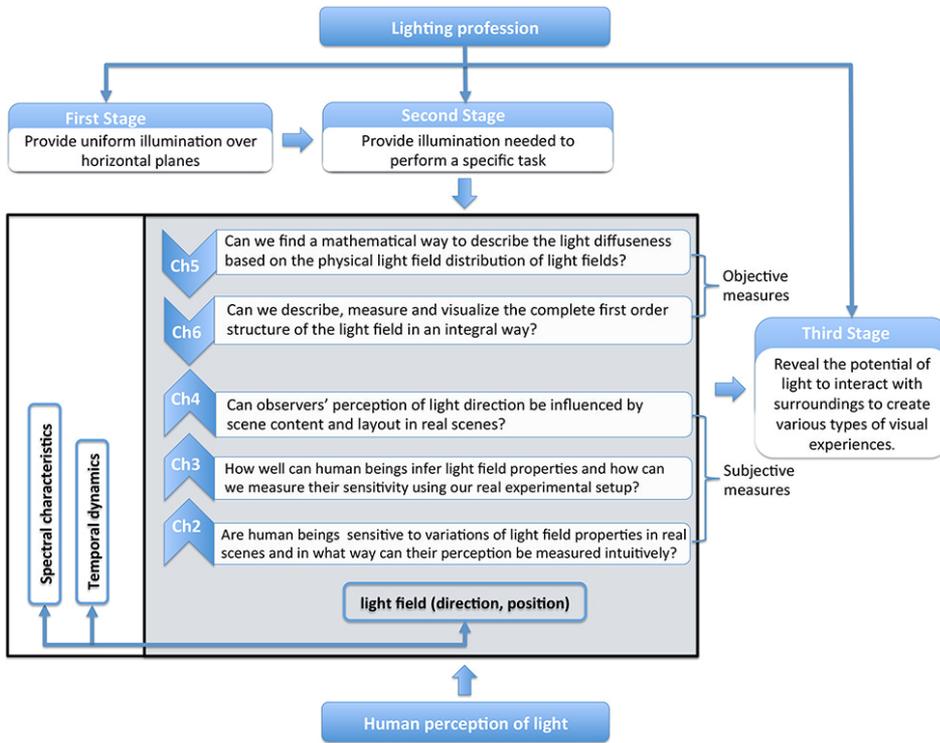
Figure 1.7: Overview of the structure of the main work presented in this thesis (marked with gray background).

- Chapter 2 based on [Xia-1], proposed a novel experimental setup to investigate human sensitivity for variations of light field properties in real scenes. This setup was developed based on the generic notion of a "probe object" by optically mixing a light probe into a real scene. Observers' sensitivities for low order properties of the light field (i.e., light density, direction and diffuseness) in real scenes were evaluated.

- Chapter 3 based on [Xia-2], used the method of adjustment to quantitatively measure human observers' sensitivity for the low order properties of the light field. Two experiments were conducted using the experimental setup proposed in Chapter 2, in which human observers' abilities to infer the light density, direction and diffuseness independently and simultaneously were studied.

- Chapter 4 based on [Xia-3], presents a systematic exploration of the effect of scene content and layout on light direction perception in space. Again, two experiments

1

were conducted based on the experimental setup proposed in Chapter 2. The first experiment focused on studying whether types of shapes and scene layout influence light direction estimation and the second experiment focused on studying how the shape properties, scene layout and light direction estimation impact each other.

• Chapter 5 based on [Xia-4], we reviewed the four most frequently used light diffuseness metrics and proposed a diffuseness metric based on the mathematical description of the physical light distribution in a space. This work is an extension of Mury's work on describing the light field's structure in terms of flux density and direction variations in 3D spaces based on the spherical harmonics representation of the light field. The relationships between the five diffuseness metrics were examined using a model named "probe in a sphere" and each of them was examined against our criteria proposed for a general purpose diffuseness metric.

• Chapter 6 based on [Xia-5], introduced an integral way to describe, measure and visualize the flux density, light vector and diffuseness (variations) of the light field based on the spherical harmonics representation of the light field. A way to simultaneously measure the light density, light vector and diffuseness (variations) of the light using a cubic illumination meter was introduced. This approach was applied to six light probe images of natural scenes and four real scenes built in our lab. Furthermore, a cubic meter was built using commercially available components and laser-cutting MDF boards.

In the end, Chapter 7 concludes this thesis by summarizing the main contributions and findings. In addition, limitations and possible directions for future research are discussed. Some of the relevant research that has not been shown in previous chapters will be presented in the Appendix.

1.6. List of Publications

Journal Articles

[Xia-1] **XIA, L.**, PONT, S. C. & HEYNDERICKX, I. The visual light field in real scenes. *i-Perception*, 5, 613-629. 2014.

[Xia-2] **XIA, L.**, PONT, S. C. & HEYNDERICKX, I. Testing separate and simultaneous adjustment methods for lighting intensity, direction and diffuseness. *i-Perception* (submitted).

[Xia-3] **XIA, L.**, PONT, S. C. & HEYNDERICKX, I. Effects of scene content and layout on the perceived light direction in 3D spaces. *Journal of Vision* (accepted).

[Xia-4] **XIA, L.**, PONT, S. C. & HEYNDERICKX, I. Light diffuseness metric, Part 1: Theory. *Lighting Research and Technology*. 1477153516631391, 2016.

[Xia-5] **XIA, L.**, PONT, S. C. & HEYNDERICKX, I. 2016. Light diffuseness metric, Part 2: Describing, measuring and visualising the light flow and diffuseness in three-dimensional spaces. *Lighting Research and Technology*, 1477153516631392, 2016.

Conference proceedings

[Xia-6] **XIA, L.**, PONT, S. C. & HEYNDERICKX, I. Probing light in real scenes using optical mixtures. *Proceedings of the ACM Symposium on Applied Perception*, Dublin, Ireland, August 2013: 137.

[Xia-7] **XIA, L.**, PONT, S. C. & HEYNDERICKX, I. The influence of scene layout and content on the perception of light direction in real scenes. *Journal of Vision*, Florida, USA. 14(10), August 2014: 71.

[Xia-8] **XIA, L.**, PONT, S. C. & HEYNDERICKX, I. The sensitivity of observers to light field in real scenes. *Proceedings of EXPERIENCING LIGHT 2014, International Conference on the Effects of Light on Wellbeing*, Eindhoven, the Netherlands, November 2014: 120.

[Xia-9] **XIA, L.**, PONT, S. C. & HEYNDERICKX, I. Simultaneous measurement and visualisation of light flow and diffuseness in 3D spaces. *Proceedings of 28th CIE Session*, Manchester, UK, June 2015: 556-563.

References

[1] Edward H Adelson. Zjˆ±lightness perception and lightness illusions. *New Cogn. Neurosci*, 339, 2000.

[2] Edward H Adelson and James R Bergen. The plenoptic function and the elements of early vision, chapter 1, 1991.

[3] Peter N Belhumeur, David J Kriegman, and Alan L Yuille. The bas-relief ambiguity. *International journal of computer vision*, 35(1):33–44, 1999.

[4] AW Beuttell et al. An analytical basis for a lighting code. a method of computing values of illumination for various classes of work. *Illuminating Engineer*, 27:5–11, 1934.

[5] Marina Bloj, Caterina Ripamonti, Kiran Mitha, Robin Hauck, Scott Greenwald, and David H Brainard. An equivalent illuminant model for the effect of surface slant on perceived lightness. *Journal of Vision*, 4(9):6–6, 2004.

[6] Brian Bowers and Paul Anastas. *Lengthening the day: a history of lighting technology*. oxford university Press New York, 1998.

[7] Huseyin Boyaci, Katja Doerschner, and Laurence T Maloney. Perceived surface color in binocularly viewed scenes with two light sources differing in chromaticity. *Journal of Vision*, 4(9):1–1, 2004.

[8] Hussein Boyaci, Lawrence T Maloney, and Sarah Hersh. The effect of perceived surface orientation on perceived surface albedo in binocularly viewed scenes. *Journal of Vision*, 3(8):2–2, 2003.

[9] Peter R Boyce. Lighting quality: the unanswered questions. In *Orlando, First CIE (Commission International d'Eclairage) Symposium on Lighting Quality*, 1998.

[10] Peter Robert Boyce. *Human factors in lighting*. Crc Press, 2014.

[11] PR Boyce. Age, illuminance, visual performance and preference. *Lighting Research and Technology*, 5(3):125–144, 1973.

[12] David H Brainard. Color constancy in the nearly natural image. 2. achromatic loci. *JOSA A*, 15(2):307–325, 1998.

[13] David H Brainard, Wendy A Brunt, and Jon M Speigle. Color constancy in the nearly natural image. 1. asymmetric matches. *JOSA A*, 14(9):2091–2110, 1997.

[14] David Brewster. On the optical illusion of the conversion of cameos into intaglios and of intaglios into cameos, with an account of other analogous phenomena. *Edinburgh Journal of Science*, 4(1826):99–108, 1826.

[15] B Constantatos. Uniformity as the key element in present developments in lighting design (or-why there seems to be an apparent dichotomy between artificial and natural lighting schemes). *Lighting Research and Technology*, 14(2):102–105, 1982.

[16] Stanley Coren and Melvin K Komoda. The effect of cues to illumination on apparent lightness. *The American journal of psychology*, pages 345–349, 1973.

[17] C Cuttle. Lighting patterns and the flow of light. *Lighting research and Technology*, 3(3):171–189, 1971.

[18] C Cuttle. Towards the third stage of the lighting profession. *Lighting Research and Technology*, 42(1):73–93, 2009.

[19] C Cuttle. A new direction for general lighting practice. *Lighting Research and Technology*, 45(1):22–39, 2013.

[20] Christopher Cuttle. *Lighting by design*. Routledge, Oxford: Architectural Press, 2008.

[21] PS Defoe. Light: how much is right? *Building Services Journal*, 10(8):54–5, 2008.

[22] K Doerschner, H Boyaci, and LT Maloney. Testing limits on matte surface color perception in three-dimensional scenes with complex light fields. *Vision research*, 47(28):3409–3423, 2007.

[23] Katja Doerschner, Huseyin Boyaci, and Laurence T Maloney. Human observers compensate for secondary illumination originating in nearby chromatic surfaces. *Journal of Vision*, 4(2):3–3, 2004.

[24] Ron O Dror, Edward H Adelson, and Alan S Willsky. Estimating surface reflectance properties from images under unknown illumination. In *Photonics West 2001-Electronic Imaging*, pages 231–242. International Society for Optics and Photonics, 2001.

[25] James Thomas Duff. The 2012 sll code for lighting: the impact on design and commissioning. *SDAR* Journal of Sustainable Design & Applied Research*, 1(2):4, 2012.

[26] Neil H Eklund, Peter R Boyce, and S Noel Simpson. Lighting and sustained performance: modeling data-entry task performance. *Journal of the Illuminating Engineering Society*, 30(2):126–141, 2001.

[27] Terrence W Faulkner and Thomas J Murphy. Lighting for difficult visual tasks. *Human Factors: The Journal of the Human Factors and Ergonomics Society*, 15(2):149–162, 1973.

[28] Sophus Frandsen. The scale of light–a new concept and its application. In *Paper on 2nd European Conference on Architecture*, pages 4– 8, 1989.

[29] Andreī Gershun. The light field (translated by moon, parry hiram and timoshenko, gregory). *Journal of Mathematics and Physics*, 18(1):51–151, 1939.

[30] Alan Gilchrist, Christos Kossyfidis, Frederick Bonato, Tiziano Agostini, Joseph Cataliotti, Xiaojun Li, Branka Spehar, Vidal Annan, and Elias Economou. An anchoring theory of lightness perception. *Psychological review*, 106(4):795, 1999.

1

[31] Alan L Gilchrist. When does perceived lightness depend on perceived spatial arrangement? *Perception & Psychophysics*, 28(6):527–538, 1980.

[32] David Gledhill. *Gas lighting*, volume 65. Osprey Publishing, 1999.

[33] Richard Langton Gregory. *The intelligent eye*. ERIC, 1970.

[34] Donald D Hoffman. *Visual intelligence: How we create what we see*. WW Norton & Company, 2000.

[35] Mitsuo Ikeda, Hiroyuki Shinoda, and Yoko Mizokami. Phenomena of apparent lightness interpreted by the recognized visual space of illumination. *Optical review*, 5(6):380–386, 1998.

[36] Kevin Kelly and James Duff Mr. Lighting design in europe: Aligning the demands for lower energy usage with better quality. *Civil Engineering and Architecture*, 9:283–290, 2015.

[37] Richard Kelly. Lighting as an integral part of architecture. *College Art Journal*, pages 24–30, 1952.

[38] Byung-Geun Khang, Jan J Koenderink, and Astrid ML Kappers. Perception of illumination direction in images of 3-d convex objects: Influence of surface materials and light fields. *Perception*, 35(5):625–645, 2006.

[39] Frederick AA Kingdom. Lightness, brightness and transparency: A quarter century of new ideas, captivating demonstrations and unrelenting controversy. *Vision Research*, 51(7):652–673, 2011.

[40] Jan J Koenderink, Sylvia C Pont, Andrea J van Doorn, Astrid ML Kappers, and James T Todd. The visual light field. *PERCEPTION-LONDON-*, 36(11):1595, 2007.

[41] Jan J Koenderink, Andrea J van Doorn, Astrid ML Kappers, Sylvia C Pont, and James T Todd. The perception of light fields in empty space. *Journal of Vision*, 5(8):558–558, 2005.

[42] Jan J Koenderink, Andrea J van Doorn, Astrid ML Kappers, Susan F Te Pas, and Sylvia C Pont. Illumination direction from texture shading. *JOSA A*, 20(6):987–995, 2003.

[43] M. Madsen and M Donn. Experiments with a digital 'light-flow-meter' in daylight art museum buildings. In *presented at the 5th International Radiance Scientific Workshop, UK: Leicester, Sep 13-14*, 2006.

[44] Laurence T Maloney. Illuminant estimation as cue combination. *Journal of Vision*, 2(6):6–6, 2002.

[45] Yaniv Morgenstern. *The role of low-pass natural lighting regularities in human visual perception*. York University, 2011.

[46] Alexander A Mury, Sylvia C Pont, and Jan J Koenderink. Light field constancy within natural scenes. *Applied Optics*, 46(29):7308–7316, 2007.

[47] Alexander A Mury, Sylvia C Pont, and Jan J Koenderink. Spatial properties of light fields in natural scenes. In *Proceedings of the 4th symposium on Applied perception in graphics and visualization*, pages 140–140. ACM, 2007.

[48] James P O'Shea, Maneesh Agrawala, and Martin S Banks. The influence of shape cues on the perception of lighting direction. *Journal of vision*, 10(12):21, 2010.

[49] Alex P Pentland. Finding the illuminant direction. *JOSA*, 72(4):448–455, 1982.

[50] Sylvia C Pont. Spatial and form-giving qualities of light. *Handbook of Experimental Phenomenology: Visual Perception of Shape, Space and Appearance*, pages 205–222, 2013.

[51] Sylvia C Pont and Jan J Koenderink. Matching illumination of solid objects. *Perception & psychophysics*, 69(3):459–468, 2007.

[52] Vilayanur S Ramachandran. Perception of shape from shading. *Nature*, 1988.

[53] Peter Raynham. Standards and codes. 2013.

[54] PJ Raynham. *The SLL Code for Lighting*. The Society of Light and Lighting, UK, 2012.

[55] Mark S Rea. Toward a model of visual performance: Foundations and data. *Journal of the Illuminating Engineering Society*, 15(2):41–57, 1986.

[56] Mark S Rea and Michael J Ouellette. Relative visual performance: A basis for application. *Lighting Research and Technology*, 23(3):135–144, 1991.

[57] Caterina Ripamonti, Marina Bloj, Robin Hauck, Kiran Mitha, Scott Greenwald, Shannon I Maloney, and David H Brainard. Measurements of the effect of surface slant on perceived lightness. *Journal of Vision*, 4(9):7–7, 2004.

[58] David Rittenhouse. Explanation of an optical deception. *Transactions of the American Philosophical Society*, 2:37–42, 1786.

[59] Rocco Robilotto and Qasim Zaidi. Limits of lighness identification for real objects under natural viewing conditions. *Journal of Vision*, 4(9):9–9, 2004.

[60] James A Schirillo. We infer light in space. *Psychonomic bulletin & review*, 20(5):905–915, 2013.

[61] AI Slater, MJ Perry, and DJ Carter. Illuminance differences between desks: Limits of acceptability. *Lighting Research and Technology*, 25(2):91–103, 1993.

[62] Anthony I Slater and Peter R Boyce. Illuminance uniformity on desks: Where is the limit? *Lighting Research and Technology*, 22(4):165–174, 1990.

1

[63] Jacqueline Leigh Snyder, Katja Doerschner, and Laurence T Maloney. Illumination estimation in three-dimensional scenes with and without specular cues. *Journal of Vision*, 5(10):8–8, 2005.

[64] Susan F te Pas and Sylvia C Pont. A comparison of material and illumination discrimination performance for real rough, real smooth and computer generated smooth spheres. In *Proceedings of the 2nd symposium on Applied perception in graphics and visualization*, pages 75–81. ACM, 2005.

[65] James T Todd, J Farley Norman, and Ennio Mingolla. Lightness constancy in the presence of specular highlights. *Psychological Science*, 15(1):33–39, 2004.

[66] HC Weston. Rationally recommended illumination levels. *Lighting Research and Technology*, 26(1 IEStrans):1–16, 1961.

[67] Hubert Claude Weston et al. The relation between illumination and visual efficiency-the effect of brightness contrast. *Industrial Health Research Board Report. Medical Research Council*, (87), 1945.

2

SUJECTIVE SENSITIVITY FOR THE VISUAL LIGHT FIELD IN REAL SCENES

Abstract

Human observers' ability to infer the light field in empty space is known as the "visual light field". While most relevant studies were performed using images on computer screens, we investigate the visual light field in a real scene by using a novel experimental setup. A "probe" and a scene were mixed optically using a semi-transparent mirror. Twenty participants were asked to judge whether the probe fitted the scene with regard to the illumination intensity, direction and diffuseness. Both smooth and rough probes were used to test whether observers use the additional cues for the illumination direction and diffuseness provided by the 3D texture over the rough probe. The results confirmed that observers are sensitive to the intensity, direction and diffuseness of the illumination also in real scenes. For some lighting combinations on scene and probe, the awareness of a mismatch between the probe and scene was found to depend on which lighting condition was on the scene and which on the probe, which we called the "swap effect". For these cases the observers judged the fit to be better if the average luminance of the visible parts of the probe was closer to the average luminance of the visible parts of the scene objects. The use of a rough instead of smooth probe was found to significantly improve observers' abilities to detect mismatches in lighting diffuseness and directions.

2.1. Introduction

The interplay between lighting, geometry and materials in a scene shapes the architectural space and the light field in it. The structure of the light field depends on the spatial and spectral characteristics of the light sources, and on the shape, 3D texture (corrugation) and material reflectance properties of the patches in the light field that receive and re-emit the light. According to Gershun, if color and temporal variations are neglected, the light field is a 5-dimensional function, that describes the light traveling in every direction (θ, ϕ) through any point (x, y, z) in space [8]. Gershun's light field is essentially the radiance distribution over space and directions. The theory of the light field developed by Gershun describes light physically (optically). It describes everything that can potentially be seen and in psychology this concept was called the "plenoptic function" by Adelson and Bergen [1].

Our interest mainly concerns the perception of the light field; are people able to discern all aspects of the optical light field? A detection study done by Ostrovsky[20] showed that observers were remarkably insensitive to inconsistencies of illumination direction. They used both computer renderings consisting of identical but randomly oriented cubes and photographs of real scenes in which local inconsistencies of illumination were created. Their results suggest that the visual system does not verify the global consistency for locally derived estimates of illumination direction. However, Koenderink et al. found that human observers have expectations of how an object would look like when it was introduced at an arbitrary location in a scene [11]. It means that human observers can infer the light field even in the empty space around them, which the authors called the "visual light field". Later, Schirillo confirmed this theory on the basis of a review study [26]. In this study, Schirillo presented both direct and indirect evidence of our awareness of the light field.

Which properties of the light field can human observers perceive? The light field can strongly influence the appearance of a scene and inversely, its properties can be reflected by the appearance of a scene. The light field in natural scenes is highly complicated due to intricate optical interactions, containing low and high frequencies in the radiance distribution function. Nonetheless, the human visual system (HVS) is able to distinguish the intensity, the primary illumination direction, and the diffuseness, which are basic (low-order) properties of a light field [5, 7, 12, 14–16, 19, 21, 24, 27]. Mury et al [17] described the relations between the mathematical structure and physical meaning of the light field components, plus a manner to measure and visualize the light field. The intensity corresponding to "radiant flux density" in Gershun's theory describes a constant illumination from all directions, which is usually known as 'ambient light' in computer graphics. The "light vector" describes the average illumination direction and strength. Diffuseness of light was not mathematically described by Gershun or Mury and it ranges from fully collimated via hemispherical diffuse to completely diffuse light. An overcast sky generates hemispherical diffuse light, while direct sunlight is a typical example of collimated light and a polar whiteout of completely diffuse light.

The next question is how to reliably measure the perceived light field properties. Koenderink et al.'s experiment [11] adopted a method based upon the generic notion of a "gauge object". Their stimuli were stereo photographs of a scene consisting of matte

white painted penguins facing each other. A suitable "gauge object" was introduced at various locations in the photographic scenes and the observers were asked to adjust the appearance of the gauge object to visually fit the scene with respect to the lighting. Three properties of the light field (i.e., intensity, direction and diffuseness) could be adjusted simultaneously. The results suggested that observers could accurately match the illumination at arbitrary locations in a static scene. The high reliability of the observers on their settings also demonstrated the validity of the method of using a "gauge object" to measure the visual fit with a scene. In our research, a similar experiment with the same method is conducted. However, instead of using photographs, we perform our experiment in a real scene by optically mixing a gauge object into a group of scene objects.

Looking at a real scene is totally different than looking at a picture of it, even when stereo pictures are used. There are a few reasons. Firstly, there is a big difference in the dynamic range (DR) of luminance values between the real world and a computer screen. The real world has about ten orders of dynamic range for luminance values spread across the spectrum from darkness to brightness while a computer screen has only approximately two to three [18]. Secondly, some depth cues also induce differences between the real world and synthetic stereo images. The depth cue "motion parallax" is one of them. Observers can't stay absolutely still. When they move, the apparent relative motion of several stationary objects against a background gives hints about their relative distance, which can provide absolute depth information if the direction and velocity of the movement are known [6]. Besides head movements, eye movements can also provide additional information about the observed objects [28].

In this paper, we will implement a novel experimental setup to introduce a real gauge object into a real scene [29]. A similar setup was firstly used in a material perception study in which real objects with different materials were optically mixed together [22]. The key point of this setup lies in the use of a semitransparent mirror. The scene and probe are located inside two separated boxes and they are mixed together optically by a semitransparent mirror (see Figure 4.1). In this way, the properties of lighting for the probe and scene can be changed separately without any mutual interference. We will focus on testing observers' sensitivities for illumination direction, diffuseness and intensity because former studies into picture perception showed that observers are sensitive to these low-order characteristics of light. Observers have to judge the visual 'fit' of the probe in the scene.

In the experiment, two types of probes will be used, a smooth sphere and a rough sphere (golf ball). Theoretically, the illuminance flow or texture contrast gradients over the sphere due to the roughness of the golf ball give cues about its illumination additional to shading [10, 23]. It has been found that observers are sensitive to such gradient orientations on flat rough surfaces [13], but to our knowledge this is the first systematic study of whether observers use such cues on 3D objects to judge specific illumination characteristics.

2.2. Experimental setup

We made a setup to optically mix the scene and probe object, as shown in Figure 4.1. Three $30cm \times 30cm \times 30cm$ cubes formed the main framework of this setup. In cube B,

there were five colourful geometrical shapes forming a simple scene. In the center of cube C, there was a white sphere, which served as the probe. Because a white object has a higher albedo than an object with any other colour, one of the colourful geometrical shapes was painted white to provide an anchor. Inside Cube A, a semi-transparent optical mirror was placed vertically at the diagonal, which was at 45 degrees with respect to the viewing direction. Due to this mirror, the probe was seen through the mirror within the scene via its reflection in the mirror. The edges of the mirror could not be seen through the viewing hole. All cubes' insides were covered with light absorbing black-out material (black flocked paper, from Edmund Optics) to avoid too much scattering from the background, optical cross-talk through, and haze on the mirror. Occlusions between the probe and the shapes in the scene were prevented. Thus, when observers looked through the viewing hole, they saw the optical mixture of the scene and probe as if they were put together, as illustrated in Figure 2.2. The lighting of the scene and probe were provided by one LCD screen on top of cube B and one on top of cube C. Independent images were displayed on the two screens to determine the individual lighting for the scene and for the probe.

To make sure that both the probe and scene contributed 50% to the final superpositioned scene, we calibrated our setup. Firstly, the relationship between the screens' luminance and their pixel values was measured. Then we measured the reflectivity and transmission of the semi-transparent mirror, being 41% and 59% respectively (adding up to 100%, since this was a high quality semi-transparent mirror). By multiplying the luminance of screen B with the reflectivity of the mirror, we calculated the "simulated luminance" for screen B. In the same way, we calculated the "simulated luminance" for screen C by multiplying the luminance of screen C with the transmission of the mirror.
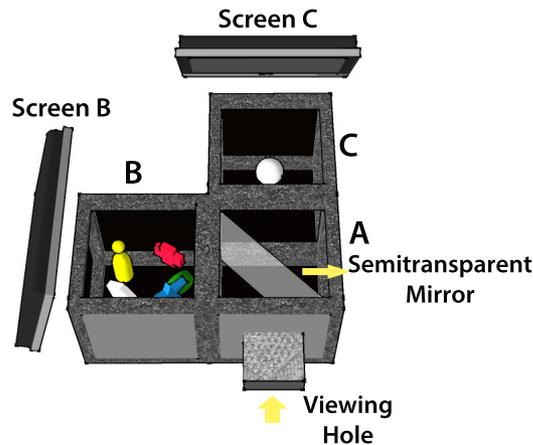
Figure 2.1: Illustration of the setup. The setup consists of three $30cm \times 30cm \times 30cm$ cubes, of which the inside is covered with black velvet paper. In cube B, we made a simple scene with five geometrical shapes. In cube C, we placed a white sphere, which served as the probe. A semi-transparent mirror was placed vertically at the diagonal of box A. Two LCD screens, one covering the top of cube B and one the top of cube C, provided the lighting which could thus be varied independently for the scene and probe

2

(a)   (b)
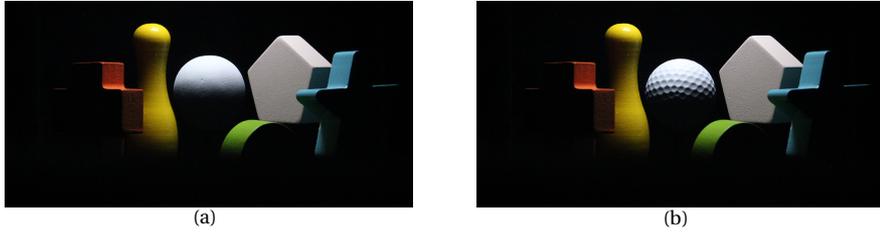
Figure 2.2: Optical mixture of scene and probe photographed from the viewing hole, with a smooth probe (left image), and a rough probe (right image).

2.2.1. Lighting stimuli

Two groups of images were used to simulate the light sources on the scene and probe, as depicted in Figure 2.3. The first group of stimuli was made to simulate intensity variations (group I) and a second group of stimuli was made to simulate variations in direction and diffuseness (group II).

In stimulus group I, we investigated whether human beings are sensitive to variations in lighting intensity over a scene. The lighting intensity variations were achieved by varying the pixel value of an image consisting of a white disk in the center of the LCD screen. The diameter of the white disk was L/3 (L=25 cm, which was the width of the cube's top window). Three levels of intensity were used, marked as I_1, I_2 and I_3 (with $I_1 > I_2 > I_3$) . For each level of intensity, we selected pixel values such that the "simulated luminance" of screen B and screen C were the same, as given in Table 2.1. It has long been known that the HVS has a nonlinear response to luminance. This nonlinearity can be quantified using the concept of JND (Just Noticeable Difference), which represents the luminance difference between two patches that the average human observer can just perceive under given viewing conditions. Following the definition, the difference between two luminance levels on the perceptual scale is proportional to the number of JNDs between them [30]. Based on the Barten model [3, 4], Rosslyn et al. [2] developed a Grayscale Standard Display Function which describes the relationship between luminance and Just-Noticeable Differences. When selecting three intensity levels, we made sure that the difference in luminance between I_1 and I_2, and between I_2 and I_3 had the same number of JNDs. The I_1 and I_3 were selected such that the difference when I_1 illuminated the scene and I_3 illuminated the probe, or vice versa, was obvious (based on a pilot experiment with 7 observers). The difference in luminance between I_1 and I_2, and between I_2 and I_3 were 60 JNDs.

In stimulus group II, we varied the position and the size of the disk to investigate whether human beings are sensitive to the average direction as defined by the light vector [8, 16, 17] and to the diffuseness as defined by the scale of light of a light source [7]. We displayed white disks with a diameter of L/3 in the center and in two opposite corners of the screen to vary the direction, and displayed white disks with diameters L/3, 2L/3 and L to investigate the sensitivity to diffuseness. The simulated luminance for screen B and screen C was set to their maximum of 77 cd/m^2, corresponding to I_1. As we needed to

keep the total emitted luminous flux for the three diameters of the white disk the same, we used the same number of white pixels as for L/3, but randomly distributed them over the disk when its diameter was larger than L/3. This created a noise pattern in the LCD image mimicking the light source (as shown in Figure 2.3), but didn't impact the light on the probe or scene objects. We also varied the position of the disk for the diameters L/3 and 2L/3 to investigate the interaction between direction and diffuseness. We refer to the stimuli in Group II by D_1 to D_7.
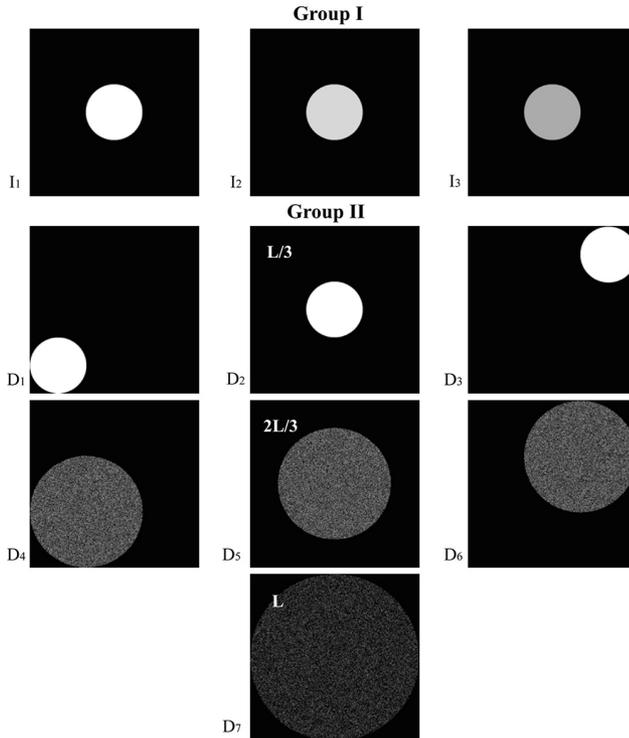
Figure 2.3: Lighting stimuli: Group I, variations in intensity which were achieved by changing the pixel values of the image of a disk (diameter of L/3, L=25 cm) in the center of the LCD screen; Group II, variations in direction and diffuseness which were achieved by changing the position and the size of the displayed white disks. The disks were displayed in the center and in two opposite corners and had a diameter of L/3, 2L/3 and L (L=25cm).

2.2.2. Probe

This experiment was performed with two different probe objects, i.e., a smooth sphere and a golf ball (see Figure 2.2), in order to check whether human beings are sensitive to illuminance flow over a rough probe. The dimples on the golf ball resulted in 3D texture contrast gradients over the ball, which generated "illuminance flow" and provided cues additional to the shading.

Table 2.1: Pixel values, simulated luminance values and their corresponding JND levels for three levels of intensity.

	I_1	I_2	I_3
Pixel values of screen B	255	135	85
Pixel values of screen C	156	103	68
Simulated luminance (cd/m^2)	77	47	28
JND values	441	381	321

2.2.3. Task

The task of the observer was to judge whether the white probe fitted the scene with regard to its lighting. If the observer thought the lighting of the scene and probe was the same, they had to press "Yes" on the keyboard. Otherwise, they had to press "No". After they had given their answer, they had to press "confirm" to proceed to the next trial. As illustrated in Figure 2.3, stimulus group I consisted of 3 lighting conditions, and so, resulted in 9 combinations for scene and probe. Stimulus group II consisted of 7 lighting conditions, and so, resulted in 49 combinations for scene and probe. So, among the total of 58 combinations, 48 had different lighting settings for scene and probe and 10 had the same lighting settings for scene and probe. We repeated the 10 "same combinations" for 3 times to improve the balance between the number of same and different combinations, resulting in a total of 78 comparisons to be made for one probe. As we used two probes, this resulted in 156 trials in total. Before the formal experiment started, all participants were asked to do a few practice trials to become familiar with the procedure. The whole experiment was divided into two sessions, where a different type of probe was evaluated in each session. Since only one type of scene layout was used, there could be learning effects. In order to minimize the effects on the outcome, all stimuli were randomly given within each session and the order of the two sessions was balanced across participants. Between the first and second session, the observers took a break. The whole experiment took about half an hour for each participant.

2.2.4. Participants

Twenty observers participated in this experiment, 11 females and 9 males, two of whom were the first and second author. Observers ranged in age from 24 to 43 and the median age was 30. The participants were naive with respect to the setup of this experiment except for the two authors. All participants had normal or corrected-to-normal vision. They all gave written, informed consent. All experiments were done in agreement with local ethical guidelines, Dutch Law and the Declaration of Helsinki.

2.3. Results

This results section is organized as follows: firstly, we analyze the overall percentages of correct answers; after that we use the data of Group I to investigate how sensitive our

Table 2.2: Percentages of correct answers split up for stimuli with the same lighting setting on scene and probe and stimuli with different lighting setting on scene and probe (N = total number of answers, Percentage = percentage of correct answers)

Stimuli	Type of probe	Stimuli with same lighting		Stimuli with different lighting	
		N	Percentage	N	Percentage
Group I	Smooth	180	77%	120	66%
	Rough	180	73%	120	67%
Group II	Smooth	420	80%	840	61%
	Rough	420	78%	840	65%

observers are to variations in lighting intensity; then the data of Group II are used to check how sensitive they are to the variations of lighting direction and diffuseness. For all statistical tests applied below, we measured the significance at the 0.05 level.

When examining the overall percentages of correct answers, we distinguish two options: for the stimuli with the same lighting on probe and scene, "Yes" was the correct answer, while for the stimuli with different settings, "No" was the correct answer. Consequently, we split the data into two categories, one category "stimuli with same lighting" and another category "stimuli with different lighting". The percentages of correct answers are given in Table 2.2. We used one-sample binomial tests to check whether these percentages were significantly different from 50%. The results showed that they all were significantly different from chance level.

Before we go into a more detailed analysis, we introduce the phenomenon of the "swap effect". For some combinations of the scene and probe lighting, participants judged the probe to fit the scene well, yet swapping the lighting over the probe with that over the scene dramatically shifted participants' judgments. One example is given in Figure 2.4, where the optical mixture of a lower intensity I_3 on the probe and a higher intensity I_2 on the scene (Figure 2.4(a)) looks as a good fit between probe and scene (only 35% of the observers recognized a mismatch between probe and scene), while the optical mixture of a higher intensity I_2 on the probe and a lower intensity I_3 on the scene (Figure 2.4(b)) does not look as a good fit between probe and scene (indeed 75% of the observers recognized the mismatch in illumination on probe and scene). Because of this asymmetry, we take this "swap effect" into consideration in the rest of our analysis. To quantify the combinations of lighting on probe and scene as susceptible to the "swap effect", we used the Pearson's Chi-square test on the percentages of correct answers for the combinations of mirrored lighting on probe and scene. The lighting combinations that resulted in a significant difference are marked with a red solid frame in the matrix graphs of Figure 5, Figure 6, Figure 8 and Figure 10.

2.3.1. Group I results: intensity sensitivity

The percentages of correct answers to compare lighting intensity on probe and scene are visualized in Figure 2.5 for each possible combination. The gray level indicates the percentage of correct answers, where black means that 0% of answers is correct. One-

(a)   (b)

Figure 2.4: "Swap effect" for lighting settings with different intensity: (a) lower intensity on the probe and higher intensity on the scene (percentage of correct answers: 35%), (b) lower intensity on the scene and higher intensity on the probe (percentage of correct answers: 75%)

sample binomial tests were performed to check whether the percentage of right answers was significantly different from chance. Cells in the matrix graph of Figure 2.5 for which this was the case are marked with red "∗".

Figure 2.5: Matrix graphs representing the percentages of correct answers for stimulus group I. The columns represent the intensity level on the probe, while the rows represent the intensity level on the scene. The gray level indicates the percentage of right answers. Black means that 0% of the answers was correct. For the cells marked with a red "∗", the proportion of correct answers was significantly different from 50%, according to the result of a one-sample binomial test. The paired cells marked with a red solid frame show where the swap effect occurred according to a Pearson's Chi-square test. The left graph represents the data for the smooth probe and the right graph the data for the rough probe.

We noticed that the data in Figure 2.5 are not symmetrical with respect to the black dashed diagonal (from upper left to bottom right), which is due to the "swap effect". The lighting combinations where the "swap effect" occurred are marked with a red solid frame. The cells in the upper right represent lighting with lower intensity on the probe than on the scene (see Figure 2.4(a)). The cells in the bottom left represent lower intensity on the scene than on the probe (see Figure 2.4(b)). The combination "$I_1 \sim I_3$" had the largest difference in intensity (120 JNDs), and the observers were quite sensitive to

Table 2.3: Results of a binary logistic analysis for the effect of probe type, "swap effect" and intensity difference on the percentage correct answers.

Source	Wald Chi-square	df	P
Probe type	0.059	1	0.808
Swap effect	6.826	1	0.009
Intensity difference	18.994	2	<0.001
Probe type * intensity difference	0.024	2	0.988
Swap effect * intensity difference	7.426	2	0.024

it with more than 85% of correct answers. For the combinations "$I_1 \sim I_2$" and "$I_2 \sim I_3$", the difference in intensity was much smaller (60 JNDs), but still rather well perceived if the lower intensity illuminated the scene and the higher intensity illuminated the probe (except for the combination "$I_1 \sim I_2$" for the smooth probe). However, when the lower intensity illuminated the probe and the higher intensity illuminated the scene, the observers had difficulties seeing the mismatch (the percentage of correct answers was not significantly different from the chance level).

We employed a binary logistic analysis of the generalized linear model to analyze the probability that the observers could see the difference in lighting intensity between probe and scene. Only the combinations with different intensity levels of lighting for scene and probe were included in this analysis. The predictable variables were the type of probe, the "swap effect" and the difference in intensity level. The "swap effect" included two cases: (1) lower intensity on the probe than on the scene, and (2) lower intensity on the scene than on the probe. Two-way interactions between probe type and intensity difference and between the "swap effect" and intensity difference were also included. The results are given in Table 2.3. There was no significant difference in percentage of correct answers between the smooth and rough probe. Also the interaction between probe type and intensity difference was not significant. The influence of the "swap effect" and intensity were both statistically significant ($p<0.05$), as well as their interaction. The latter is consistent with what we described before: people are sensitive to a small difference in intensity only when the scene is illuminated by the lower intensity and the probe by the higher intensity, but this "swap effect" disappears when the intensity difference is large enough.

2.3.2. Group II results: direction and diffuseness sensitivity

To give an overview of the data, the percentages of correct answers for different combinations of direction and diffuseness are visualized as matrix graphs in Figure 2.6. Again, the gray level in the cell represents the percentage of correct answers, where black means that 0% of the answers was correct. In Figure 2.6, it can be seen that the global patterns for the performance as a function of lighting direction and diffuseness are quite robust. In both graphs, the grey levels are not symmetrically distributed with respect to the diagonal (from upper left to bottom right) due to the "swap effect". Where it occurs, the corresponding cells are marked with a red solid frame.
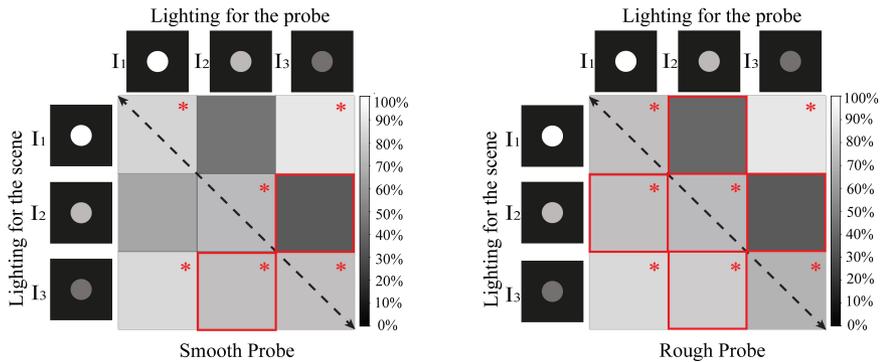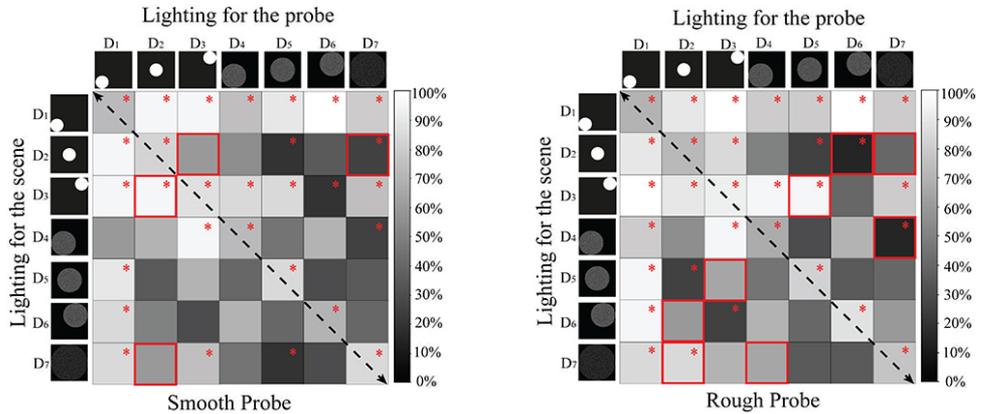
Figure 2.6: Matrix graphs representing the percentages of correct answers for stimulus group II. The columns represent the lighting setting on the probe, while the rows represent the lighting settings on the scene. The gray level indicates the percentage of correct answers. Black means that 0% of the answers was correct. For the cells marked with a red "∗", the proportion of correct answers was significantly different from 50%, according to the result of a one-sample binomial test. The paired cells marked with a red solid frame show where the swap effect occurred according to a Pearson's Chi-square test. The left graph shows the data for the smooth probe and the right graph the data for the rough probe.

For further analysis, Figure 2.7 illustrates the percentages of correct answers for lighting with different directions or different diffuseness or both, for the smooth probe and the rough probe respectively. We did not consider the "swap effect" in Figure 2.7 because the "swap effect" for directions differs from that for diffuseness. Later, we will discuss the "swap effect" for direction and diffuseness separately. The bars labeled as "same-direction" represent cases with the same direction on the probe and the scene. Since only the data for combinations with different lighting settings for scene and probe were considered here, the bar labeled as "same-direction" was absent from the diffuseness combination of "same-diffuseness" in Figure 2.7. Likewise, because the display disk with the largest diffuseness L could only be located in the center, the bars labeled as "$near \sim farther$", which represent direction variation from the near corner to far corner, were absent from the diffuseness combinations "$2L/3 \sim L$" and "$L/3 \sim L$". One-sample binomial tests were conducted to evaluate to what extent the percentages correct answers differed from a chance level of 50%. If the latter was the case, the corresponding bar in Figure 7 is marked with a red "∗". If the percentage was significantly lower than the chance level, it indicated that the observers consistently saw the lighting on the scene and probe to fit. If the percentage was significantly higher than the chance level, it implied that the observers had no difficulty to perceive the mismatch in lighting on scene and probe.

Again we used a binary logistic analysis of a generalized linear model to analyze the probability that the observers could see the mismatch in lighting for the probe and the scene. The predictable variables were the type of probe, the difference in direction and
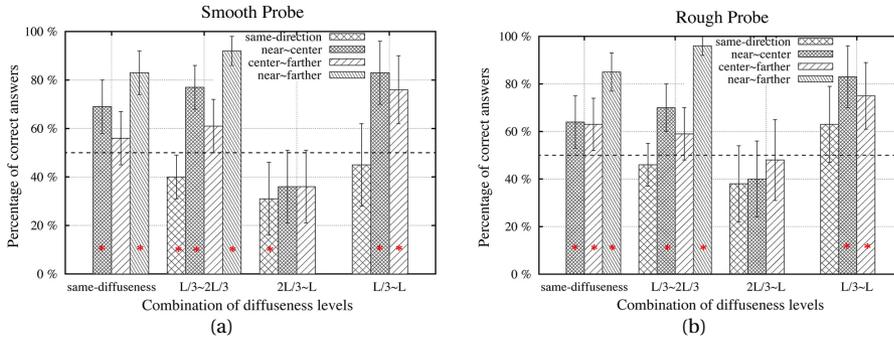
Figure 2.7: Percentages of correct answers as a function of the difference in diffuseness for different pairs of directions. The left graph represents the data for the smooth probe and the right graph for the rough probe. The bars marked with red "∗" had a percentage of correct answers significantly different from 50%. Error bars show the 95% confidence interval

the difference in diffuseness. All two-way interactions were included. Since the "swap effect" for direction and diffuseness was different and will be discussed separately later, we did not introduce the "swap effect" into this analysis. The results in Table 2.4 reveal that the influence of probe type was statistically significant (P<0.05). Thus, as we expected, the probe type did have an effect on the detection of combined direction and diffuseness differences while it had no effect on the detection of intensity differences. Overall the percentage of correct answers was higher for the rough probe than for the smooth probe. The effects of differences in direction and in diffuseness were both highly significant. The first set of bars in Figure 2.7 (i.e., differences in direction for the same diffuseness) illustrates that as the difference in direction increased, more and more people could see that the directions did not fit. Generally, as the difference in diffuseness became larger (i.e., illustrated by the same type of bars in different sets in Figure 2.7), more of the observers could detect the mismatch. The percentage of correct answers was especially low for the combination "$2L/3 \sim L$". We also found a significant interaction between direction and diffuseness differences. These results were in agreement with what Figure 2.7 showed. In general, observers were very sensitive to differences in lighting direction, but this sensitivity was affected by the lighting diffuseness. When the diffuseness was relatively large, but different for probe and scene (i.e., for the combination $2L/3 \sim L$), most of the observers tended to be uncertain whether the scene and probe fit each other (since both in Figure 2.7(a) for the smooth probe and in Figure 2.7(b) for the rough probe most of the bars were not significantly different from chance level).

2.3.3. Swap effect

The influence of the "swap effect" for direction and diffuseness was analyzed separately to investigate what happened when the lighting with only different directions or only different diffuseness was swapped between probe and scene. We selected the data with only one kind of difference either in direction or in diffuseness, to avoid mutual impact.

2

Table 2.4: Results of a binary logistic analysis for sensitivity to differences in lighting direction and diffuseness, including the effect of probe type

Source	Wald Chi-square	df	P
Probe type	3.963	1	0.047
Direction difference	103.719	3	0.001
Diffuseness difference	60.926	3	0.001
Direction difference * diffuseness difference	14.166	6	0.028
Probe type * direction difference	4.258	3	0.235
Probe type * diffuseness difference	1.957	3	0.581

The "swap effect" for direction included two conditions: (1) farther lighting on the probe and closer on the scene, and (2) farther lighting on the scene and closer on the probe. Similarly, the "swap effect" for diffuseness included also two conditions: (1) larger diffuseness on the probe and smaller on the scene, and (2) larger diffuseness on the scene and smaller on the probe.

For lighting settings with different directions but same diffuseness, both stimuli with diffuseness of L/3 and 2L/3 were selected as shown in Figure 2.8. The cells right above the black dashed diagonal (from upper left to bottom right) in the matrix graph represent farther lighting on the probe than on the scene, while the cells left below the diagonal represent farther lighting on the scene than on the probe.

Generally speaking, both graphs in Figure 2.8 were symmetrically mirrored with respect to the black dashed diagonal except for the combination $D_2 - D_3$ when a smooth probe was used (as marked with a red solid frame in Figure 2.8 left graph). The result of a binomial test showed that when D_3 was on the probe and D_2 on the scene (as illustrated in the left image of Figure 2.9), the observers were just guessing whether both lighting conditions fitted. However, when D_3 and D_2 were swapped (as illustrated in the right image of Figure 2.9), the observers were quite sure that the light on the probe did not fit the light on the scene. We have no specific explanation for this observation, but just noticed (as can be seen from Figure 2.9) that the mixed scene looked more disharmonious with a brighter illumination on the probe when the center lighting was on the probe and the far lighting on the scene. A binary logistic analysis of a generalized linear model was performed using the probe type, the "swap effect", the difference in direction as well as their two-way interactions as predictor variables. However, the result showed that the "swap effect" did not statistically significantly influence observers' awareness of the mismatches the probe and scene ($Chi^2 = 1.179, p = 0.278$).

For lighting settings with different diffuseness but same direction on scene and probe, stimuli in the center, in the near left corner and in the far right corner were selected as shown in Figure 2.10. In each group of cells the ones right above the black dashed diagonal (from upper left to bottom right) have a higher diffuseness on the probe than on the scene, while the ones left below the black dashed diagonal have higher diffuseness on the scene than on the probe. In general, each group of cells is pretty well mirrored with respect to its diagonal, suggesting that the "swap effect" was small, except for the combination $D_2 - D_7$. Again, a binary logistic analysis of a generalized linear model was
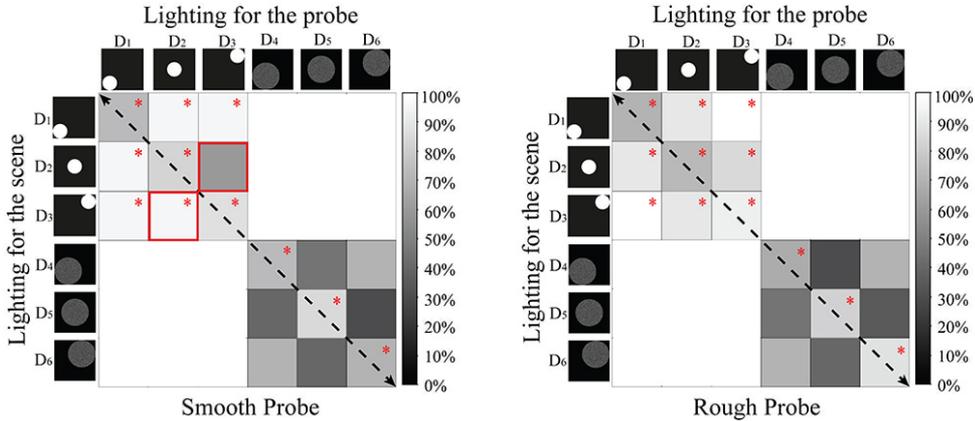
Figure 2.8: Matrix graphs representing the percentages of correct answers for combinations of different directions but same diffuseness on the probe and the scene. The columns represent the lighting condition on the probe, while the rows represent the lighting condition on the scene. The gray level in each cell indicates the percentage of correct answers. Black means that 0% of the answers was correct. The cells marked with red "$*$" indicate that the proportion of correct answers for this combination of lighting on probe and scene was significantly different from 50%. The paired cells marked with a red solid frame show where the swap effect occurred according to a Pearson's Chi-square test. The left graph represents the data for the smooth probe and the right graph for the rough probe.

performed, using the probe type, "swap effect" and difference in diffuseness as main predictor variables, including their two-way interactions. We did not find a significant main effect of the "swap effect" ($Chi^2 = 2.991, p = 0.084$), but we did find a significant interaction between "swap effect" and "difference in diffuseness" ($Chi^2 = 12.432, p = 0.002$). The latter was already suggested by our observations in Figure 2.10. With small "difference in diffuseness" between the probe and scene ($L/3 \sim 2L/3 : D_2 - D_5, D_1 - D_4, D_3 - D_6; 2L/3 \sim L : D_5 - D_7$), observers often had difficulties to see the mismatch in illumination diffuseness and there was no significant "swap effect". However, when the "difference in diffuseness" was relatively large ($L/3 \sim L : D_2 - D_7$), the "swap effect" was significant. In the latter case, the percentage of correct answers was higher when the lighting on the scene was more diffuse than on the probe, while the percentage of correct answers was much lower when the lighting on the probe was more diffuse than on the scene.

2.4. Discussion

We have used a novel experimental setup to investigate human sensitivity for lighting intensity, direction and diffuseness in real scenes. One advantage of this setup is that it allows us to introduce a real probe object into a real scene while the lighting of the scene and the probe can be varied separately without any mutual interference. Furthermore, the task to judge the visual "fit" of the illuminated probe in a scene allows us to obtain a

2

(a)   (b)
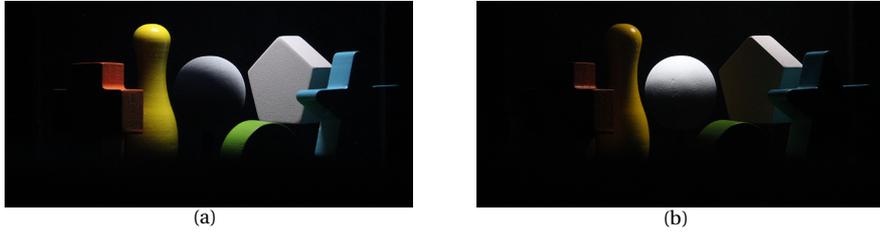
Figure 2.9: Optical mixture of scene with center lighting (D_2) and right far lighting (D_3): The left image represents center lighting on the scene and right far lighting on the probe; The right image represents center lighting on the probe and right far lighting on the scene
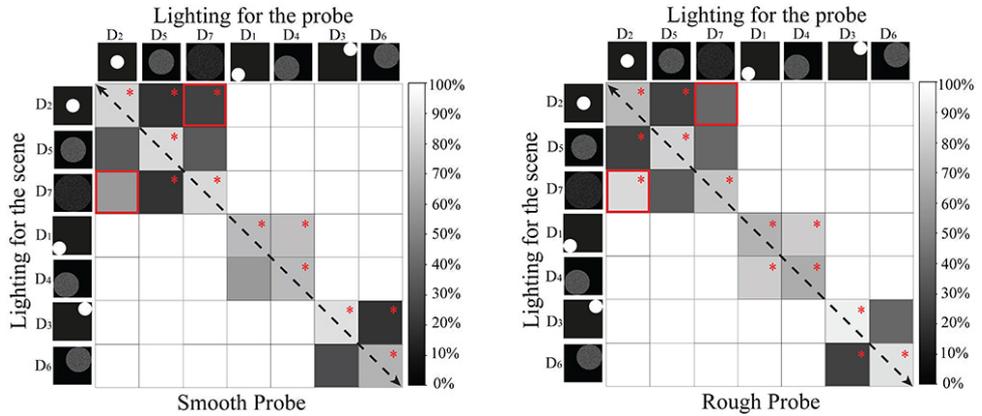
Figure 2.10: Matrix graphs representing the percentages of correct answers for combinations of different diffuseness but the same direction on the probe and the scene. The columns represent the lighting condition on the probe, while the rows represent the lighting condition on the scene. The gray level in each cell indicates the percentage of correct answers. Black means that 0% of the answers was correct. The cells marked with red "∗" indicate that the proportion of correct answers for this combination of lighting on probe and scene was significantly different from 50%. The paired cells marked with a red solid frame show where the swap effect occurred according to a Pearson's Chi-square test. The left graph represents the data for the smooth probe and the right graph for the rough probe.

direct operational measure, which quantifies what the observer sees with a purely visual "yardstick" [9, 11]. During the experiment, observers had little trouble with the task and none of them doubted that the probe and scene were actually not located in the same box.

Where previous studies [11, 12, 25] asked participants to adjust the lighting on the (virtual) probe such that it fitted into the (virtual) scene, we here simplified the task by asking observers only to indicate (with "yes" or "no") whether the lighting of the probe fitted the scene. We repeated the stimuli with the same lighting on probe and scene three times each, so that the number of same combinations was 60, and the number of

different combinations was 96 (see also section 2). Table 2.2, however, shows that the number of "yes" and "no" responses was balanced. Indeed, for stimuli with the same lighting conditions (N=60) participants on average had 78% correct answers (and so, on average 47 "yes" and 13 "no" responses), whereas for stimuli with different lighting conditions (N=96) participants on average had 63% correct answers (and so, on average 36 "yes" and 60 "no" responses). So, the sum of the "yes" responses and "no" responses was much more balanced than what could be expected from the number of stimuli with the same or different lighting conditions. We don't think that this tendency of balancing the "yes" and "no" responses has influenced our findings, since it in principle affected all stimuli in a similar way.

We found that the observers were sensitive to variations of the light intensity, direction and diffuseness, which confirmed the results of former studies. A study conducted by Pont et al. found that observers were able to match the direction and diffuseness of a light field [25]. The visual light field study by Koenderink et al. certified observers' ability on estimating the direction and diffuseness in natural scenes and found that the observers were also sensitive to the variations in light field intensity [11]. While their studies were all performed based on the use of images on computer screens, this study was conducted in real scenes. Hence, this study confirmed that observers' sensitivity to intensity, direction and diffuseness of the light field also holds for real scenes. As expected, we found that as the difference in intensity, direction and diffuseness increased, the observers were better aware of the mismatches between the scene and probe. Since the methods used in the former studies (adjustment to create visual fit) and in the current study (yes/no to visual fit) are so different, it is not possible to compare the results in terms of sensitivity.

It should be noted that the current study only used one particular, relatively simple real scene to demonstrate the measurement of the visual light field in a real scene. As participants assessed 156 stimuli with this particular scene, we cannot exclude a learning or adaptation effect to this scene. However, all stimuli in the experiment were provided to each participant in a different random order, and so, possible learning/adaptation to the stimuli is not expected to affect our findings. Obviously, more scenes need to be investigated to evaluate the generalizability of our findings to other scenes. We do expect that also in other real scenes people will be sensitive to the intensity, direction and diffuseness of the light field, though possibly with different sensitivity.

We discovered in some cases a "swap effect", which means that whether the mismatch in lighting between probe and scene was visible dependent on which of the two lighting conditions was on the scene and which on the probe. We listed the optical mixtures for all the cases where the "swap effect" occurred in Figure 2.11. For lighting conditions differing in intensity and diffuseness, the "swap effect" occurred with both the smooth probe and rough probe. The "swap effect" for one of the combinations of different directions of the lighting only occurred with the smooth probe.

To investigate why the "swap effect" happened, we examined all optical mixtures for which it happened in Figure 2.11. The observers were significantly more aware of the mismatch between scene and probe for the conditions in the left column than for those in the right column according to the percentage of correct answers (PoCA). We noticed that the probes in the left column seemed to be brighter with respect to their

2

Figure 2.11: Optical mixtures of scene and probe for all the cases where the "swap effect" occurred. The lighting on the probe was marked as "P" (i.e. P: I_2 means the probe was illuminated with intensity I_2) and the lighting on the scene was marked as "S". "PoCA" represents the percentage of correct answers. The higher the PoCA is, the more observers were aware of the "mismatch in lighting between scene and probe"

surrounding scene than in the right column. Therefore we calculated the ratios be-
tween the average luminance of the probe and the average luminance of the scene ($R = Lum\_probe/Lum\_scene$) for the images of the optical mixtures in both the left and right
columns, see Figure 2.12. Since we took the photographs using the same setting of the
camera, the average luminance could be estimated via the average pixel luminance. To
exclude the dark areas and noise in the photographs, only the pixels whose luminance
was larger than 0.1 were considered. Figure 2.12 shows that the luminance of the probe
with respect to the scene was indeed higher for all the optical mixtures in the left col-
umn. These results indicate that indeed the observers might have judged the mixes in
the right column as a better fit because the average luminance of the visible parts of
the probe were closer to the average luminance of the visible parts of the scene objects
whereas in the left column the probe is clearly much higher in luminance.
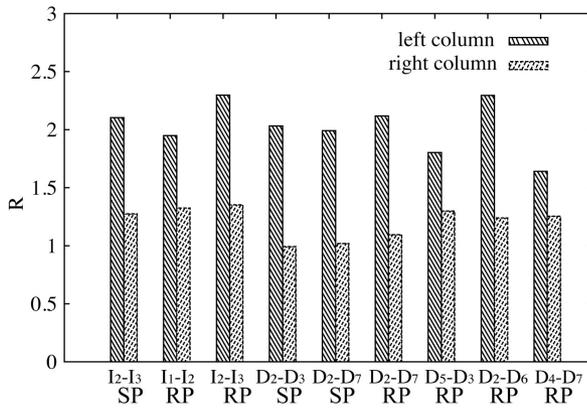
Figure 2.12: The ratio between the average luminance of the probe and the average luminance of
the scene ($R = Lum\_probe/Lum\_scene$) for all the lighting combinations where the "swap effect"
occurred. The bars labelled as "left column" and "right column" represent the optical mixtures in
the left column and right column of Figure 2.11 respectively. The label SP represents results for the
smooth probe and RP for the rough probe.

In our experiment, the mean illuminance over the probe decreased as the diffuseness
increased. Figure 2.13 illustrates the illumination over the probe under three diffuseness
levels: from left to right, the diameter of the disk changes from L/3 (8 cm) to 2L/3 (16
cm) and L (25 cm), and the corresponding scale of light is 24%, 43% and 59% according
to the definition by Frandsen [7]; so, the mean illuminance over the probe decreases by
a factor of 92% and 83% in the middle and right image in comparison to the left image.
This observation triggered another question, namely whether the observers detected the
difference of diffuseness by just comparing the mean illumination on the probe and the
scene. If so, they would have difficulties in judging where the inhomogeneity originated
from: from the difference in intensity or from the difference in diffuseness, not to men-
tion estimating the diffuseness and intensity simultaneously. Therefore, our next study
will focus on whether observers can simultaneously match the intensity, direction and
diffuseness in real scenes.
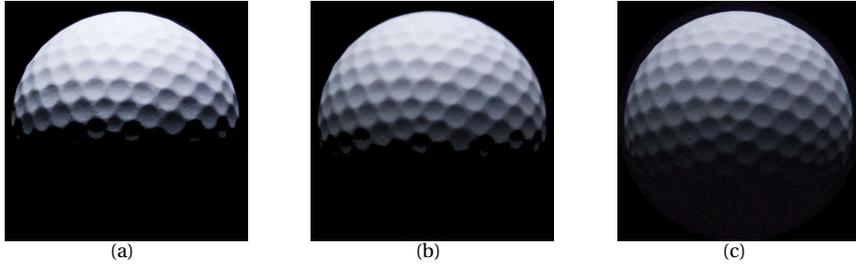
Figure 2.13: The illumination over the probe under different levels of diffuseness, the diameter of the disk being L/3 (8 cm) in the left image, 2L/3 (16 cm) in the middle image and L (24 cm) in the right image.

Finally, our findings show that the use of a rough probe did not help the observers to detect the mismatch in intensity of the lighting between the scene and probe, but it helped them to find the mismatch in the combination of lighting direction and diffuseness between scene and probe. This proved our expectation that for real 3D objects, human observers can use the illuminance flow to judge illumination properties. In computational vision, the illuminance flow is derived from the roughness on the mesoscale. The variation of illuminance on the macroscale is usually denoted as "shading" and the variation of illuminance on the mesoscale as "3D texture" [23]. In theory, the illuminance flow generated by 3D texture gradients can give additional cues about the illumination to the "shading" [10]. This theory was confirmed for flat surfaces by asking subjects to adjust the elevation and azimuth of a probe for a series of pictures of natural textures [13]. In our experiment, the illuminance flow or texture contrast gradients over the rough probe give information about the direction and diffuseness. However, it doesn't give information about the intensity because the texture gradient structure is invariant for intensity changes. So, as expected, the 3D texture on the rough probe did not improve judgments of the mismatches in lighting intensity, but it did for diffuseness and direction. To our knowledge this is the first systematic study proving that observers use the illuminance flow over 3D objects to judge specific illumination characteristics.

2.5. Conclusions

In summary, we implemented a novel experimental setup to investigate human sensitivity to low-order properties of light fields in real scenes, namely the intensity, direction and diffuseness. We found that observers are able to detect whether a probe fits a scene with respect to these light qualities. However, in some cases with different lighting on the probe and scene, the awareness of the mismatch depended on which lighting condition was on the scene and which on the probe, which we called the "swap effect". For these cases we found that observers judged the fit to be better if the average luminance of the visible parts of the probe were closer to the average luminance of the visible parts of the scene objects. Finally, adding roughness to the spherical probe improved judgments of

the mismatch in direction and the diffuseness of the lighting, showing that human observers use illuminance flow as a cue to the light.

References

[1] Edward H Adelson and James R Bergen. The plenoptic function and the elements of early vision, chapter 1, 1991.

[2] National Electrical Manufacturers Association, American College of Radiology, et al. *Digital imaging and communications in medicine (DICOM)*. National Electrical Manufacturers Association, 1998.

[3] Peter GJ Barten. Physical model for the contrast sensitivity of the human eye. In *SPIE/IS&T 1992 Symposium on Electronic Imaging: Science and Technology*, pages 57–72. International Society for Optics and Photonics, 1992.

[4] Peter GJ Barten. Spatiotemporal model for the contrast sensitivity of the human eye and its temporal aspects. In *IS&T/SPIE's Symposium on Electronic Imaging: Science and Technology*, pages 2–14. International Society for Optics and Photonics, 1993.

[5] Christopher Cuttle. *Lighting by design*. Routledge, Oxford: Architectural Press, 2008.

[6] Steven H Ferris. Motion parallax and absolute distance. *Journal of experimental psychology*, 95(2):258, 1972.

[7] Sophus Frandsen. The scale of light–a new concept and its application. In *Paper on 2nd European Conference on Architecture*, pages 4– 8, 1989.

[8] Andreī Gershun. The light field (translated by moon, parry hiram and timoshenko, gregory). *Journal of Mathematics and Physics*, 18(1):51–151, 1939.

[9] J. J. Koenderink and A. J. van Doorn. *Painting to Marble*. The Clootcrans Press, 2012.

[10] Jan J Koenderink and Sylvia C Pont. Irradiation direction from texture. *JOSA A*, 20(10):1875–1882, 2003.

[11] Jan J Koenderink, Sylvia C Pont, Andrea J van Doorn, Astrid ML Kappers, and James T Todd. The visual light field. *PERCEPTION-LONDON-*, 36(11):1595, 2007.

[12] Jan J Koenderink, Andrea J van Doorn, Astrid ML Kappers, Sylvia C Pont, and James T Todd. The perception of light fields in empty space. *Journal of Vision*, 5(8):558–558, 2005.

[13] Jan J Koenderink, Andrea J van Doorn, Astrid ML Kappers, Susan F Te Pas, and Sylvia C Pont. Illumination direction from texture shading. *JOSA A*, 20(6):987–995, 2003.

[14] Yaniv Morgenstern. *The role of low-pass natural lighting regularities in human visual perception*. York University, 2011.

[15] Yaniv Morgenstern, Wilson S Geisler, and Richard F Murray. Human vision is attuned to the diffuseness of natural light. *Journal of vision*, 14(9):15, 2014.

[16] Alexander A Mury, Sylvia C Pont, and Jan J Koenderink. Light field constancy within natural scenes. *Applied Optics*, 46(29):7308–7316, 2007.

[17] Alexander Alexeevich Mury. *The light field in natural scenes*. PhD thesis, TU Delft, Delft University of Technology, 2009.

[18] Karol Myszkowski, Rafal Mantiuk, and Grzegorz Krawczyk. High dynamic range video. *Synthesis Lectures on Computer Graphics and Animation*, 1(1):1–158, 2008.

[19] James P O'Shea, Maneesh Agrawala, and Martin S Banks. The influence of shape cues on the perception of lighting direction. *Journal of vision*, 10(12):21, 2010.

[20] Yuri Ostrovsky, Patrick Cavanagh, and Pawan Sinha. Perceiving illumination inconsistencies in scenes. *Perception*, 34(11):1301–1314, 2005.

[21] Alex P Pentland. Finding the illuminant direction. *JOSA*, 72(4):448–455, 1982.

[22] SC Pont, JJ Koenderink, AJ Van Doorn, MWA Wijntjes, and SF Te Pas. Mixing material modes. In *IS&T/SPIE Electronic Imaging*, pages 82910D–82910D. International Society for Optics and Photonics, 2012.

[23] Sylvia Pont and Jan Koenderink. Surface illuminance flow. In *3D Data Processing, Visualization and Transmission, 2004. 3DPVT 2004. Proceedings. 2nd International Symposium on*, pages 2–9. IEEE, 2004.

[24] Sylvia C Pont. Spatial and form-giving qualities of light. *Handbook of Experimental Phenomenology: Visual Perception of Shape, Space and Appearance*, pages 205–222, 2013.

[25] Sylvia C Pont and Jan J Koenderink. Matching illumination of solid objects. *Perception & psychophysics*, 69(3):459–468, 2007.

[26] James A Schirillo. We infer light in space. *Psychonomic bulletin & review*, 20(5):905–915, 2013.

[27] Susan F te Pas and Sylvia C Pont. A comparison of material and illumination discrimination performance for real rough, real smooth and computer generated smooth spheres. In *Proceedings of the 2nd symposium on Applied perception in graphics and visualization*, pages 75–81. ACM, 2005.

[28] DA Wismeijer, CJ Erkelens, Raymond van Ee, and M Wexler. Depth cue combination in spontaneous eye movements. *Journal of vision*, 10(6):25, 2010.

[29] Ling Xia, Sylvia C Pont, and Ingrid Heynderickx. Probing light in real scenes using optical mixtures. In *Proceedings of the ACM Symposium on Applied Perception*, pages 137–137. ACM, 2013.

[30] An Xu, Anindita Saha, Gabriele Guarnieri, Giovanni Ramponi, and Aldo Badano. Display methods for adjustable grayscale and luminance depth. In *Medical Imaging*, pages 69190Q–69190Q. International Society for Optics and Photonics, 2008.

2

3

SUBJECTIVE ADJUSTMENT OF THE LIGHT FIELD PROPERTIES IN REAL SCENES

Abstract

3

Previously, we probed lighting perception in a real scene by asking whether the light on a "probe object" that was optically mixed with a same or differently lighted real scene was the same or different [36]. But how well are observers able to interactively adjust the lighting (i.e., intensity, direction and diffuseness) on a "probe object" to its surrounding real scene? Image ambiguities can result in perceptual interactions between light properties. Such interactions formed a major problem for the "readability" of the illumination direction and diffuseness on a matte smooth spherical probe [21]. We found that light direction and diffuseness judgments using a rough sphere (i.e., a golfball) as probe were slightly more accurate than when using a smooth sphere, due to the 3D texture [36]. We here extended the previous work by testing independent and simultaneous adjustments of light intensity, direction and diffuseness using a rough probe. Independently inferred light intensities were close to the veridical values and the simultaneously inferred light intensity interacted somewhat with the light direction and diffuseness. The independently inferred light directions showed no statistical difference with the simultaneously inferred directions. The observers could coarsely infer the light diffuseness. In summary, observers were able to adjust the basic light properties through both independent and simultaneous adjustments. The light intensity, direction and diffuseness are well "readable" from our rough probe. Our method allows "tuning the light" in interfaces for design or perception research.

3.1. Introduction

Light fields in the real world are highly complex due to the spectral and spatial characteristics of light sources within a scene and the inter-reflections of light between surfaces, generating various shading, shadowing and vignetting effects. Nevertheless, the human visual system (HVS) is sensitive for the intensity, the primary illumination direction, and the diffuseness, which are basic properties of a light field [15, 18, 19, 23, 26, 27]. Light intensity, direction and diffuseness are the first order properties of the light field represented using spherical harmonics [24].

Human observers' awareness of the light field in the empty space of a scene was called the "visual light field" [18]. Many studies into surface colour and lightness perception gave indirect evidence of our awareness of the light field [1, 7–10, 13, 14, 16, 22, 30, 32, 34]. Some studies focused on observers' estimations of single properties of the illumination, with the illumination direction being studied most intensively [17, 19, 23, 27]. The independent adjustment of one lighting property is a method of controlled variable tuning and it influences appearance unilaterally. However, the light intensity, direction and diffuseness can vary simultaneously in real environments and all of them result in appearance changes of the objects inside it. The simultaneous adjustment of lighting properties is much more complicated than the independent adjustment because the tuning has more degrees of freedom.

Koenderink et al. have tested simultaneous estimations of all three basic properties of the light field using displayed images [18]. They found that the "visual light field" could be revealed via people's expectations of how a given object would appear if it was introduced in a displayed scene. We successfully probed this kind of expectation in real scenes by introducing a real gauge object into a real scene using optical mixtures in a novel experimental setup [35, 36]. The results confirmed that observers were sensitive to intensity, direction and diffuseness differences also in real scenes.

However, the influences of these lighting properties on the appearance of a scene or gauge object are in no way "orthogonal" but can interfere with each other due to basic image ambiguities. For example, Pont and Koenderink [29] used artificial Lambertian smooth spheres and images of real rough spherical objects with various surface textures to investigate light direction and diffuseness estimations. They found that illumination direction estimates interacted with illumination diffuseness estimates, because more frontal lighting or more diffuse lighting resulted in quite similar changes in object appearance (i.e., "diffuseness-direction ambiguity"). Madsen and Donn [21] found that this interaction formed a major "readability" problem in applying a smooth matte sphere as a light probe in architectural lighting applications.

In a previous study [36], the use of a golf ball in comparison to a smooth sphere was found to significantly help observers detect mismatches in light direction and diffuseness between the scene and the probe. This improvement was caused by 3D texture gradients that gave information complementary to the shading [28], partly resolving the direction-diffuseness ambiguity. Light intensity discrimination was not improved by the probe roughness, as expected, since the related brightness changes did not influence the 3D texture patterns. However, this study was done using a "fit"/ "no fit" paradigm instead of a method of adjustment. In order to develop our probing method and its in-

terface further, for perception experiments and as a practical tool for lighting designers, it is necessary to know how accurately people are able to adjust the three basic properties of a light field.

In this study, we evaluated observers' abilities to adjust and fit the three basic lighting properties both independently and simultaneously using a rough probe in a real scene. Based on former results, we expect to find that both methods will work well and differ only slightly, because of possible interactions between the simultaneously inferred lighting properties. It will answer whether simultaneous adjustment of all first order lighting properties on a rough light probe is a feasible approach in a lighting interface for lighting design and perception experiments.

3.2. General methods

A novel type of experimental setup was used to optically introduce a real gauge object into a real scene (see Figure 4.1 (a)). The scene was located in cube B and consisted of five colourful geometrical shapes. The probe was a white golf ball put in the centre of cube C. Because a white object has a higher albedo than an object with any other colour, one of the colorful geometrical shapes was painted white to provide an anchor [13]. The scene and probe were optically mixed together by a semitransparent mirror put at 45° with respect to the viewing direction. When the observers looked through the viewing hole, they saw the optical mixture of the scene and probe as if they were put together (see Figure 4.1 (b)). The lighting on the scene and the probe was provided by an LCD screen on top of cube B and cube C, respectively (hereafter referred to screen B and screen C). Independent images were displayed on the two screens to provide independent lighting on the scene and on the probe. The inner width of the cubes was 25 cm and the top of cube B and C was covered by a 930 pixels×930 pixels square area on the LCD screens. We refer to [35, 36] for more information on the experimental setup.

The intensity variation was achieved by varying the pixel value of a disk displayed on the LCD screen. The average light direction, defined by the light vector [12, 24] with respect to the probe, was varied by displaying a disk at different positions on the LCD screen. The light diffuseness as defined by the scale of light [11], which is derived from the comparison between the size of a light source and that of an illuminated object, was varied by changing the size of the disk on the screen. To keep the total emitted luminous flux constant for the same intensity level when changing this size, we started from the number of pixels needed to fill a disk of 6.5 cm diameter, and randomly distributed these pixels over the required (larger) size. So, this created a noise pattern on the LCD image (see Figure 3.7).

The experiments in this study were based on a within-subject design. In the first experiment, the observers were asked to separately estimate the light direction, diffuseness and intensity. After a short break we started the second experiment, in which the observers were asked to simultaneously estimate these properties. The observers spent around 1 hour finishing both experiments.

The experiments were performed in a dark room. The observers looked at the optical mixture of the scene and the probe through the viewing hole. We provided different lighting stimuli on the scene. The task of the observer was to adjust the lighting on the
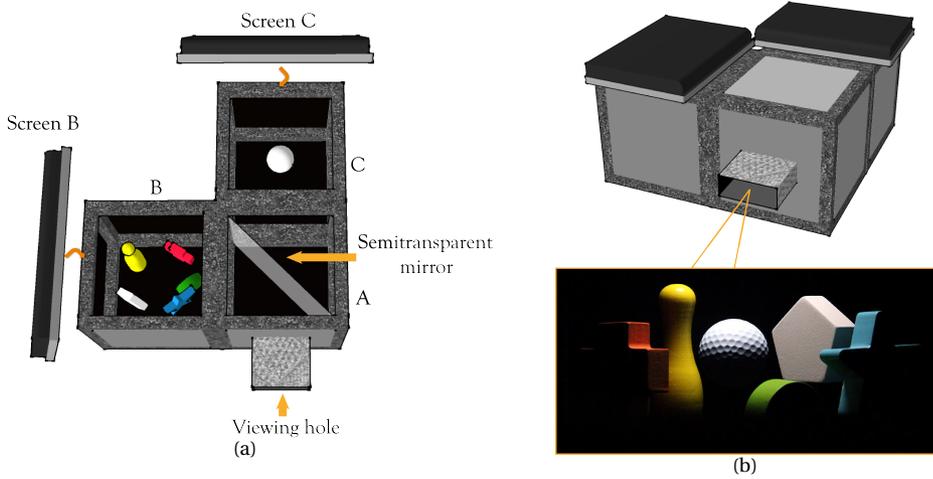
Figure 3.1: Illustration of the setup. (a)The setup consists of three $30cm \times 30cm \times 30cm$ cubes, of which the inside is covered with black velvet paper (the inner width of the cubes was 25cm excluding the width of the frames). In cube B, we made a simple scene with five geometrical shapes. In cube C, we placed a white painted golf ball which served as the probe. A semi-transparent mirror was placed vertically at the diagonal of box A. Two LCD screens covering the top of cube B and cube C provided the lighting which could thus be varied independently for the scene and the probe. (b) The setup and an optical mixture of the scene and the probe photographed through the viewing hole.

probe to fit the scene. The observers used four arrow keys to adjust the light direction, and the up and down arrow keys to increase and decrease the light diffuseness or light intensity. Furthermore, the observers could take small steps or big steps by pressing corresponding keys on the keyboard when performing the adjustment.

Once the big step was selected, each time the key was pressed, the centre of the disk was moved 30 pixels (approximately 0.8 cm) in the selected direction, or the diameter of the disk increased/decreased by 30 pixels, or the pixel value increased/decreased by 10 grey levels depending on the session. Otherwise, if the small step was used, the centre of the disk was moved 10 pixels, the diameter of the disk increased/decreased by 10 pixels, or the pixel value increased/decreased by 3 grey levels. The big steps were selected such that the differences between the lighting effects on the probe were obvious (based on a pilot experiment with 4 observers), and the small steps to generate just noticeable variations of lighting effects. In Experiment 2, the participants first had to decide which lighting property (direction, diffuseness or intensity) they wanted to vary by pressing corresponding keys. If the direction, diffuseness or intensity exceeded a boundary, the computer gave a warning sound.

3.2.1. Participants

Six female observers and nine male observers (two of whom were the first and second author), aged between 20 and 44 years old, participated in this study. The participants were naive with respect to the setup of this experiment except for the two authors. All participants had normal or corrected-to-normal vision. They all gave written, informed consent. All experiments were done in agreement with local ethical guidelines, the Dutch Law and the Declaration of Helsinki, and were approved by the TUDelft Human Research Ethics Committee (HREC).

3.3. Experiment 1: adjusting intensity, direction and diffuseness independently

We first investigated how well observers can adjust and fit the light direction, diffuseness and intensity independently in real scenes. This experiment was divided into three sessions for the three lighting properties and the order of these three sessions was randomized per participant. After each session, the observers were asked to rank the five shapes inside the scene from 1 to 5 according to the information these shapes gave introspectively during the adjustment, with 1 meaning the least information and 5 the most information.

3.3.1. Group I: Sensitivity for independent light intensity adjustment

Lighting stimuli

The stimuli in Group I were designed to investigate how sensitive observers were to variations in light intensity. A disk with diameter D1 (7 cm, 264 pixels) and varying grey value was displayed in the centre of screen B to serve as a light source with different intensity level on the scene. Five levels of intensity were used, marked from I1 to I5 (with I1>I2>I3>I4>I5, see Figure 3.2). Because of the nonlinear response of the HVS to luminance, we adopted a constant difference in the number of JNDs between the adjacent luminance levels, namely 30 JNDs [2, 37]. The pixel values, the luminance values and the JND values for each of the intensity levels are listed in Table 3.1. It should be noted that the different light intensity levels were generated by changing the pixel values on the screen, which were parameterized by luminance values of the sources. Although different terms are used here, they result in the same brightness changes on the object's /scene's appearance.

On the probe side, a disk with the same diameter was displayed in the centre of screen C, whose luminance value was randomly generated between 0 to 89 cd/m^2. The task of the observers was to adjust the intensity of the light source on the probe to fit the scene.

Each stimulus was repeated for 3 times, resulting in $5 \times 3 = 15$ trials for each participant. Since we weren't interested in differences between participants (we nowhere discuss them except shortly in the discussion) and since we didn't distinguish inter- from intra-variance in participants we considered all measurements independently in the sta-

tistical analyses. . The same applies to the data analysis for all the repeated stimuli in this study.

(a) 75.0 cd/m^2 (b) 60.0 cd/m^2 (c) 47.4 cd/m^2 (d) 36.7 cd/m^2 (e) 28.9 cd/m^2
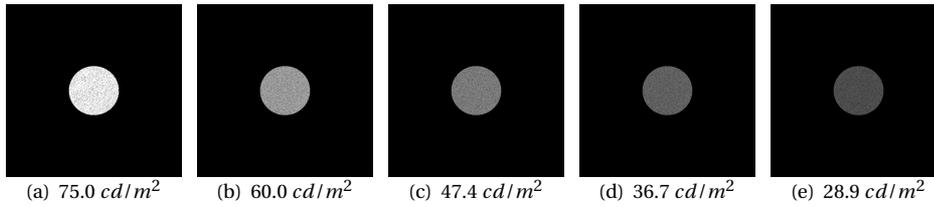
Figure 3.2: Group I stimuli: five intensity levels on the scene were achieved by varying the grey value of a white disk with a diameter of 7cm (264 pixels) located in the centre of screen B.

Table 3.1: The five intensity levels of the light source on the scene that were used in stimuli group I. The pixel values, luminance values and their JND values are listed.

Intensity levels	I1	I2	I3	I4	I5
Pixel value	255	169	135	106	85
Luminance (cd/m^2)	75.0	60.0	47.4	36.7	28.9
JND	441	411	381	351	321

Results

Table 3.1 shows the luminance values of the light source on the scene and the mean of the corresponding adjusted luminance values on the probe. Their relationship is illustrated in Figure 3.3. We noticed that the adjusted luminance on the probe was well in line with the luminance on the scene except for a slight offset.
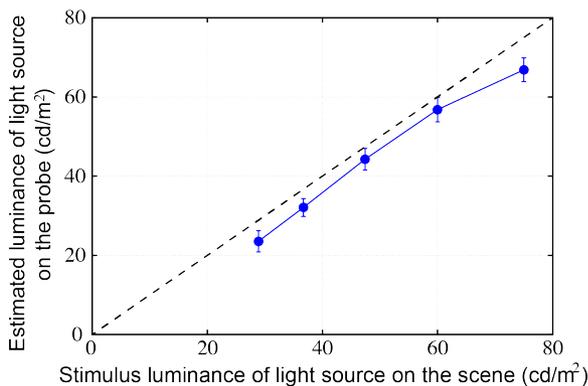
Figure 3.3: Mean of the adjusted luminance on the probe as a function of the luminance on the scene. The error bars show the 95% confidence interval (for N=45 measurements).

A repeated-measures ANOVA showed that the fitted intensity on the probe was significantly affected by the intensity level on the scene ($F(4, 176) = 242.83$, $p < 0.001$). Besides that, the post-hoc test revealed that the fitted intensity for each intensity level from I1 to I5 was statistically significantly different from each other. A simple linear regression resulted in an R^2 of 0.74 with a systematic offset of -2.5 cd/m^2. Thus, observers could quite accurately distinguish all intensity levels we used as stimulus on the scene.

3.3.2. Group II: Sensitivity for independent light direction adjustment

Lighting stimuli

The stimuli in Group II were designed to investigate how sensitive observers were to variations in light direction. A disk was displayed in one of nine different positions on screen B. In this specific setup, the position of the disk is a convenient parameterization of the light direction with respect to the probe. The bird's eye view of these nine positions is depicted in Figure 3.4, including their labels from P1 to P9 and their x and y co-ordinates on the screen. The positions of the disk were selected within a certain distance from the edges of the cube to make sure that there was enough space to adjust the setting of the light direction. On the probe side, a disk was displayed in a random position on screen C. The task of the observer was to adjust the position of the light source on the probe to fit the scene.

Each stimulus was repeated for 3 times, resulting in 9 × 3 = 27 trials for each participant.
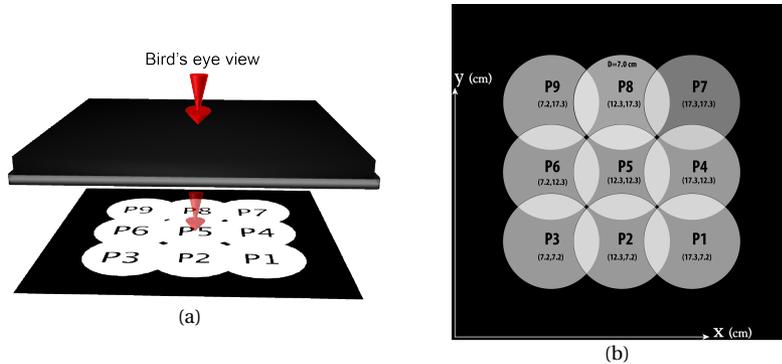
Figure 3.4: (a) illustration of the bird's eye view of Group II stimuli on the scene: variation in direction was achieved by changing the position of a displayed white disk. Nine positions from P1 to P9 were used, as shown in the figure. The diameter of the disk was 264 pixels, and the width of the full window was 930 pixels (25cm). (b) Detailed information of the disk's positions.

Results

Figure 3.5 illustrates the positions of the light source above the scene (white disks) and the estimated positions of the light source above the probe (pink disks). The estimated

positions were averaged across all 15 observers. The error bars on the pink disks show the 95% confidence intervals.
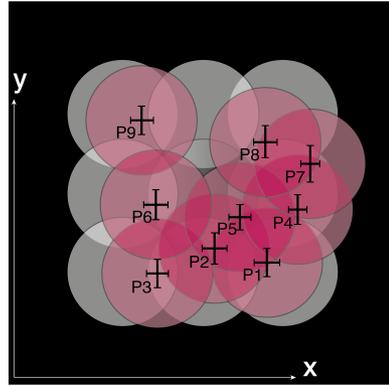
Figure 3.5: The white disks represent the positions of the light source above the scene and the pink disks represent the averaged positions of the light source above the probe, inferred by the observers. The error bars on the pink disks show the 95% confidence intervals (for $N = 45$ measurements).

The position of the light source was converted into its direction with respect to the probe, which is defined by two angles, namely the slant and tilt, as described in Figure 3.6. The slant of the light source is the angle between the viewing direction and the vector from the centre of the probe to the centre of the light source ($\vec{PS}$). The tilt of the light source is the angle between the positive x-axis and the projection of ($\vec{PS}$) on the surface XPZ.

Both the slant and tilt angles for the nine light sources above the scene and for the inferred positions above the probe were calculated, as listed in Table 3.2 and Table 3.3, respectively. The slant of the light source on the scene was approximately 74° for the front row (P1, P2, P3 in Figure 3.4), 90° for the second row (P4, P5, P6) and 106° for the back row (P7, P8, P9). Comparing these values to the inferred slants, we found the biggest difference for P7, namely 10° with a standard deviation of 12°. Similarly, the tilt of the light source was 73° for the right column (P1, P4, P7 in Figure 4), 90° for the middle column (P2, P5, P8) and 107° for the left column (P3, P6, P9). We compared these values to the fitted tilts on the probe and found that the biggest difference was 13° for P8, with a standard deviation of 8°. Furthermore, we found that the standard deviations of the inferred slant angles were slightly larger than those of the inferred tilt angles. The results indicated that, generally, the observers were able to estimate the light direction in our scenes.

We performed a 3 (stimulus row)×3 (stimulus column) repeated-measures ANOVA for the inferred slants and tilts, respectively. For the inferred slants, we found a significant main effect of the stimulus row ($F(2,88) = 166.95, p < 0.001$). The post-hoc test revealed that the inferred slants in the front row were significantly smaller than those in the middle row ($p < 0.001$), and the inferred slants in the middle row were significantly smaller than those in the back row ($p < 0.001$). For the inferred tilts, we found a sig-

3
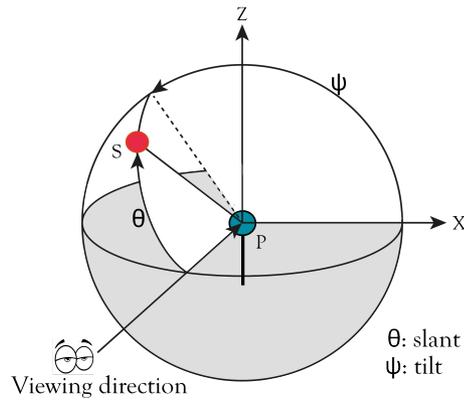
Figure 3.6: Illustration of slant and tilt. The red spot represents the light source and the blue spot the probe. The slant θ is defined as the angle between the viewing direction and the vector from the centre of the probe to the centre of the light source ($\vec{PS}$). The tilt ψ is defined as the angle between the positive x-axis and the projection of ($\vec{PS}$) on the surface XPZ.

Table 3.2: The slant angle of the 9 light sources on the scene and the corresponding mean angle on the probe as inferred by the participants (SD= Standard Deviation).

Slant	P1	P2	P3	P4	P5	P6	P7	P8	P9
Scene	74°	73°	74°	90°	90°	90°	106°	107°	106°
Probe	76°	78°	73°	87°	85°	88°	96°	100°	105°
SD	9.8°	11.3°	9.9°	10.3°	9.2°	10.7°	12.4°	11.2°	9.8°

Table 3.3: The tilt angle of the 9 light sources on the scene and the corresponding mean angle on the probe as inferred by the participants (SD= Standard Deviation).

Slant	P1	P2	P3	P4	P5	P6	P7	P8	P9
Scene	73°	90°	107°	73°	90°	107°	73°	90°	107°
Probe	76°	87°	100°	70°	82°	100°	68°	77°	103°
SD	9.1°	9.2°	7.9°	6.3°	8.1°	8.7°	6.5°	8.4°	8.2°

nificant main effect of the stimulus column ($F(2, 88) = 439.74, p < 0.001$). The post-hoc test showed that the tilts for the right column were significantly smaller than those in the middle column ($p < 0.001$), and the tilts for the middle column were significantly smaller than that in the left column ($p < 0.001$). These results indicate that generally, the observers were able to make a distinction between the slants in different stimulus rows and the tilts in different stimulus columns.

Unexpectedly, we also found a significant effect of the stimulus row on the tilt estimation ($F(2, 88) = 17.83, p < 0.001$). The post-hoc test revealed that the fitted tilts of the front row were significantly larger than those of the middle row ($p = 0.001$) and the back row ($p < 0.001$). Both for the estimation of slant and tilt, a significant interaction between the stimulus row and the stimulus column was found ($slant : F(4, 176) = 7.36, p < 0.001; tilt : F(4, 176) = 10.66, p < 0.001$). This interaction together with the influence of the stimulus row on the tilt estimation were consistent with the observation in Figure 3.5 that the inferred position of the light source on the probe was systematically contracted to the back right corner.

The observers ranked the five shapes inside the scene according to the information they thought these shapes gave (the first and second author did not answer the questionnaire). The bowling pin was ranked 10 times out of the 13 answers as the shape providing the most information for the light direction estimation. This introspective result seems to agree with the measurements; the estimated direction of the light source on the scene was found to be contracted to the back right corner where a white pentagon was located, but not near the bowling pin.

3.3.3. Group III: Sensitivity for independent light diffuseness adjustment

Lighting stimuli

The stimuli in Group III were designed to investigate how sensitive the observers were to variations in light diffuseness. To this end a disk with a diameter of 264 pixels (7.0 cm), 398 pixels (10.5 cm), 532 pixels (14.0 cm), 666 pixels (17.6 cm) or 800 pixels (21.1 cm) (a stepwise increase of 134 pixels) was displayed in the centre of screen B (see Figure 3.7). The five diffuseness levels were labeled from D1 to D5. Frandsen et al. [11] scaled the diffuseness levels in the range from fully collimated to hemispherical diffuseness based on the ratio of the area of the semi-shadow on a sphere to the area of the whole sphere. According to his theory, the corresponding scale of light value was calculated for the diffuseness levels from D1 to D5, as listed in Table 3.4.

On the probe side, a white disk with a randomly generated diameter between 250 pixels and 930 pixels was displayed in the centre of screen C. The task of the observer was to adjust the diffuseness on the probe to fit the scene. Although the diameter of the light sources varied, the total number of white pixels inside each light source was kept constant to make sure they had the same total emitted luminous flux.

Each stimulus was repeated for 3 times, resulting in $5 \times 3 = 15$ trials for each participant.

(a) D1 (7cm)   (b) D2 (10.5cm)   (c) D3 (14.0cm)   (d) D4 (17.6cm)   (e) D5 (21.1cm)
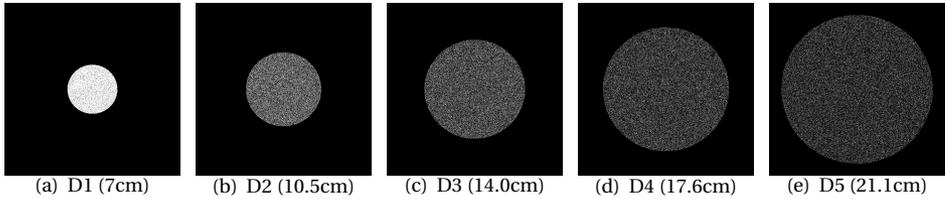
Figure 3.7: Group III stimuli: five diffuseness levels were achieved by changing the size of a white disk on screen B, while keeping the total number of white pixels constant.

Table 3.4: The diffuseness levels on the scene used in stimuli group III, and their scale of light values, calculated according to the definition by Frandsen [11].

Diffuseness levels	D1	D2	D3	D4	D5
Diameter (pixel)	264	398	532	666	800
Diameter (cm)	7.0	10.5	14.0	17.6	21.1
Scale of light	21%	30%	39%	47%	54%

Results

Table 3.5 gives the comparison between the diffuseness levels (parameterized by the scale of light) on the scene and the corresponding adjusted values on the probe averaged across the observers. The relationship is illustrated in Figure 3.8. Overall, the adjusted diffuseness on the probe increased as the diffuseness levels on the scene increased. However, the adjusted diffuseness levels on the probe were generally larger than the diffuseness levels on the scene and contract towards the range 37%-50%.

Table 3.5: The diffuseness levels on the scene used in stimuli group III, and their scale of light values, calculated according to the definition by Frandsen [11].

Scale of light	D1	D2	D3	D4	D5
Scene	21%	30%	39%	47%	54%
Probe	37%	42%	45%	50%	49%
SD	10%	12%	10%	9%	11%

We performed a repeated-measures ANOVA to test the differences between adjusted diffuseness levels. We found that the adjusted diffuseness levels were significantly affected by the diffuseness levels on the scene ($F(4, 176) = 11.14, p < 0.001$). The post-hoc test revealed that the inferred D1 was not significantly different from the inferred D2, the inferred D2 was not significantly different from the inferred D3, and the inferred D3 was not different from the inferred D4 and D5. This indicates that the observers could not detect all the diffuseness levels we simulated. A simple linear regression yielded a low R^2 of 0.157. Participants' predicted diffuseness levels increased slower than the stimuli's diffuseness with a slope of 0.38 and a systematic offset of 0.30.
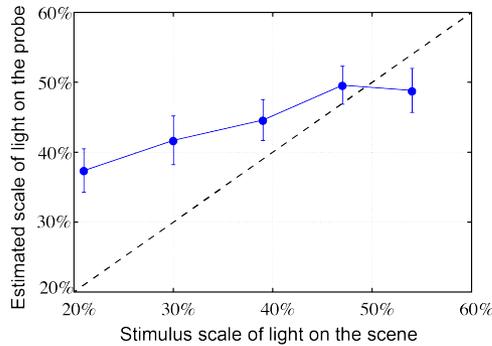
Figure 3.8: Mean of the fitted diffuseness levels (parameterized by the scale of light) on the probe as a function of the diffuseness levels on the scene. The error bars show the 95% confidence interval (for N=45 measurements).

3.4. Experiment 2: adjusting intensity, direction and diffuseness simultaneously

The aim of Experiment 2 is to investigate whether the observers can adjust and fit the light intensity, direction and diffuseness simultaneously using a rough probe. Adjusting the three lighting properties simultaneously might seem challenging because it requires the ability to discriminate the lighting effects for each of these three properties.

3.4.1. Lighting stimuli

The stimuli in Group IV are shown in Figure 3.9. The disk was put in one of three positions: P1 (the front right corner; $slant$: 74°; $tilt$: 73°), P5 (in the center; $slant$: 90°; $tilt$: 90°) or P9 (the back left corner; $slant$: 106°; $tilt$: 107°). In each of the three positions, the disk varied between two diffuseness levels: D1 (diameter: 7cm; scale of light of 21%) and D2 (diameter: 10.5cm; scale of light of 30%). For the disk in the centre (P5), one more diffuseness D3 (diameter: 14.0; scale of light of 39%) was added. Two intensity levels were used: I1 (75.0 cd/m^2) and I4 (36.7 cd/m^2). Thus, there were $2 \times 3 \times 2 + 1 \times 2 = 14$ stimuli on the scene in total.

On the probe side a disk with random diameter between 250 and 600 pixels and random luminance between 0 to 89 cd/m^2 was displayed in a random position. The task of the observers was to adjust the direction, diffuseness and intensity on the probe simultaneously to make it fit the scene.

Each stimulus was repeated for 3 times, resulting in $14 \times 3 = 42$ trials for each participant.

3.4.2. Results

The results for the fitted slant, tilt, diffuseness (parameterized by the scale of light) and intensity (parameterized by luminance) for the light source on the probe are listed in

3

Table 3.6: The mean fitted slant, tilt, diffuseness and intensity levels of the light source on the probe. SD means standard deviation. The rows in gray indicate stimuli that were used both in Experiment 1 and Experiment 2. Results for these stimuli will be compared at the end of this paper (Section 5).

Direction (slant, tilt)	Diffuseness (scale)	Intensity (cd/m^2)	N	Slant fitted	Slant SD	Tilt fitted	Tilt SD	Diffuseness (scale) fitted	Diffuseness (scale) SD	Luminance (cd/m^2) fitted	Luminance (cd/m^2) SD
P1(74°, 73°)	D1(21%)	I4(36.7)	45	81.2°	11.2°	78.8°	6.9°	31%	8.4%	22.9	13.8
P1(74°, 73°)	D1(21%)	I1(75.0)	45	79.4°	9.5°	75.3°	7.2°	29%	8.4%	68.9	14.1
P1(74°, 73°)	D2(30%)	I4(36.7)	45	79.5°	9.2°	79.1°	6.8°	32%	10.0%	30	14.4
P1(74°, 73°)	D2(30%)	I1(75.0)	45	78.4°	8.6°	76.7°	5.9°	31%	7.2%	67.0	13.6
P5(90°, 90°)	D1(21%)	I4(36.7)	45	85.0°	8.6°	81.4°	7.3°	32%	8.6%	40.4	12.7
P5(90°, 90°)	D1(21%)	I1(75.0)	45	87.1°	6.8°	81.7°	7.0°	32%	9.5%	71.7	11.4
P5(90°, 90°)	D2(30%)	I4(36.7)	45	88.8°	9.3°	84.1°	8.7°	34%	10.2%	38.4	11.6
P5(90°, 90°)	D2(30%)	I1(75.0)	45	88.1°	7.8°	82.1°	6.6°	34%	8.9%	66.1	12.3
P5(90°, 90°)	D3(39%)	I4(36.7)	45	87.0°	10.4°	84.9°	7.5°	35%	10.4%	37.8	18.6
P5(90°, 90°)	D3(39%)	I1(75.0)	45	85.3°	7.2°	83.7°	6.0°	38%	10.4%	63.2	13.2
P9(106°, 107°)	D1(21%)	I4(36.7)	45	100.8°	11.0°	101.1°	6.6°	30%	7.9%	33.7	10.8
P9(106°, 107°)	D1(21%)	I1(75.0)	45	101.9°	8.7°	101.9°	7.2°	28%	8.7%	57.0	14.9
P9(106°, 107°)	D2(30%)	I4(36.7)	45	98.2°	9.8°	99.4°	7.0°	32%	10.1%	32.8	12.5
P9(106°, 107°)	D2(30%)	I1(75.0)	45	99.3°	9.7°	101.9°	6.6°	30%	8.1%	51.1	18.7

(a) D1, I1   (b) D2, I1   (c) D3, I1   (d) D1, I2   (e) D2, I2   (f) D3, I2
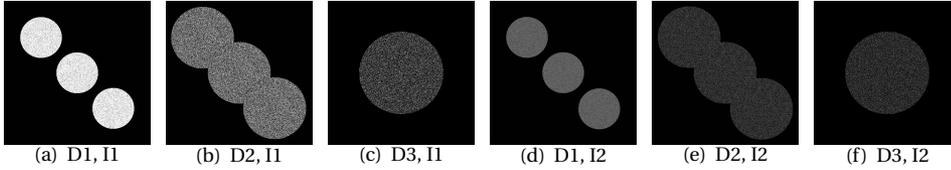
Figure 3.9: Group IV stimuli: three positions (P1, P5, P9), two diffuseness levels (D1, D2) and one extra diffuseness level (D3) on P5, and two intensity levels (I1, I4), resulting in 14 different stimuli in total. (a) D1 with I1 in P1, P5 and P9, (b) D2 with I1 in P1, P5 and P9, (c) D3 with I1 in P5, (d) D1 with I2 in P1, P5 and P9, (e) D2 with I2 in P1, P5 and P9, (f) D3 with I2 in P5.

Table 3.6. The average fitted slants and tilts were all within 9° of the veridical angles. The standard deviation was within 11° and the standard deviation for fitted slants was bigger than that for fitted tilts. Generally, the fitted diffuseness on the probe increased as the diffuseness on the scene increased, and the fitted intensity on the probe increased as the intensity on the scene increased.

Since the light source in position P5 had one more diffuseness level D3, we divided the statistical analysis into two parts. In part one, we analyzed the influence of all three properties (three positions: P1, P5, P9; two diffuseness levels: D1, D2; two intensity levels: I1, I4) on the adjustments. In part two, we analyzed the influence of three diffuseness levels (D1, D2, D3) and two intensity levels (I1, I4) of the source in P5.

Part one:

From the illustrations in Figure 3.10 we noticed that, in general, the fitted directions of the light source on the probe (pink disks) aligned with the light source direction on the scene (white disks). The fitted directions tended to contract towards the centre of the screen. In Figure Figure 3.10(a) and (c), the fitted diameters of the light source on the probe were much larger than the diameter D1 of the light source on the scene.

Figure 3.11 shows the fitted luminance on the probe for I1 and I4 in positions P1, P5 and P9, averaged over two diffuseness levels (D1 and D2). The veridical luminance values of I1 and I4 are marked with dashed lines. The fitted luminance values correlate well with the veridical values and again show (in most cases) a negative offset as in Experiment 1.

We performed a 3 (position)×2 (diffuseness)×2 (intensity) repeated-measures ANOVA for the fitted slant, tilt, diffuseness and intensity. We found a significant main effect of the light source position on the estimated slant ($F(2,88) = 106.53, p < 0.001$) and tilt ($F(2,88) = 323.85, p < 0.001$) of the light source on the probe. The post-hoc test revealed that the three estimated slants were significantly different from each other, and so were the three estimated tilts. We also found a significant main effect of diffuseness level of the scene on the estimated diffuseness on the probe ($F(1,44) = 6.69, p = 0.013$); the estimated diffuseness level for D1 ($M = 30\%, SD = 0.011$) was smaller than the estimated diffuseness level for D2 ($M = 32\%, SD = 0.008$). Also, we found a significant main effect of intensity levels on the estimated light intensity on the probe ($F(1,44) = 603.60, p < 0.001$), which was consistent with the observation in Figure 3.11.

(a) D1, I1

(b) D2, I2

(c) D1, I4

(d) D2, I4
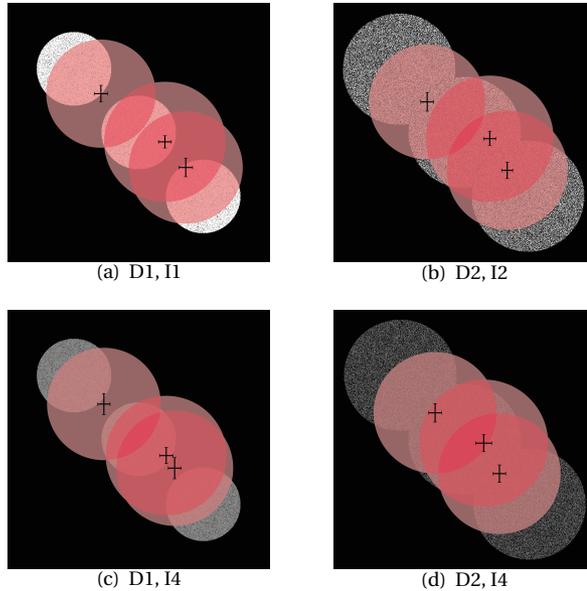
Figure 3.10: The white disks represent the light source on the scene and the pink disks represent the mean light source on the probe estimated by the observers. Light sources in position P1, P5 and P9 with (a) diameter D1 and intensity level I1, (b) diameter D2 and intensity level I1, (c) diameter D1 and intensity level I4, and (d) diameter D2 and intensity level I4. The error bars on the pink disks show the 95% confidence intervals (for N=45 measurements).
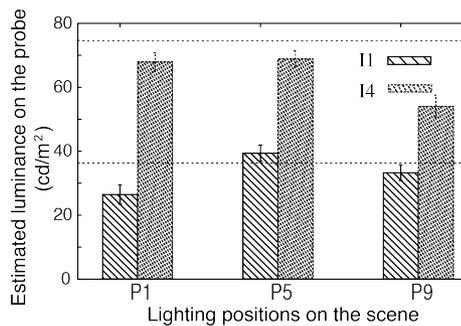
Figure 3.11: Mean fitted luminance on the probe for I4 (the most densely dashed bars) and I1 on the scene in position P1, P5 and P9 averaged over two diffuseness levels (D1 and D2). The error bars show the 95% confidence intervals (for N=90 measurements). The dashed horizontal lines show the veridical values of I1 and I4.

Unexpectedly, we found a significant main effect of the light source position on the fitted intensity on the probe ($F(2, 88) = 28.136, p < 0.001$). The post-hoc test indicated that the adjusted intensity for P5 was significantly higher than for P1 ($p < 0.001$) and P9

($p < 0.001$).

Part two:

In this part, only the estimated lighting properties for P5 were investigated. A 3 (diffuseness)×2 (intensity) repeated-measures ANOVA was performed for the fitted slant, tilt, diffuseness and intensity. As expected, we found a significant main effect of diffuseness on the fitted diffuseness ($F(2,88) = 6.378, p = 0.003$). As Figure 3.12 shows, the estimated diffuseness values on the probe increased as the diffuseness on the scene increased. The post-hoc test showed that the estimated diffuseness (parameterized by the scale of light) for D3 was significantly larger than that of D1 ($p = 0.004$) and D2 ($p = 0.013$). We also found a significant main effect of the intensity on the estimated light intensity on the probe ($F(1,44) = 335.96, p < 0.001$), in that the estimated light luminance for I4 was significantly lower than that for I1, as shown in Figure 3.13.
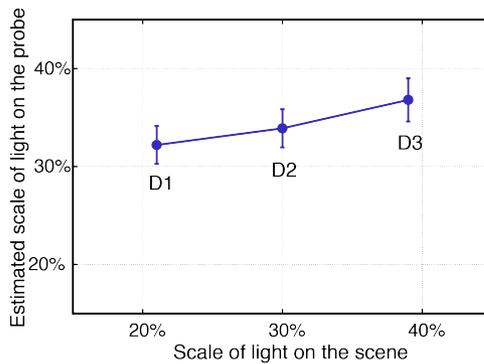
Figure 3.12: Mean estimated scale of light on the probe as a function of the scale of light on the scene averaged over intensity levels I4 and I1. The error bars show the 95% confidence intervals (for N=90 measurements).

Unexpectedly, the analysis showed that the diffuseness levels on the scene significantly influenced the estimated intensity on the probe ($F(2,88) = 4.753, p = 0.011$). As illustrated in Figure 3.13, generally, the estimated intensity on the probe decreased with the diffuseness on the scene increased. The post-hoc test showed that the estimated intensity for D1 was significantly higher than for D3 ($p = 0.011$).

3.5. Comparison between independent and simultaneous adjustments in Experiment 1 and 2

We analyzed the results for the lighting stimuli that were used in both Experiment 1 and Experiment 2 (marked in gray in Table 3.6) to compare the results of independent and simultaneous estimation.
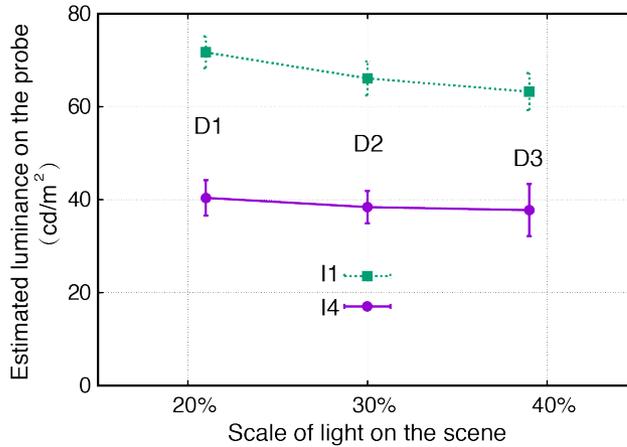
Figure 3.13: Mean estimated light intensity (parameterized by luminance) on the probe for I4 (the lower solid line) and I1 (the upper dashed line) on the scene for diffuseness levels D1, D2 and D3. The error bars show the 95% confidence interval (for N=45 measurements).

3.5.1. Comparison between independent and simultaneous adjusted light intensity

For the light intensity, the common stimuli on the scene for Experiment 1 and Experiment 2 were I1 and I4 in position P5 with diffuseness D1. The results of paired-samples t-tests showed that the estimated intensity in Experiment 2 was higher than that in Experiment 1 both for I1 (difference: $4.9 cd/m^2$, $t(44) = 2.21$, $p = 0.032$) and I4 (difference: $8.3 cd/m^2$, $t(44) = 4.11$, $p < 0.001$), as shown in Table 3.7. However, we found that in Experiment 2, the simultaneously estimated diffuseness for D1 was significantly larger than in Experiment 1, both for a light intensity of I1 (difference: 11%, $t(44) = 7.94$, $p < 0.001$) and I4 (difference: 11%, $t(44) = 8.58$, $p < 0.001$). It shows the interaction between the estimated light intensity and diffuseness. When the light intensity on the probe was evaluated to be higher than in Experiment 1, the diffuseness was evaluated to be larger.

Table 3.7: Comparison between mean estimated light luminance in Experiment 1 (inferred independently) and in Experiment 2 (inferred simultaneously) for stimuli with a light source in P5 having a diffuseness level D1 and an intensity of I4 or I1 on the scene.

Intensity levels (cd/m^2)	I1	I4
Scene	75.0	36.7
Probe in EXP 1	66.8	32.1
Probe in EXP 2	71.7	40.4

3.5.2. Comparison between independent and simultaneous adjusted light direction

For the slant and tilt, we compared the results of the stimuli for positions P1, P5 and P9 with diffuseness D1 and intensity I1 (see Table 3.8) in Experiment 1 and Experiment 2. The results of paired-samples t-tests indicated that neither the estimated slants nor the estimated tilts in Experiment 2 were statistically significantly different from those in Experiment 1.

Table 3.8: Comparison between slant and tilt on the probe in Experiment 1 (inferred independently) and in Experiment 2 (inferred simultaneously) for stimuli with a light source in positions P1, P5 and P9 having a diffuseness level D1 and intensity I1 on the scene.

Direction	Slant			Tilt		
	P1	P5	P9	P1	P5	P9
Scene	74°	90°	106°	73°	90°	107°
Probe in EXP 1	75°	85°	106°	76°	82°	103°
Probe in EXP 2	79°	87°	102°	75°	81°	102°

3.5.3. Comparison between independent and simultaneous adjusted light diffuseness

For the light diffuseness, we compared the levels D1, D2 and D3 on the scene for intensity I1 in position P5. The results of paired-samples t-tests showed that the estimated diffuseness on the probe in Experiment 2 was significantly smaller than that in Experiment 1 for D1 (difference: -5%, $t(44) = -3.41$, $p = 0.001$), D2 (difference: -8%, $t(44) = -4.47$, $p < 0.001$) and D3 (difference: -6%, $t(44) = -2.73$, $p = 0.009$), as shown in Table 10. Additionally, we found that the simultaneously estimated luminance in Experiment 2 were smaller than those of the stimuli in Experiment 1 (i.e. I1) for all three diffuseness levels D1 (difference: $-3.3 cd/m2$, $t(44) = -1.93$, $p = 0.06$), D2 (difference: $-8.9 cd/m^2$, $t(44) = -4.86$, $p < 0.001$) and D3 (difference: $-11.8 cd/m^2$, $t(44) = -5.97$, $p < 0.001$). This again shows the interaction between the estimated light intensity and diffuseness; a lower estimate of diffuseness went together with a lower estimate of the intensity.

Table 3.9: Comparison between the mean diffuseness in Experiment 1 (inferred independently) and in Experiment 2 (inferred simultaneously) for stimuli with a light source in position P5 having an intensity of I1 and a diffuseness level of D1, D2 or D3.

Diffuseness levels (scale of light: %)	D1	D2	D3
Scene	21%	30%	39%
Probe in EXP 1	37%	42%	45%
Probe in EXP 2	32%	34%	38%

3.5.4. Comparison between independent and simultaneous adjusted probe appearances

Figure 3.14 shows pixelwise correlations between the gray scale photograph of the probe taken under the average adjustment of Experiment 1 and Experiment 2, for the common stimuli of intensity and diffuseness estimates. The results show that the distribution in the scatter plots is well in line with the x-y diagonal, and so, that the average adjustment in Experiment 1 corresponds well to the average adjustment in Experiment 2 for the same stimuli. The correlations are quite high in that the generic R2 values for these straight pixelwise regressions are all above 0.95, while correlations for arbitrary parameter settings are found to be much lower (for instance, the R2 for the photographs of the probe under P1 and P9 with diffuseness level D1 and intensity level I1 is 0.44). That the images for the adjusted lighting correlate so well is surprising, because the adjustments in Experiment 1 and Experiment 2 are performed in different sessions and the probe appearance could not be compared directly between the sessions. Thus, consistent with the previous finding, it indicates that the observers have an internal expectation of how a probe would look like and this expectation is rather consistent. Furthermore, the observers are able to rely on this expectation to adjust the lighting properties.

3.6. Discussion

3.6.1. Methods

In this study, we investigated observer's abilities to infer light field properties in a real scene both independently and simultaneously using an adjustment method and optical mixing of a scene and rough probe. In a previous study by Xia et al. [36], the same scene was used but with a forced-choice method, in which observers indicated yes/no to "visual fit". The results of the previous study showed that the observers had difficulty to see the mismatch between the probe and the scene for scales of light of 24% and 43%. However, in this study, their estimated diffuseness for a scale of light of 21% was statistically different from that of 39%. Similarly, in the previous study the observers could not see the mismatch between I1 and I3 and between I3 and I5 when the probe was illuminated by the lower intensity and the scene by the higher intensity. However, in this study, the estimated five intensity levels were all statistically significantly different from each other. We conjecture that the method of adjustment is a more sensitive method than the yes/no method. A possible reason may be that the dynamic changes in object appearance due to the adjustment can help the observers to infer the lighting conditions in our experimental setup.

3.6.2. Estimated light intensity

We found that the observers were quite good at inferring the light intensity. Especially in Experiment 1, the independently estimated luminance values were surprisingly close to the veridical ones. It was found that in Experiment 1, the regression slope varied from 0.58 to 1.27 among 15 observers with an average value of 0.95. In Experiment 2, the slope
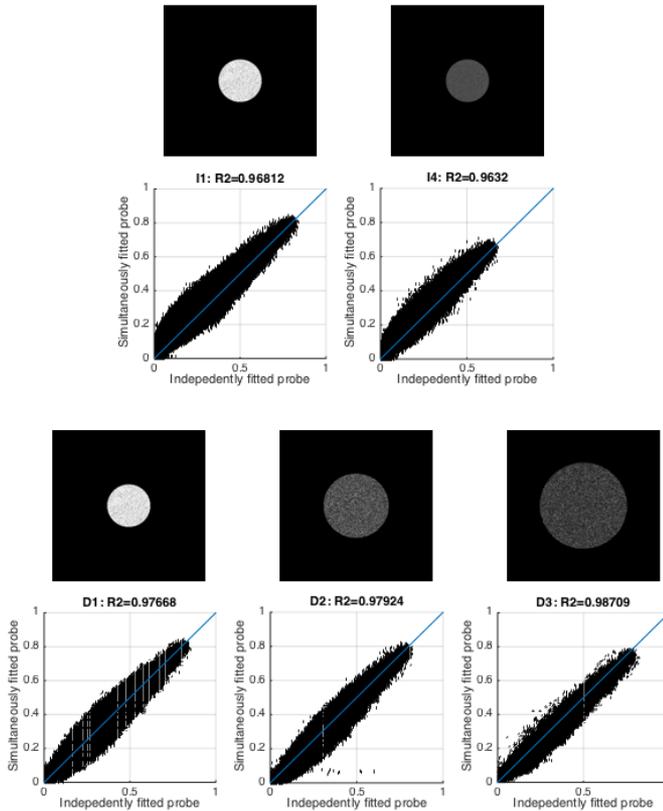
Figure 3.14: Scatterplots of the gray scale photograph of the probe taken under the average adjust-ment in Experiment 1 versus that in Experiment 2, for intensity levels (a) I1 and (b) I4 in position P5 with diffuseness D1, and for diffuseness level (c) D1, (d) D2 and (e) D3 on the scene for intensity I1 in position P5.

varied from 0.48 to 1 among 15 observers with an average value of 0.78. In a previous study using photographs [18], the estimated intensities were found to be monotonically related to the physical intensity values and to obey the "inverse squares law" of photom-etry at least semi-quantitatively. They found that the slopes of the linear regression of the intensity observations against the veridical values varied from 0.35 to 0.85 among 8 observers, and the average slope was around 0.58. Photographs are different from real scenes in that photographs usually have only two or three orders of dynamic range (DR) of luminance, while the real world has about ten orders [25]. The results in this study suggest that the observers might be much more sensitive to variations in light intensity in real scenes than what is reflected in photographs. However, the measurements by Koenderink et al. were done in various positions in a scene, and therefore the difference in the results may also reflect effects due to the global structure of the light field.

It has been extensively studied whether observers can extract the reflectance of surfaces under varying illumination conditions [1, 13, 31, 34]. Their results showed that often the visual system can discount the illumination conditions and viewing conditions resulting in lightness constancy. Human's lightness perception is not perfectly veridical but without the ability of inferring the luminous flux falling on a surface, observers would be unable to infer surface reflectance. Our results for the intensity adjustments can be seen as a direct proof of this ability.

3.6.3. Estimated light direction

For the light direction, the independently estimated directions and the simultaneously estimated ones showed no statistically significant difference and the observers could fit the light direction rather well in our real scene. The average fitted slant and tilt were overall within a few degrees of the veridical values. However, both in Experiment 1 and Experiment 2, we found that the standard deviation for the inferred tilt was smaller than for the inferred slant. This result is consistent with existing literature [18, 19, 29]. Pont et al. introduced the concept of "surface illuminance flow" to describe the 3D texture gradients due to illuminated surface mesorelief [20, 28]. The variation of illuminance on the macroscale is usually denoted as "shading". The "surface illuminance flow" provides cues about the lighting additional to the "shading". Xia et al. showed that the "surface illuminance flow" over a rough sphere was indeed helpful in estimating the light direction and diffuseness in real scenes [36]. Besides the "illuminance flow" over rough surfaces, Pont et al. showed that the "illuminance flow" could also be estimated from images of arbitrary natural images [28]. The shading patterns and patterns of shadow contour variations over the scene give information about the "illuminance flow" over the scene and thus provide salient information about the illumination direction. However, it is difficult to estimate the depth of the light source ("slant angle") due to basic ambiguities in the (retinal) images, such as the bas-relief ambiguity [3]. The results of the current study suggest that the " illuminance flow" over the scene was also used as a cue for the illumination.

3.6.4. Estimated light diffuseness

In our study, we found that the observers could infer the light diffuseness, but, consistent with previous research [18, 29], in a very coarse manner. The sequence of adjustment of the three lighting properties in Experiment 2 was recorded. We checked all the 630 stimuli (15 participants×14 stimuli × 3 times) and found that the light direction was chosen as the first property to adjust for 290 times, and the intensity for 310 times, while the diffuseness only for 30 times. This result suggests that the diffuseness is the most difficult property to adjust. The difficulty in inferring the light diffuseness was also reflected in the observers' performance.

Our results also show that the fitted diffuseness levels were generally larger than the veridical values especially for D1 (scale of light of 21%) and D2 (scale of light of 30%). According to Frandsen, scales of light of 21% and 30% represent light fields dominated by parallel light. Koenderink et al. also found that observers inferred the light to be

more diffuse than the veridical values in their collimated light condition [18]. Furthermore, five recent psychophysical studies have investigated assumptions that observers make about light diffuseness when estimating shape and reflectance. They found that observers tend to assume high levels of diffuseness - often higher than the actual diffuseness of the light in the scene being viewed [4–7, 33]. Morgenstern et al. made 570 measurements of the diffuseness levels in natural scenes and found that the mean diffuseness level indicator ICE ranged from 0.41 to 0.66 in these scenes. ICE ranges from 0 for a completely uniform, ambient light source to 1.29 for a distant point light source. So, the range 0.41-0.66 represented relatively high diffuseness levels [23]. Thus, most of the light encountered in daily life is relatively diffuse instead of being collimated. This might explain the observers' bias towards more diffuse rather than collimated light.

3.6.5. Interactions between the estimated light properties

We found an interaction between the estimated light intensity and light direction and an interaction between the light intensity and light diffuseness in Experiment 2. These interactions suggest that the observers are quite sensitive to the luminous flux falling on the probe. Figure 3.15 illustrates the variation in physical brightness of a probe under lighting stimuli in different directions (in the first row) or with different diffuseness levels (in the second row). The light source in P5, compared to that in P1 and P9, generates more luminous flux in the centre of the scene where the probe was supposed to be located. As a result, the observers might have adjusted the intensity above the probe in P5 to be higher than that in P1 and P9. Similarly, with smaller diffuseness levels on the scene, more luminous flux falls on the central area of the scene. Thus, the observers might have estimated the intensity for D1 to be higher than for D3.

In a similar experiment performed on a display screen, Koenderink et al. did pixel-wise regressions of the actual probe images to predicted images that were computed for the veridical settings and found that these correlations were quite high [18]. In a previous study, it was found that observers judged the fit to be better if the average luminance of the visible parts of the probe was closer to the average luminance of the visible parts of the scene objects [36]. Combining the findings above, it indicates that the observers rely on their expectation of the probe appearance (i.e. their visual light field as defined by Koenderink et al.) to judge whether the probe fits the scene, within which the brightness is an essential cue. The light intensity, direction and diffuseness are not "orthogonal" in influencing the appearance of the probe. For instance, as the second row in Figure 3.15 shows, with higher diffuseness levels, the top of the probe gets darker. Comparing Experiment 1 with Experiment 2, for the stimuli whose diffuseness was inferred to be larger in Experiment 2, the intensity was inferred to be higher and vice versa. Since the light intensity is directly correlated with the brightness, it is probable that the observers attributed part of the brightness loss because of the higher estimated diffuseness to lower intensity and they compensated for the lost luminous flux by adjusting the intensity to be higher.

In addition to the intensity-diffuseness and the intensity-direction interactions we found here, Pont et al. found that simultaneous judgments of light direction and light diffuseness from the appearance of a matte white sphere interact with each other (i.e.,

3

(a) P1   (b) P2   (c) P3

(d) D1   (e) D2   (f) D3   (g) D4   (h) D5

Darker ➤ Brighter

(i) Legend
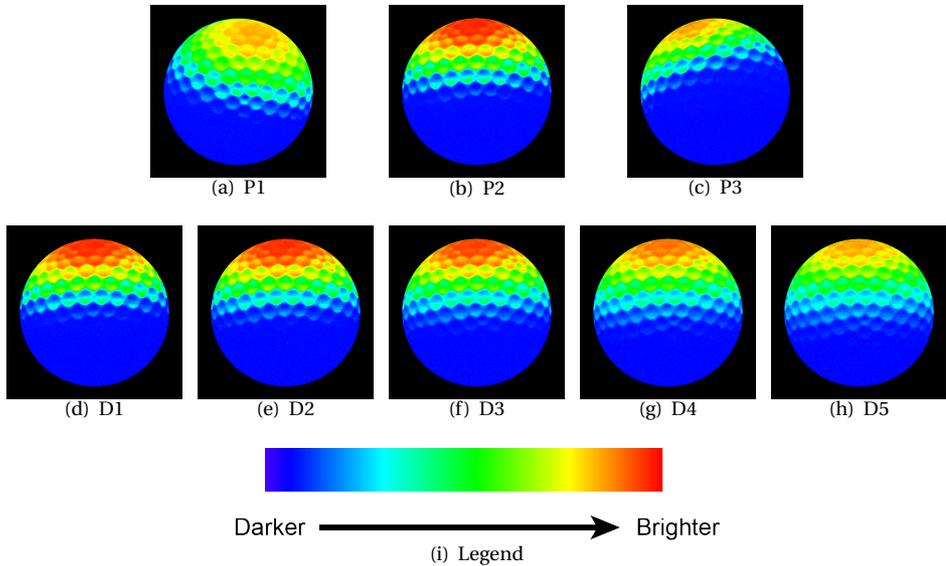
Figure 3.15: Color mapped photographs of the probe under different light directions (the first row) or light diffuseness levels (the second row). The photographs were taken along the observers' viewing direction. First row: the light source on screen C is in position (a) P1, (b) P5, (c) P9; Second row: the light source located in position P5 with diffuseness levels (d) D1, (e) D2, (f) D3, (g) D4, (h) D5. (i) legend of the color map, from left to right, blue represents the darkest area and red represents the brightest area.

the "diffuseness-direction interaction") [29]. Such perceptual interactions are to be expected on the basis of image-based analyses of the incoming optical structure or proximal stimulus, since there is no unique solution to the so-called inverse problem (inferring the physical light properties from the appearance of the probe object). Thus the image (of the scene and of the probe) is ambiguous with regard to certain light properties, or, in other words, the light properties are confounded in the resulting object appearance. This applies to any natural luminous environment. Nevertheless, we argue that simultaneous adjustment of the light intensity, direction and diffuseness is a suitable method for perception experiments and lighting interfaces, especially in combination with the use of a rough white matte spherical probe. Despite the image ambiguities, the light intensity, direction and diffuseness have well distinguishable effects on the appearance of such objects. Indeed our results of Experiment 2 show that, using a rough golf ball, the interactions were relatively small and the three parameters were adjusted quite accurately - in comparison to the results of Experiment 1 and former results using a yes/no fit method [36]. To summarize, simultaneous adjustment of all first order lighting properties is a feasible approach in a lighting interface, in which the designers/observers can use these properties as "buttons" to "tune the light". More specifically, our results show that an interface on which these properties can be adjusted in a blended manner, in combination with a visual representation of the resulting appearance, is a practically

feasible manner to vary the spatial distribution of the light (as an observer in a perception experiment, or as a designer designing a light plan). However, we should keep in mind that perceptual interactions between these lighting properties may happen because of basic image ambiguities.

3.7. Summary

In this study, we used an adjustment method to measure the observers' abilities of inferring the light intensity, direction and diffuseness. Two experiments were conducted using a "probe object" approach in an experimental setup, which optically mixed a scene and a probe together. We used a matte white rough spherical probe, which provides surface illuminance flow in addition to shading cues. In Experiment 1, the observers were asked to estimate the three basic lighting properties independently, while in Experiment 2 they were asked to estimate these lighting properties simultaneously.

In Experiment 1, we found that the observers were quite sensitive to the variation of light direction and light intensity, but estimated the light diffuseness much more coarsely. In Experiment 2, we found that although the inferred light properties interacted slightly, the observers were well able to infer all three properties simultaneously. Thus, the simultaneous adjustment method using an optically mixed scene and probe was proved to be an efficient way to measure observers' sensitivity for light field characteristics in real scenes. Simultaneous adjustment of light intensity, direction and diffuseness of light is thus feasible in lighting interfaces, in which the users can use these properties as "tuning buttons".

References

[1] Edward H Adelson. Zjˆ±lightness perception and lightness illusions. *New Cogn. Neurosci*, 339, 2000.

[2] Peter GJ Barten. Physical model for the contrast sensitivity of the human eye. In *SPIE/IS&T 1992 Symposium on Electronic Imaging: Science and Technology*, pages 57–72. International Society for Optics and Photonics, 1992.

[3] Peter N Belhumeur, David J Kriegman, and Alan L Yuille. The bas-relief ambiguity. *International journal of computer vision*, 35(1):33–44, 1999.

[4] Marina Bloj, Caterina Ripamonti, Kiran Mitha, Robin Hauck, Scott Greenwald, and David H Brainard. An equivalent illuminant model for the effect of surface slant on perceived lightness. *Journal of Vision*, 4(9):6–6, 2004.

[5] Huseyin Boyaci, Katja Doerschner, and Laurence T Maloney. Perceived surface color in binocularly viewed scenes with two light sources differing in chromaticity. *Journal of Vision*, 4(9):1–1, 2004.

[6] Huseyin Boyaci, Katja Doerschner, and Laurence T Maloney. Cues to an equivalent lighting model. *Journal of Vision*, 6(2):2–2, 2006.

[7] Hussein Boyaci, Lawrence T Maloney, and Sarah Hersh. The effect of perceived surface orientation on perceived surface albedo in binocularly viewed scenes. *Journal of Vision*, 3(8):2–2, 2003.

[8] David H Brainard. Color constancy in the nearly natural image. 2. achromatic loci. *JOSA A*, 15(2):307–325, 1998.

[9] David H Brainard, Wendy A Brunt, and Jon M Speigle. Color constancy in the nearly natural image. 1. asymmetric matches. *JOSA A*, 14(9):2091–2110, 1997.

[10] Stanley Coren and Melvin K Komoda. The effect of cues to illumination on apparent lightness. *The American journal of psychology*, pages 345–349, 1973.

[11] Sophus Frandsen. The scale of light–a new concept and its application. In *Paper on 2nd European Conference on Architecture*, pages 4– 8, 1989.

[12] Andreī Gershun. The light field (translated by moon, parry hiram and timoshenko, gregory). *Journal of Mathematics and Physics*, 18(1):51–151, 1939.

[13] Alan Gilchrist, Christos Kossyfidis, Frederick Bonato, Tiziano Agostini, Joseph Cataliotti, Xiaojun Li, Branka Spehar, Vidal Annan, and Elias Economou. An anchoring theory of lightness perception. *Psychological review*, 106(4):795, 1999.

[14] Mitsuo Ikeda, Hiroyuki Shinoda, and Yoko Mizokami. Phenomena of apparent lightness interpreted by the recognized visual space of illumination. *Optical review*, 5(6):380–386, 1998.

[15] Byung-Geun Khang, Jan J Koenderink, and Astrid ML Kappers. Perception of illumination direction in images of 3-d convex objects: Influence of surface materials and light fields. *Perception*, 35(5):625–645, 2006.

[16] Frederick AA Kingdom. Lightness, brightness and transparency: A quarter century of new ideas, captivating demonstrations and unrelenting controversy. *Vision Research*, 51(7):652–673, 2011.

[17] Jan J Koenderink and Sylvia C Pont. Irradiation direction from texture. *JOSA A*, 20(10):1875–1882, 2003.

[18] Jan J Koenderink, Sylvia C Pont, Andrea J van Doorn, Astrid ML Kappers, and James T Todd. The visual light field. *PERCEPTION-LONDON-*, 36(11):1595, 2007.

[19] Jan J Koenderink, Andrea J van Doorn, Astrid ML Kappers, Susan F Te Pas, and Sylvia C Pont. Illumination direction from texture shading. *JOSA A*, 20(6):987–995, 2003.

[20] Jan J Koenderink, Andrea J Van Doorn, and Sylvia C Pont. Perception of illuminance flow in the case of anisotropic rough surfaces. *Perception & psychophysics*, 69(6):895–903, 2007.

[21] M. Madsen and M Donn. Experiments with a digital 'light-flow-meter' in daylight art museum buildings. In *presented at the 5th International Radiance Scientific Workshop, UK: Leicester, Sep 13-14*, 2006.

[22] Laurence T Maloney. Illuminant estimation as cue combination. *Journal of Vision*, 2(6):6–6, 2002.

[23] Yaniv Morgenstern, Wilson S Geisler, and Richard F Murray. Human vision is attuned to the diffuseness of natural light. *Journal of vision*, 14(9):15, 2014.

[24] Alexander A Mury, Sylvia C Pont, and Jan J Koenderink. Light field constancy within natural scenes. *Applied Optics*, 46(29):7308–7316, 2007.

[25] Karol Myszkowski, Rafal Mantiuk, and Grzegorz Krawczyk. High dynamic range video. *Synthesis Lectures on Computer Graphics and Animation*, 1(1):1–158, 2008.

[26] James P O'Shea, Maneesh Agrawala, and Martin S Banks. The influence of shape cues on the perception of lighting direction. *Journal of vision*, 10(12):21, 2010.

[27] Alex P Pentland. Finding the illuminant direction. *JOSA*, 72(4):448–455, 1982.

[28] Sylvia Pont and Jan Koenderink. Surface illuminance flow. In *3D Data Processing, Visualization and Transmission, 2004. 3DPVT 2004. Proceedings. 2nd International Symposium on*, pages 2–9. IEEE, 2004.

[29] Sylvia C Pont and Jan J Koenderink. Matching illumination of solid objects. *Perception & psychophysics*, 69(3):459–468, 2007.

3

[30] Rocco Robilotto and Qasim Zaidi. Limits of lighness identification for real objects under natural viewing conditions. *Journal of Vision*, 4(9):9–9, 2004.

[31] MD Rutherford and DH Brainard. Lightness constancy: A direct test of the illumination-estimation hypothesis. *Psychological Science*, 13(2):142–149, 2002.

[32] James A Schirillo. We infer light in space. *Psychonomic bulletin & review*, 20(5):905–915, 2013.

[33] Andrew J Schofield, Paul B Rock, and Mark A Georgeson. Sun and sky: Does human vision assume a mixture of point and diffuse illumination when interpreting shape-from-shading? *Vision research*, 51(21):2317–2330, 2011.

[34] James T Todd, J Farley Norman, and Ennio Mingolla. Lightness constancy in the presence of specular highlights. *Psychological Science*, 15(1):33–39, 2004.

[35] Ling Xia, Sylvia C Pont, and Ingrid Heynderickx. Probing light in real scenes using optical mixtures. In *Proceedings of the ACM Symposium on Applied Perception*, pages 137–137. ACM, 2013.

[36] Ling Xia, Sylvia C Pont, and Ingrid Heynderickx. The visual light field in real scenes. *i-Perception*, 5(7):613–629, 2014.

[37] An Xu, Anindita Saha, Gabriele Guarnieri, Giovanni Ramponi, and Aldo Badano. Display methods for adjustable grayscale and luminance depth. In *Medical Imaging*, pages 69190Q–69190Q. International Society for Optics and Photonics, 2008.

4

EFFECTS OF SCENE CONTENT AND LAYOUT ON THE SUBJECTIVE LIGHT DIRECTION PERCEPTION

Abstract

The lighting, together with the furnishing of an interior space (i.e., the reflectance of its materials, the geometries of the furnishing and their arrangement) determines the appearance of this space. Conversely, human observers infer lighting properties from the space appearance. We conducted two psychophysical experiments to investigate how the perception of the light direction is influenced by a scene's objects and their layout using real scenes. In the first experiment, we confirmed that the shape of the objects in the scene and the scene layout influence the perceived light direction. In the second experiment, we systematically investigated how specific shape properties influenced the estimation of the light direction. The results showed that increasing the number of visible faces of an object, ultimately using globally spherical shapes in the scene supported the veridicality of the estimated light direction. Furthermore, symmetric arrangements in the scene improved the estimation of the tilt direction. Thus, human perception of light should integrally consider materials, scene content and layout.

4

4.1. Introduction

Light makes objects visible without being visible itself in empty space. The combination of the spatial and spectral characteristics of the light source(s), and the materials, scene content and layout determines the appearance of a space (the so-called "forward problem" of computer graphics). As such, the space's appearance is the main cue for the perception of its lighting and materials, scene content and layout. However, there is no unique solution to the so-called inverse problem (i.e. inferring the physical scene properties from the scene's appearance) because of basic image ambiguities. Therefore, light, material, scene content and layout perception are expected to be confounded. Several studies addressed perceptual interactions between light and material perception [6, 13, 14]. Here we present a first systematic exploration of the effect of scene content and layout on the perceived light direction in a space.

In the past years, research on light direction detection from images of surfaces has drawn a lot of attention both in computer vision and psychophysics. In computer vision, the light direction is one of the key elements that determine the shading patterns on an illuminated object, and therefore its estimation is used in shape-from-shading (SFS) algorithms. In psychophysics, understanding how human beings account for the variations in light field properties (i.e., light direction, intensity and diffuseness) is essential for research on color/lightness constancy [3, 4, 8, 19], human perception of "illuminance flow" [16, 17, 25] and to understand how human beings estimate 3D shape from shading [15, 21].

However, every biological or artificial visual system faces the problem that images are ambiguous, in the sense that every image can be the result of an infinite number of possible combinations of shapes, surface materials, and lighting conditions. Thus, to recover the light direction from the appearance of an image is challenging because there is no unique solution. Pentland investigated how well humans could estimate the illumination direction from an image [24]. He provided a sheet with a series of disks with varying surface normals. The observers were asked to select from these disks the one with its surface normal closest to the illumination direction in test pictures of natural objects. The results showed that the observers could estimate both tilt and slant of the illuminant direction with an average deviation of 6° from the veridical direction and a standard deviation less than 12°. Koenderink et al. did a study on estimating illumination orientation from textures in images [16]. The participants were asked to match the illumination direction of a probe (i.e., a hemispherical boss on a plane) to the illumination direction of the textures. They found that participants were generally quite good at estimating the illumination orientation with a standard deviation of 13.6°, but not its direction because 180° flips happened quite frequently due to the "convex/concave ambiguity" [5, 9, 27]. Connected with this finding, they confirmed the "light-from-above bias" [10, 27, 28], which means that participants almost invariably judged the illumination to be from above rather than from below. Moreover, they found that participants were much worse at estimating the elevation of the illumination than the orientation, as the "bas-relief ambiguity" theory predicts [1]. The lower performance for estimating elevation than for azimuth was confirmed in an experiment done by Pont and Koenderink [26] in which artificial Lambertian spheres and images of real rough spherical objects

with various surface textures were used. They varied the diffuseness of the illumination in addition to the direction of the illumination. They found that illumination direction estimates interacted with illumination diffuseness estimates, because more frontal lighting or more diffuse lighting resulted in quite similar changes in object appearance (i.e., "diffuseness-direction ambiguity").

It is already known that human beings can detect the light direction on an illuminated object from the "shading", "shadowing" and "highlight" at the level of significant global surface curvature on the macroscale [2, 23]. For objects with rough surfaces, there is an additional source of optical information named "surface illumination flow", which is the variation of the surface texture over the object surface due to illuminated corrugations on the mesoscale. Koenderink et al. found that observers could estimate the illumination orientation of isotropic rough surfaces rather precisely [16], but that for anisotropic rough surfaces observers made very systematic errors depending on the level of anisotropy-causing specific deformations of the "surface illumination flow" [17]. Also, Khang et al. found that the estimated illumination direction in images of 3-D convex shapes differed for different types of reflectances-causing different types of shading variations [14]. Thus, shading, shadowing and 3D texture patterns are important cues for light direction estimation and systematic deformations of those patterns may result in specific deviations in the estimates.

The studies mentioned above were all performed using images on screens. In real scenes, observations may be less ambiguous for several reasons: (1) observers can move their eyes, head and body, which results in many extra cues, for instance motion parallax and multiple views, and (2) observers may rely on stereoscopic vision and a higher dynamic range. We used an optical mixture setup to test human observers' sensitivity for the low order lighting properties, such as intensity, direction and diffuseness in real scenes [34]. The observers were asked to adjust the lighting on a probe to make it appear like it fit the scene. The scene consisted of five small different geometrical shapes (a bowling pin, a pentagon body, a disk body, a cross body and a star body), which were arbitrarily selected and scattered in the space. The results showed that humans were quite sensitive to variations in light intensity in the scene and that they could also infer the light diffuseness, albeit with a bigger variance. However, one interesting phenomenon found in this study caught our attention and impelled the study described in this paper. The results showed that although observers' estimations of the light direction correlated well with the veridical light direction, they showed a significant deviation near a pentagon body, and not near a bowling pin [32].

We noticed that, both in psychophysical research and interior design, it appears to be neglected that objects placed within a 3D space might influence the perception of light - and, more particularly the perception of the light direction - in this space. Empirical evidence for the influence of the shape and arrangement of objects in real scenes on the perceived light direction is still missing.

The experiments in this paper were designed to investigate the following two research questions:

1. Whether the shape and layout of objects in a real scene influence the perceived light direction.

2. If the answer to the first question is yes, how the shape properties and light direction estimation are related.

4.2. General methods

We conducted an adjustment task based on the generic notion of a "gauge object". We used an experimental setup, in which a real gauge object was optically introduced into a real scene [33, 34]. Our setup is illustrated in Figure 4.1 (a). The scene consisted of five colorful painted matte wooden geometrical shapes and was located in cube B. A painted matte white golf ball, serving as the probe, was put in the center of cube C. Because a white object has a higher albedo than an object with any other color, one of the shapes in the scene was also painted white to provide an anchor [8]. The scene and probe were optically mixed together by a semitransparent mirror put in cube A at $45_{\circ}$ with respect to the viewing direction. The observers saw the optical mixture of the scene and probe through a viewing hole as if they were put together as illustrated in Figure 4.1 (b). The lighting on the scene and probe was provided by an LCD screen on top of cube B and cube C, respectively. Independent images were displayed on the two screens to provide individual lighting for the scene and for the probe. We refer to [34] for more information on the experimental setup.

The width of the cubes was 30 cm and the top of cube B and cube C was covered with a $930\,pixels \times 930\,pixels$ squared area on the screens. The average light direction as defined by the light vector [7, 22] was varied by displaying a white disk with a diameter of 7cm (i.e., 264 pixels) at different positions on the LCD screen. In the sections explaining the experimental setup, analysis and results we will describe these variations in terms of position, but it should be remembered that this is just a convenient parameterization of the direction in this specific setup. When illuminating the scene, the white disk was displayed at one out of nine fixed positions on the LCD screen. The bird's eye view of these nine positions is depicted in Figure 4.2 and they are labeled from P1 to P9. Their location on the LCD screen is marked using x- and y-coordinates. These positions of the disks were selected within a certain distance from the edges of the cube to make sure that there was enough space to adjust the light direction.

The direction of the light source on the scene can be converted into two angles, i.e., the slant and tilt angle, as listed in Table 4.1. As Figure 4.3 shows, the slant of the light source is the angle θ between the viewing direction and the vector from the center of the probe to the center of the light source ($\vec{PS}$) (using a light source in P3 as an example). The tilt of the light source is the angle ϕ between the positive x-axis and the projection of $\vec{PS}$ onto an eye-centered reference frame (i.e., the surface XPZ). The light sources in the same row of Figure 4.2 have the same slant angle, being 74° for the front row ($P1, P2, P3$), 90° for the second row ($P4, P5, P6$) and 106° for the back row ($P7, P8, P9$). Similarly, the light sources in the same column have the same tilt angle, being 73° for the right column ($P1, P4, P7$), 90° for the middle column ($P2, P5, P8$) and 107° for the right column ($P3, P6, P9$).

On the probe side, a disk with the same diameter was displayed in a random position serving as the light source that had to be adjusted.

The experiments were performed in a dark room. The observers looked at the optical

4

(a)

(b)
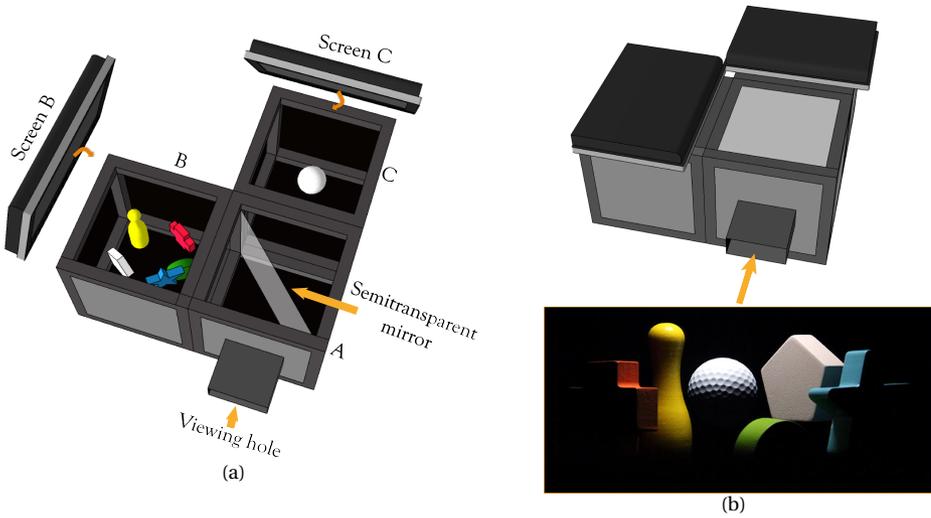
Figure 4.1: Illustration of the setup. (a)The setup consists of three $30cm \times 30cm \times 30cm$ cubes, of which the inside is covered with black velvet paper (the inner width of the cubes was 25cm excluding the width of the frames). In cube B, we made a simple scene with five geometrical shapes. In cube C, we placed a white painted golf ball which served as the probe. A semi-transparent mirror was placed vertically at the diagonal of box A. Two LCD screens covering the top of cube B and cube C provided the lighting which could thus be varied independently for the scene and the probe. (b) The setup and an optical mixture of the scene and the probe photographed through the viewing hole.

Table 4.1: The slant and tilt angles for the nine positions of the light source on the scene.

position	P1	P2	P3	P4	P5	P6	P7	P8	P9
Slant θ	74°	73°	74°	90°	90°	90°	106°	107°	106°
Tilt ϕ	73°	90°	107°	73°	90°	107°	73°	90°	107°

mixture of the scene and the probe through the viewing hole and were asked to adjust the light direction on the probe to fit the light direction on the scene. The four arrow keys on a keyboard were used to adjust the light direction. The observers could choose to take small steps or big steps by pressing corresponding keys on the keyboard when performing the adjustment. Once the "big step" was selected, each time the arrow key was pressed, the center of the light source moved 30 pixels (approximately 0.8 cm) in the selected direction. Otherwise, if "small step" was used, the center of the light source moved 10 pixels for each push on the key. If the position of the adjusted light source reached one of the boundaries, the computer gave a warning sound.
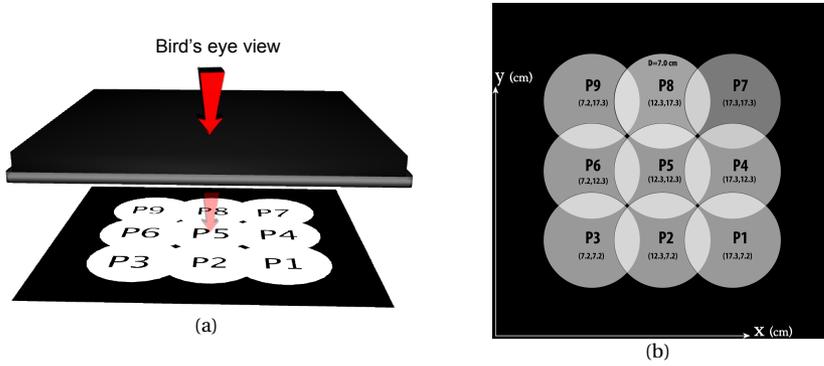
Figure 4.2: illustration of the bird's eye view of the stimuli on the scene: variation in direction was achieved by changing the position of a displayed white disk. Nine positions from P1 to P9 were used, as shown in the figure. The diameter of the disk was 264 pixels, and the width of the full window was 930 pixels (25cm). (b) Detailed information of the disk's positions.
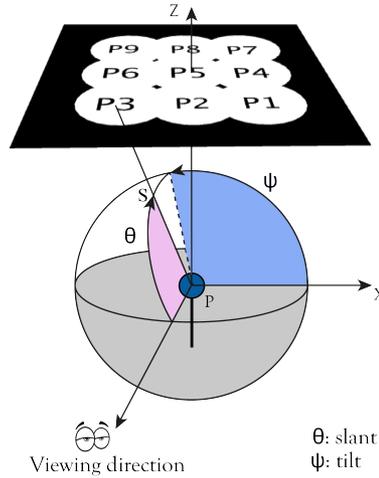
Figure 4.3: Illustration of slant and tilt for the light source located in P3. The blue spot shows where the probe is located. The slant θ is defined as the angle between the viewing direction and the vector from the center of the probe to the center of the light source ($\vec{PS}$). Tilt ϕ is defined as the angle between the positive x-axis and the projection of $\vec{PS}$ into eye-centered reference frame (i.e., surface XPZ).

4.3. Experiment 1: Is the perceived light direction in real scenes influenced by the shapes and scene layout?

In a former study by Xia et al. [32], the observers were asked to adjust the light direction of a probe to fit the light direction on a scene. The results showed that the estimated

light direction correlated well with the veridical light direction, but with a significant contraction near a pentagon body and not near a bowling pin. These results suggested that human's perception of light direction might be influenced by the shape and layout of the objects in the scene. To test this conjecture, the first experiment was designed.

4.3.1. Experimental design

Four scenes were created with five shapes in each scene: a bowling pin, a cylinder, a pentagon body, a star body, and a cross body, as Figure 4.1 shows. Scene A was originally used in Xia et al 's experiment [33, 34]. The bird's eye view of the projected position for each of the five shapes in Scene A is illustrated in Figure 4.4 with a red star. The probe was in the center of the box, marked in Figure 4.4 with a red disk. In Scene B, the position of the shapes was horizontally mirrored with respect to Scene A to test whether the layout caused the systematic contraction in estimated light position (see Figure 4.5). If so, the pattern of the estimated light positions should be mirrored as well. In Scene C, the bowling pin of Scene B was replaced by another pentagon body to test whether the contraction in estimated light position occurred because of the pentagon body. In Scene D, both pentagon bodies of Scene C were replaced by bowling pins to test whether the use of bowling pins could result in a more veridical estimation of the light position than the use of pentagon bodies.

This experiment was based on a between-subject design. It was divided into four sessions with a different scene per session. In each session, the light source was displayed three times in each of the 9 positions (see Figure 4.2), resulting in 27 trials.

There were 15 participants in each session. All participants had normal or corrected-to-normal vision. They all gave written, informed consent. All experiments were done in agreement with the local ethical guidelines, Dutch Law and the Declaration of Helsinki, and were approved by the TUDelft Human Research Ethics Committee (HREC).
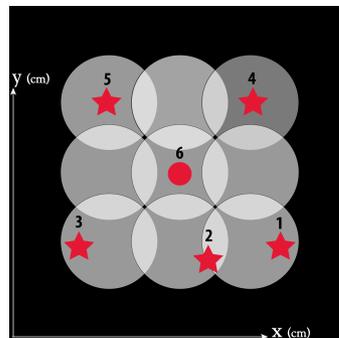

Figure 4.4: Illustration of the projected positions of the five shapes in Scene A. Number "1" represents the star body, number "2" the cylinder, number "3" the cross body, number "4" the pentagon body and number "5" the bowling pin. The red disk in the center marked with number "6" represents the position of the probe.

4.3.2. Results

Figure 4.6 shows the average estimated position of the light source above the probe (pink disks) for the nine different positions of the light source above the scene (white disks). The error bars on the pink disks show the 95% confidence intervals. We also show the raw data in Figure 4.7 as scatter plots of the estimated positions of the light source in each scene, including the 50% prediction ellipses for each light source position. The results show that the pattern of the estimated light positions was indeed mirrored when the scene was mirrored (compare Scene A and Scene B). Scene C, replacing the bowling pin with another pentagon body, resulted in a systematic contraction of the estimated light position along the y-axis (slant angle) near both pentagon bodies. Scene D, replacing both pentagon bodies with bowling pins, finally resulted in estimated light positions close to veridical ones. Furthermore, we found that the variance of the estimated light position along the Y-axis was always larger than along the X-axis (as evidenced by the error bars in Figure 4.6 and the shape of the ellipses in Figure 4.7).

(a) Scene A

(b) Scene B

(c) Scene C

(d) Scene D
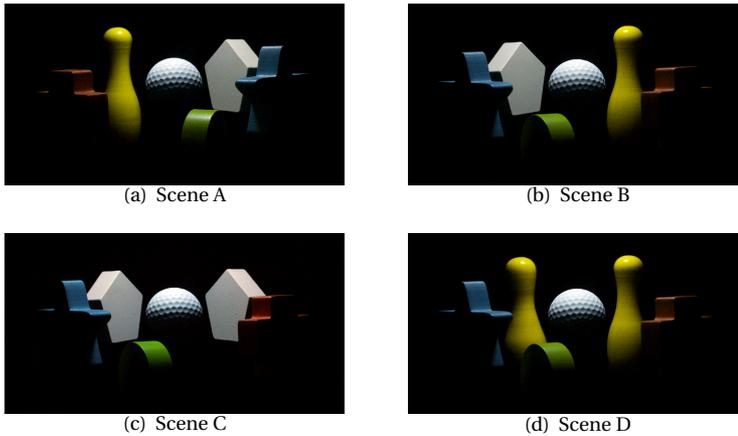
Figure 4.5: Four scenes, each consisting of five shapes (bowling pin, cylinder, pentagon body, star body, and cross body) (a) Scene A: original scene; (b) Scene B: horizontally mirrored version of Scene A; (c) Scene C: the bowling pin in Scene B was replaced by another pentagon body; (d) Scene D: both pentagon bodies in Scene C were replaced by bowling pins.

Two $3(row) \times 3(column)$ repeated-measures ANOVAs were performed, i.e., one for the estimated distances along the X-axis and one for the estimated distances along the Y-axis (hereafter referred as X-position and Y-position) of the light on the probe, for each of the 4 scenes separately. We found that in all four scenes, the estimated X-position was significantly influenced by the column, in which the light source on the scene was located ($Scene A : F(2,88) = 420, p < 0.001; Scene B : F(2,88) = 300, p < 0.001; Scene C : F(2,88) = 423, p < 0.001; Scene D : F(2,88) = 629, p < 0.001$). Similarly, the estimated Y-position was significantly influenced by the row ($Scene A : F(2,88) = 164, p < 0.001; Scene B : F(2,88) = 116, p < 0.001; Scene C : F(2,88) = 69, p < 0.001; Scene D : F(2,88) = 232, p < 0.001$). These results suggest that, generally, the observers were able to distinguish dif-

(a) for Scene A

(b) for Scene B

(c) for Scene C

(d) for Scene D
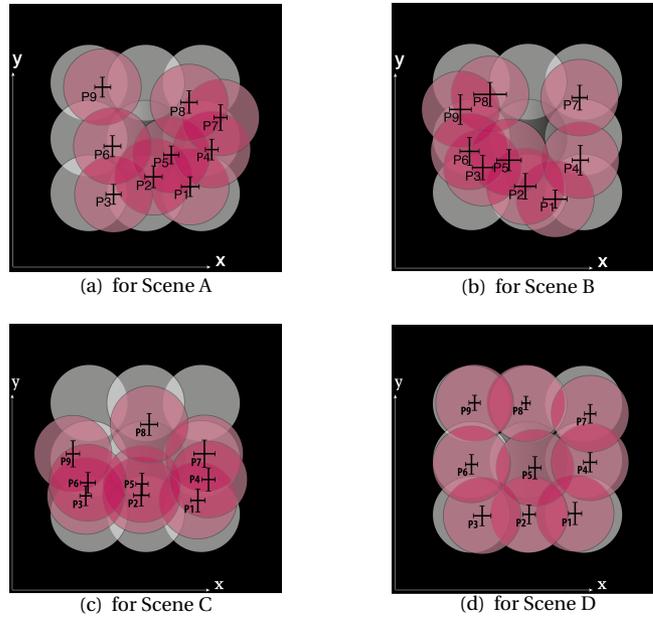
Figure 4.6: Illustration of the nine positions of the light source on the scene (white disks) and the corresponding average estimated position of the light source on the probe (pink disks) for (a) Scene A, (b) Scene B, (c) Scene C and (d) Scene D. The error bars on the pink disks show the 95% confidence intervals (for N=45 measurements).

ferent light directions in all four scenes.

Nevertheless, the estimated light source positions were closer to the veridical ones in Scene D with the two bowling pins than in the other scenes, as shown in Figure 4.6 and Figure 4.7. Together with the finding that the average estimated light position was often contracted around the position of the pentagon body, we assumed that the globally spherical smoothly curved bowling pins, in comparison with the facetted pentagon shapes, helped the observers to perceive the veridical light direction.

Scenes C and D both had a pair of the same objects (i.e., pentagon bodies and bowling pins) standing side by side in the scenes. The estimated light position along the x-axis in these two scenes was much closer to the veridical value than in Scenes A and B. According to a post-hoc analysis, the absolute difference (AD) between the estimated light position and the veridical value (expressed in terms of distance in X and Y for the position of the light disk on the LCD-screen) was significantly smaller for Scene C ($M = 1.81, SE = 0.08$) and Scene D ($M = 1.56, SE = 0.07$) than for Scene A ($M = 2.58, SE = 0.09$) and Scene B ($M = 2.90, SE = 0.11$). Thus, we conclude that symmetric arrangements within a scene improve the estimation of the tilt direction of the light source.

The results above showed that human perception of the light direction in a real scene was systematically dependent on scene layout and content.
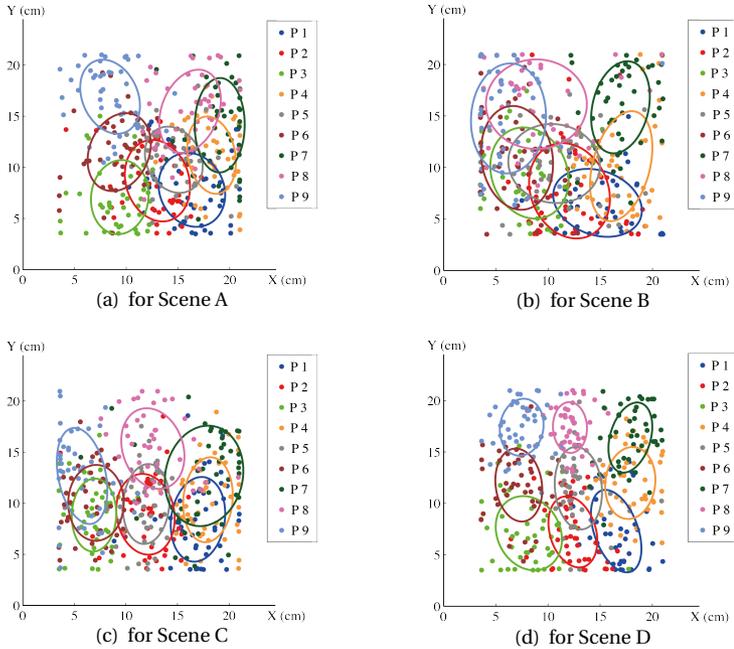
Figure 4.7: Scatter plots of the estimated position of the light source for 45 measurements in Scene A (a), Scene B (b), Scene C (c) and Scene D (d). Different colors represent the different light positions on the scene from P1 to P9 (as depicted in Figure 2). The 50% prediction ellipses for each light source position on the scene are given in the corresponding color.

4.4. Experiment 2: Which properties of shapes influence light direction estimation?

In Experiment 1, we have shown that the estimated light direction was influenced by the scene content and the scene layout. Furthermore, we found that scenes with a globally spherical smoothly curved bowling pin resulted in a more veridical estimation of the light direction than scenes with a facetted pentagon shape. This suggests that the bowling pin provides more information about the light direction than the pentagon body. The bowling pin differs from the pentagon body in two ways. First, the bowling pin has a smoothly curved surface, which generates gradual shading gradients under our lighting, while the pentagon body has facets that generate stepwise shading variations. The second difference is that the bowling pin has a close to spherical shaped top, while the pentagon body is globally flattened. Globally spherical in this study refers to a convex geometry that has symmetrical shape variations approaching or subsampling a sphere, like the top part of the bowling pin. Otherwise, if a shape is wider and taller than deep (along the line of sight), we call it globally flattened, like the pentagon body. For a global spherical geometry, the surface normals are usually rather uniformly distributed across

all directions.

As a consequence, two questions arise:

1. Will the estimation of the light direction become more veridical if the shape of the pentagon body remains globally flattened, but the number of visible facets increases?

2. Will the estimation of the light direction become more veridical if another globally spherical shape is used, but with a limited number of facets?

We designed Experiment 2 to answer these two questions.

4.5. Experimental design

We designed four new scenes in a systematic way. We kept the three shapes (i.e., the cylinder, star body, and cross body) in the front of the scene at the same position, but added a pair of new matte and white painted wooden shapes in each of the four new scenes (see Figure 4.8). Shape I, Shape II and Shape III were made starting from the pentagon body in Experiment 1, while cutting its top for Shape I, or its edges for Shape II, or both its top and its edges for Shape III. The number of perceivable facets gradually increased from Shape I, to Shape II and to Shape III. Shape IV was a pentagonal dodecahedron with a globally spherical shape, but a low number of visible facets as compared to Shape II and Shape III. As in Scene C and Scene D of Experiment 1, the new shapes were put side by side in the back of the scene, as shown in Figure 4.9.

Similar as to Experiment 1, this experiment consisted of 4 sessions with a different scene per session. The light source on the scene was displayed 3 times in each of the 9 positions (see Figure 4.2), resulting in 27 trials per session. The task of the participant was to adjust the direction of the light source on the probe to fit the light direction on the scene. This experiment was based on a within-subject design. The trials were randomly given in each session and the order of the four sessions was also randomized for each observer. The observers could have a break between sessions. After all four sessions were completed, the participant was asked to rank the sessions from 1 to 4 based on the difficulty they experienced when doing the direction estimation, where 1 stands for the most difficult session and 4 for the easiest one.

15 observers participated in this experiment. All participants had normal or corrected-to-normal vision. They all gave written, informed consent. The experiment was done in agreement with the local ethical guidelines, Dutch Law and the Declaration of Helsinki, and was approved by the TUDelft Human Research Ethics Committee (HREC).

4.5.1. Result

Figure 4.10 shows the average estimated light position on the probe side (pink disks) for the nine different positions of the light source on the scene side (white disks). The error bars on the pink disks show the 95% confidence intervals. The scatter plots of all raw data of the estimated light position on the probe are shown in Figure 4.11, together with the 50% prediction ellipses for each light source position in the scene. The results show that,

(a) Shape I

(b) Shape II

(c) Shape III
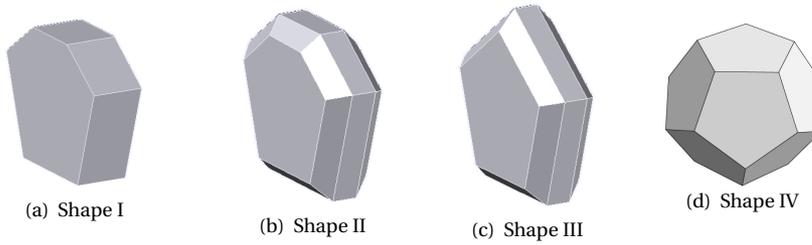
(d) Shape IV

Figure 4.8: The four shapes used in Experiment 2. Shape I, II and III were developed starting from the pentagon body by (a) cutting its top; (b) cutting its edges; (c) first cutting its top and then its edges; (d) Shape IV, a pentagonal dodecahedron with a globally spherical shape.

(a) Scene E

(b) Scene F
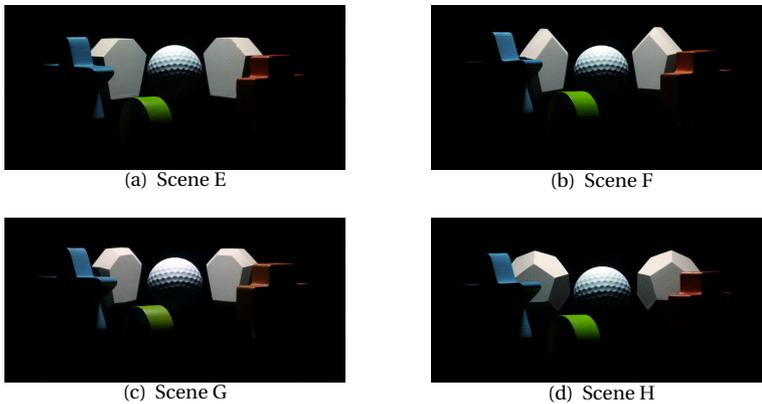
(c) Scene G

(d) Scene H

Figure 4.9: The four scenes used in Experiment 2, with in each scene a pair of shapes put side by side in the scene: (a) Shape I in Scene E, (b) Shape II in Scene F, (c) Shape III in Scene G, and (d) Shape IV in Scene H.

generally, the estimated position along the Y-axis in Scene F, Scene G and Scene H was closer to the veridical value than in Scene E. Furthermore, in general the position along the X-axis in Scene H was closer to the veridical value than in the other three scenes, especially when the light source in the scene was in Position 1 and Position 3. The shape of the ellipses with more variance along the Y-axis than along the X-axis indicates that the estimated slant angles spread wider than the estimated tilt angles.

4.5.2. Analysis on the estimated light positions

Two $3(row) \times 3(column)$ repeated-measures ANOVAs were performed, one for the estimated X-position and one for the estimated Y-position, for each of the four scenes separately. In all four scenes, the estimated X-position was significantly influenced by the column, in which the light source on the scene was located ($Scene\ E : F(2, 88) = 855, p <$

(a) for Scene E

(b) for Scene F

(c) for Scene G

(d) for Scene H
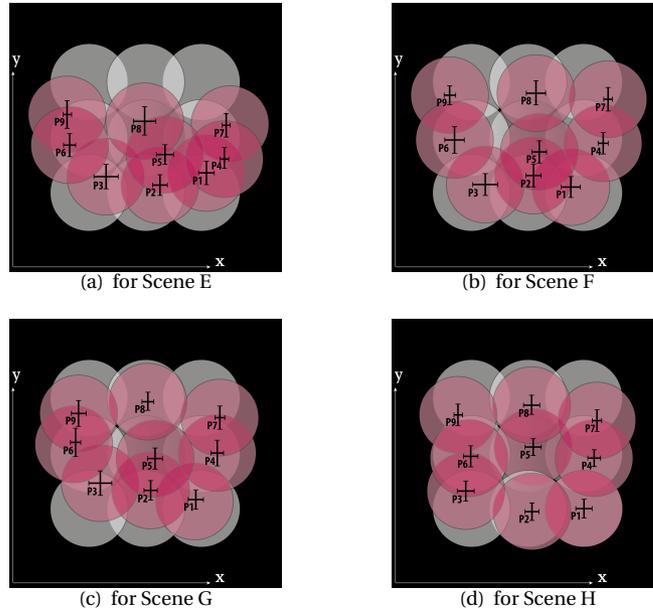
Figure 4.10: Illustration of the nine positions of the light source on the scene (white disks) and the corresponding average estimated position of the light source on the probe (pink disks) for (a) Scene E, (b) Scene F, (c) Scene G and (d) Scene H. The error bars on the pink disks show the 95% confidence interval (for N=45 measurements).

$0.001; Scene\ F : F(2,88) = 706, p < 0.001; Scene\ G : F(2,88) = 598, p < 0.001; Scene\ H : F(2,88) = 612, p < 0.001$). Similarly, the estimated Y-position was significantly influenced by the row, in which the light source on the scene was located ($Scene\ E : F(2,88) = 70, p < 0.001; Scene\ F : F(2,88) = 139, p < 0.001; Scene\ G : F(2,88) = 108, p < 0.001; Scene\ H : F(2,88) = 236, p < 0.001$). Again, these results indicate that, overall, the observers were able to distinguish different light directions in our scenes. However, we also found an interaction between the row and column of the position of the light source on the scene for the estimated X-position in all four scenes ($Scene\ E : F(4,176) = 24, p < 0.001; Scene\ F : F(4,176) = 28, p < 0.001; Scene\ G : F(4,176) = 17, p < 0.001; Scene\ H : F(4,176) = 4, p = 0.004$). As already illustrated in Figure 4.10 and Figure 4.11, the estimated light position seems shifted more to the middle column in the front row than in the other rows.

To investigate the influence of the shape type on the estimated light direction, we calculated the absolute difference (AD) between the estimated light position and the veridical one (expressed in terms of distance in X and Y for the position of the light disk on the LCD-screen). Two $4(scenes) \times 3(row) \times 3(column)$ repeated-measures ANOVAs were performed using the AD of the X-position and Y-position as dependent variable. Figure 4.12 shows the average AD of the X-position and Y-position for each scene. The paired combinations marked with a red star were significantly different from each other according to the post-hoc tests. The results show that the shape type significantly affected the
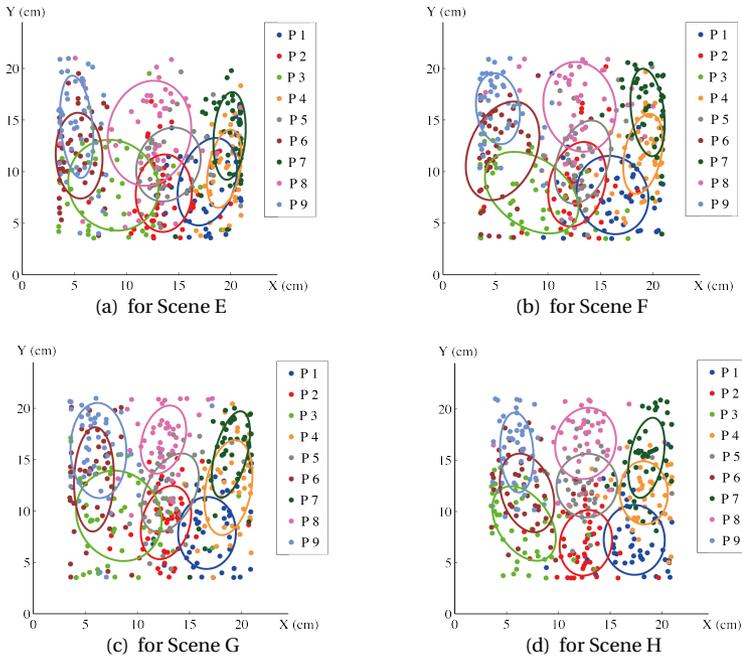
Figure 4.11: Scatter plots of the estimated position of the light source for 45 measurements in Scene E (a), Scene F (b), Scene G (c) and Scene H (d). Different colors represent the different light positions on the scene from P1 to P9, (as depicted in Figure 4.2). The 50% prediction ellipses for each light source position on the scene are given in the corresponding color.

AD of the X-position ($F(3, 132) = 9.33, p < 0.001$). The post-hoc test revealed that the AD in X-position of Scene G ($M = 1.88, SE = 0.081$) and Scene H ($M = 1.78, SE = 0.074$) were significantly smaller than of Scene E ($M = 2.27, SE = 0.094$) and Scene F ($M = 2.33, SE = 0.091$). This indicates that the estimated direction was significantly improved in Scene G and Scene H. The results also show that the column, in which the light source on the scene was located, had a significant effect on the AD in X-position ($F(2, 88) = 8.73, p < 0.001$), such that the AD in the middle column ($M = 1.77, SE = 0.084$) was significantly smaller than in the left ($M = 2.13, SE = 0.057$) and right ($M = 2.29, SE = 0.079$) columns. In other words, the estimated tilt angle in the middle column was closer to the veridical tilt angle than the estimated tilt angle in the other two columns. Also the AD of the Y-position was significantly influenced by the shape type ($F(3, 132) = 5.71, p = 0.001$), such that the AD in Scene E ($M = 3.34, SE = 0.139$) was significantly larger than in Scene F ($M = 2.82, SE = 0.117$) and Scene H ($M = 2.55, SE = 0.097$). This indicates that the observers had the worst performance inferring the slant angle in Scene E, characterized by the object with the smallest number of faces. We also found a significant influence of the column on the AD of the Y-position ($F(2, 88) = 5.84, p = 0.004$). The middle column had a significantly smaller AD in Y-position ($M = 2.72, SE = 0.101$) than the left column ($M = 3.18, SE = 0.103$), which implies that the estimated slant angle in the middle col-

umn was significantly closer to the veridical slant angle than the estimated slant angle in the left column.

Thus, altogether we found that the estimated direction became more veridical from Scene E and Scene F to Scene G, i.e., as the number of perceived faces on the object increased. Scene H, with two globally spherical pentagonal dodecahedrons gave the most veridical estimation of the light direction. The globally spherical pentagonal dodecahedron in Scene H had 5 visible faces, which was more than that of Shape I in Scene E but less than Shape II and Shape III in Scene F and Scene H. This indicates that, apart from increasing the number of the perceivable faces, the global sphericity resulted in a more veridical estimated light direction as well.
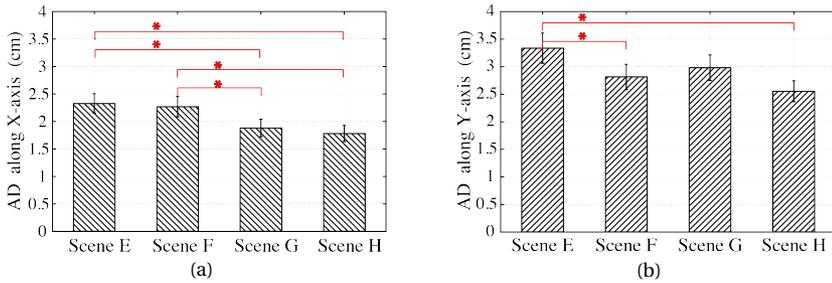
Figure 4.12: The average absolute difference (AD) between the estimated light position and the veridical one, as expressed in distance along (a) X-axis (tilt angle) and (b) Y-axis (slant angle) of the light disk on the LCD screen. The paired bars marked with a red star were significantly different from each other according to the post hoc tests. The error bars show the 95% confidence intervals (for $N = 15 observers \times 3 repeats \times 9 positions = 405$ measurements).

4.5.3. Analysis on variance between estimations

Besides comparing the estimated light direction with the veridical one, we here analyze the spread in estimated light direction (again expressed as X- or Y-position) between the participants. The standard deviation of the estimated light position was calculated for each scene and each position of the light source on the scene separately. The scenes were mutually compared using paired-samples t-tests. For the estimated X-position (i.e., the tilt angle), no statistically significant difference in standard deviation was found between any of the two scenes. For the estimated Y-position (i.e., the slant angle), we found that the standard deviation of Scene H ($M = 3.05, SE = 0.10$), compared with Scene E ($M = 3.69, SE = 0.15$), Scene F ($M = 3.53, SE = 0.11$) and Scene G ($M = 3.58, SE = 0.18$), was in all cases significantly smaller ($SceneH - E: t(8) = -5.46, p = 0.001; SceneH - F: t(8) = -3.56, p = 0.007; SceneH - G: t(8) = -3.422, p = 0.009$), but no significant difference in standard deviation was found between Scene E, Scene F and Scene G. This result indicates that the globally spherical shape used in Scene H significantly decreased the variation in estimated slant angle compared to the facetted pentagon body used in the other scenes.

4.5.4. The subjective reports on the experienced difficulty

The observers were asked to rank the scenes from 1 (most difficult) to 4 (easiest) according to the difficulty they experienced when doing the task. Table 4.2 shows the ranking order of the four scenes over all observers. Scene E was reported as the most difficult scene more frequently than the other three scenes. Scene H was reported as the easiest among all four scenes. In general, this result was consistent with the observers' performance (in terms of veridicality) on estimating the light direction in the four scenes.

Table 4.2: The ranking order of the experienced difficulty in estimating the light directions for Scene E, F G and H over 15 observers. The smaller the ranking order is, the more difficulty the observers encountered.

Scenes	Ranked as 1 (most difficult)	Ranked as 2	Ranked as 3	Ranked as 4 (easiest)
Scene E	12	1	0	2
Scene F	0	7	6	2
Scene G	2	6	7	0
Scene H	1	1	2	11

4.6. Discussion and conclusions

The aim of this study was to investigate the potential effects of scene content and layout on the perceived light direction in an interior space. It should be noted that this research was performed using a viewing box. If the observers would be able to really enter the scenes, they might get more information about the light direction from, for instance, Thermal effects of infrared radition or intraocular light scattering [29]. In this study, two experiments were designed with the first one studying whether this kind of influence exists and the second one studying which properties of the objects in the scene influence the light direction estimation in a systematic way.

We found that observers were sensitive to the light direction (the light direction was parameterized as light source position in our specific experimental setup), but its veridicality was dependent on the scene content and layout. Generally speaking, increasing the number of visible faces of the objects and using globally spherical shapes in the scene both resulted in more veridical estimations of the light direction. Furthermore, arranging scenes symmetrically improved the observer's inference of the light tilt direction.

We see two candidates for cues that help the estimation of the light direction. The first cue is the shading variation over the objects' surfaces and the second cue is the "illuminance flow" over the scene (i.e., the spatial variation in brightness over the scene due to illumination). The number of visible faces of the objects increased from Shape I to Shape II and Shape III, generating more steps in the shading pattern over the objects, which resulted in a more veridical estimation of the light direction. Khang et al. [13] found that increasing numbers of faces on 3D shapes was helpful for the interpretation of the surface reflectance variations on the shapes. To discriminate the reflectance variations, the shading effect derived from the interaction between the geometry and

lighting should be taken into account. Our results directly showed that the light direction estimation could benefit from increasing the number of faces. Furthermore, we found that a globally spherical shape resulted in a more veridical estimation of the light direction than more flattened shapes. Since our probe was also globally spherical, a reason might be the fact that the shading patterns were more comparable for this case than for the flattened shapes. Alternatively, estimation of the light direction from a shape can be expected to depend on that shape, similar to Koenderink et al.'s finding that observers' detection of light direction was systematically confounded with surface structure (e.g. comparing light direction estimation for isotropic rough surfaces with that for anisotropic rough surfaces) [17]. Let's take as an example an extreme case of a flattened shape, like a piece of paper. In such a case, observers can detect whether the light source is in front of the paper or behind the paper, but not from which direction the light comes exactly. The surface normals of a globally spherical shape are sampled rather homogeneously across all directions. In combination with a prior for global convexity [18] this could result in more veridical estimates.

The second candidate cue concerns the "illuminance flow" over the scene [17, 25]. The variation of illuminance on the macroscale is usually denoted as "shading". The "illuminance flow" provides additional cues about the light direction to the "shading". We found that mirror arrangements in the scene improved the estimation of the tilt direction, and tilt angles were consistently estimated with a smaller spread than slant angles. These two phenomena can both be explained using the "illuminance flow" theory. The "illuminance flow" is used to describe the 3D texture variation due to illuminated surface mesorelief and can also be estimated from arbitrary natural images [25]. Xia et al. proved that the "illuminance flow" over a rough sphere was helpful in estimating the light direction in real scenes [34]. Figure 4.13 shows photographs of the optical mixtures of Scene A with the probe under the nine light directions P1 to P9. These photographs were converted to grayscale and posterized from 255 to 6 gray levels in order to more clearly show the orientation of the spatial pattern in brightness gradient due to the "illuminance flow". We can see that it is difficult to estimate the depth of the light source (i.e., the slant angle) due to the lack of depth information, while the shadow patterns, e.g. the pattern of shadow edge orientations, gives salient information about the tilt angle.

To summarize, human being's light direction perception can be influenced by the scene content and layout in a space. The interplay between the lighting and the furnishing of a room (i.e., its materials, geometries and the arrangement of content inside) shapes the architectural space and the light field in it [11, 20, 30]. Human beings see the resulting scene in this space as a whole. Humans are able to distinguish the basic properties of lighting, shapes and materials through millions of years of evolution. But image ambiguities cause perceptual interactions because light, material, shape and space perception are truly confounded [1, 6, 12, 27, 31]. Thus, studying what human observers are capable of in extracting the basic properties of light, material, shape and space should be done in an integrated manner.

(a) P9   (b) P8   (c) P7

(d) P6   (e) P5   (f) P4

(g) P3   (h) P2   (i) P1
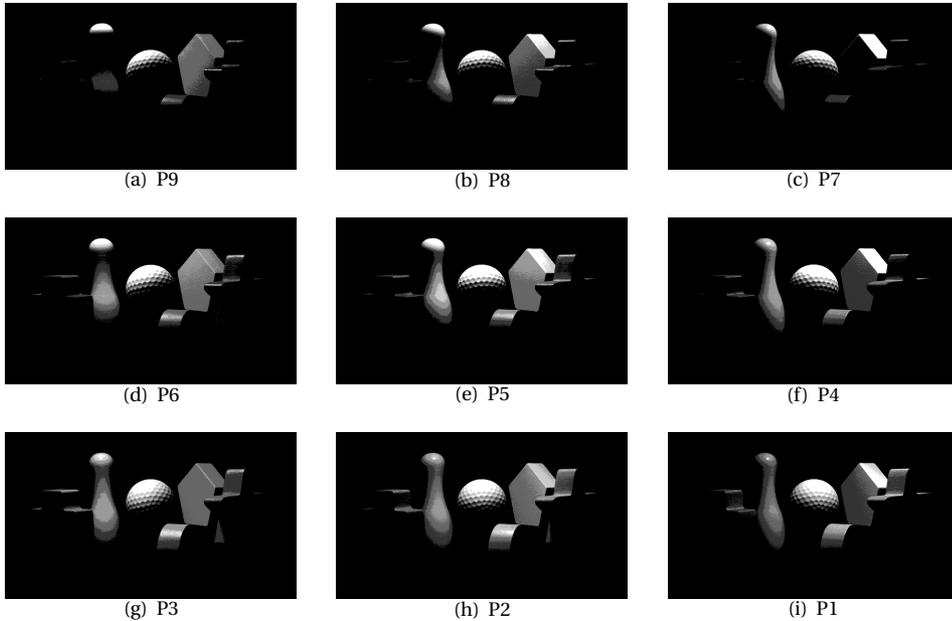
Figure 4.13: Photographs of the optical mixtures of scene A with the probe under nine light directions from P1 to P9 (shown in Figure 4.2). Note that the image was converted to grayscale and posterized from 255 to 6 gray levels.

References

[1] Peter N Belhumeur, David J Kriegman, and Alan L Yuille. The bas-relief ambiguity. *International journal of computer vision*, 35(1):33–44, 1999.

[2] Huseyin Boyaci, Katja Doerschner, and Laurence T Maloney. Cues to an equivalent lighting model. *Journal of Vision*, 6(2):2–2, 2006.

[3] David H Brainard. Color constancy in the nearly natural image. 2. achromatic loci. *JOSA A*, 15(2):307–325, 1998.

[4] David H Brainard, Wendy A Brunt, and Jon M Speigle. Color constancy in the nearly natural image. 1. asymmetric matches. *JOSA A*, 14(9):2091–2110, 1997.

[5] David Brewster. On the optical illusion of the conversion of cameos into intaglios and of intaglios into cameos, with an account of other analogous phenomena. *Edinburgh Journal of Science*, 4(1826):99–108, 1826.

[6] Ron O Dror, Alan S Willsky, and Edward H Adelson. Statistical characterization of real-world illumination. *Journal of Vision*, 4(9):11–11, 2004.

4

[7] Andreī Gershun. The light field (translated by moon, parry hiram and timoshenko, gregory). *Journal of Mathematics and Physics*, 18(1):51–151, 1939.

[8] Alan Gilchrist, Christos Kossyfidis, Frederick Bonato, Tiziano Agostini, Joseph Cataliotti, Xiaojun Li, Branka Spehar, Vidal Annan, and Elias Economou. An anchoring theory of lightness perception. *Psychological review*, 106(4):795, 1999.

[9] Richard Langton Gregory. *The intelligent eye*. ERIC, 1970.

[10] Donald D Hoffman. *Visual intelligence: How we create what we see*. WW Norton & Company, 2000.

[11] Fil Hunter, Steven Biver, and Paul Fuqua. *Light–science & Magic: An Introduction to Photographic Lighting*. Taylor & Francis, 2007.

[12] V Imamoglu. The effect of furniture on the subjective evaluation of spaciousness and estimation of size of rooms. *Architectural psychology*, pages 314–352, 1973.

[13] Byung-Geun Khang, Jan J Koenderink, and Astrid ML Kappers. Perception of surface reflectance of 3-d geometrical shapes: Influence of the lighting mode. *Perception*, 32(11):1311–1324, 2003.

[14] Byung-Geun Khang, Jan J Koenderink, and Astrid ML Kappers. Perception of illumination direction in images of 3-d convex objects: Influence of surface materials and light fields. *Perception*, 35(5):625–645, 2006.

[15] Byung-Geun Khang, Jan J Koenderink, and Astrid ML Kappers. Shape from shading from images rendered with various surface types and light fields. *Perception*, 36(8):1191–1213, 2007.

[16] Jan J Koenderink, Andrea J van Doorn, Astrid ML Kappers, Susan F Te Pas, and Sylvia C Pont. Illumination direction from texture shading. *JOSA A*, 20(6):987–995, 2003.

[17] Jan J Koenderink, Andrea J Van Doorn, and Sylvia C Pont. Perception of illuminance flow in the case of anisotropic rough surfaces. *Perception & psychophysics*, 69(6):895–903, 2007.

[18] Michael S Langer and Heinrich H Bülthoff. A prior for global convexity in local shape-from-shading. *Perception*, 30(4):403–410, 2001.

[19] Laurence T Maloney, Holly E Gerhard, Huseyin Boyaci, Katja Doerschner, LR Harris, and MRM Jenkin. Surface color perception and light field estimation in 3d scenes. *Vision in 3D environments*, pages 280–307, 2011.

[20] Lou Michel. *Light: the shape of space: designing with space and light*. John Wiley & Sons, 1995.

[21] Ennio Mingolla and James T Todd. Perception of solid shape from shading. *Biological cybernetics*, 53(3):137–151, 1986.

[22] Alexander Alexeevich Mury. *The light field in natural scenes*. PhD thesis, TU Delft, Delft University of Technology, 2009.

[23] James P O'Shea, Maneesh Agrawala, and Martin S Banks. The influence of shape cues on the perception of lighting direction. *Journal of vision*, 10(12):21, 2010.

[24] Alex P Pentland. Finding the illuminant direction. *JOSA*, 72(4):448–455, 1982.

[25] Sylvia Pont and Jan Koenderink. Surface illuminance flow. In *3D Data Processing, Visualization and Transmission, 2004. 3DPVT 2004. Proceedings. 2nd International Symposium on*, pages 2–9. IEEE, 2004.

[26] Sylvia C Pont and Jan J Koenderink. Matching illumination of solid objects. *Perception & psychophysics*, 69(3):459–468, 2007.

[27] Vilayanur S Ramachandran. Perception of shape from shading. *Nature*, 1988.

[28] David Rittenhouse. Explanation of an optical deception. *Transactions of the American Philosophical Society*, 2:37–42, 1786.

[29] TJTP Van den Berg. Importance of pathological intraocular light scatter for visual disability. *Documenta Ophthalmologica*, 61(3-4):327–333, 1986.

[30] Andrea J van Doorn, Jan J Koenderink, and Johan Wagemans. Light fields and shape from shading. *Journal of Vision*, 11(3):21–21, 2011.

[31] Christoph von Castell, Daniel Oberfeld, and Heiko Hecht. The effect of furnishing on perceived spatial dimensions and spaciousness of interior space. *PloS one*, 9(11):e113267, 2014.

[32] Ling Xia, Sylvia Pont, and Ingrid Heynderickx. The influence of scene layout and content on the perception of light direction in real scenes. *Journal of Vision*, 14(10):71–71, 2014.

[33] Ling Xia, Sylvia C Pont, and Ingrid Heynderickx. Probing light in real scenes using optical mixtures. In *Proceedings of the ACM Symposium on Applied Perception*, pages 137–137. ACM, 2013.

[34] Ling Xia, Sylvia C Pont, and Ingrid Heynderickx. The visual light field in real scenes. *i-Perception*, 5(7):613–629, 2014.

4

5

OBJECTIVE MEASURES: THEORY

Abstract

The light density, direction and diffuseness are important indicators of the spatial and form-giving character of light. Mury presented a method to describe, measure and visualize the light field's structure in terms of light density and direction variations in 3D spaces. We extend this work with a theoretical and empirical review of four diffuseness metrics leading to a novel metric proposal D_{Xia}. In particular, the relationships between these diffuseness metrics were studied using a model named "probe in a sphere". Diffuseness metric D_{Xia} re-frames the diffuseness metric of Cuttle in an integral description of the light field. It fulfils all diffuseness criteria and has the advantage that it can be used in a global, integrated description of the light flow and diffuseness throughout three-dimensional spaces.

5

5.1. Introduction

Since the lighting profession emerged, lighting standards around the world have been concerned almost exclusively with the delivery of luminous flux onto planes [43]. However, it is the distribution of light that determines the appearance of a space and the objects inside it. Inspiringly, this concept has been well acknowledged by photographers[22], painters [3, 18], designers [16] and architects [12, 32]. Rather than thinking about the illumination as a medium that makes things visible, modern designers prefer to see lighting principally in terms of how it influences the appearance of people's surroundings and create certain atmospheres [5, 8, 9, 25–27].

In their psychophysical research, Koenderink et al. found that human observers have expectations of how an object would look like when it was introduced at an arbitrary location in a scene [28]. Schirillo [45] confirmed that human observers have a mental representation of the light in a three-dimensional space through both direct and indirect evidence of our awareness of the light field. The light field in natural scenes is highly complicated due to intricate optical interactions, containing low and high frequencies in the radiance distribution function. Nonetheless, studies show that the human visual system (HVS) is able to distinguish the intensity, the primary illumination direction, and the diffuseness, which are three basic (low-order) properties of a light field [28, 29, 41, 47]. Furthermore, research showed that these low order properties of the light field stay rather constant within a certain geometry of the scene[35] and that they are sufficient to describe the appearance of most natural materials because the diffuse scattering characteristic of these materials act as a low pass filter [2, 14, 19, 42].

By introducing the notion of radiant "light density" and the notion of "light vector", Gershun [17] described the quantity and transfer direction of the radiant power through space in his 5-dimensional function of the light field. Mury et al. [38] used spherical harmonic (SH) decompositions to represent natural light as a combination of components of different orders. He found that the zeroth order component of the SH decomposition corresponds to Gershun's "density of light", which describes a constant illumination from all directions and is usually known as "ambient light" in computer graphics; the first order component was found to correspond to the "light vector" as defined by Gershun, which describes the net transport of radiant energy. However, neither Gershun nor Mury mentioned diffuseness of light in their mathematical descriptions of the physical light field.

The local light diffuseness describes the isotropy of a light distribution around a point in a space. It ranges from fully collimated light via hemispherical diffuseness to completely diffuse light. Fully collimated light comes from a single direction; in contrast, completely diffuse light comes from a sphere of directions. Light diffuseness can highly influence the appearance of scenes and objects in it, because shading, shadowing and vignetting effects co-vary with the diffuseness, as can be seen in Figure 5.1. Direct sunlight is a typical example of collimated light, an overcast sky of hemispherical diffuse light and a polar whiteout of completely diffuse light. Collimated light creates an effect of focusing by generating hard, crisp-edged body shadows and a large brightness contrast, like the visual effect on sculptures in a museum created by spotlights. Hemispherical diffuse light is the level of diffuseness that we encounter in daily life most frequently, for in-
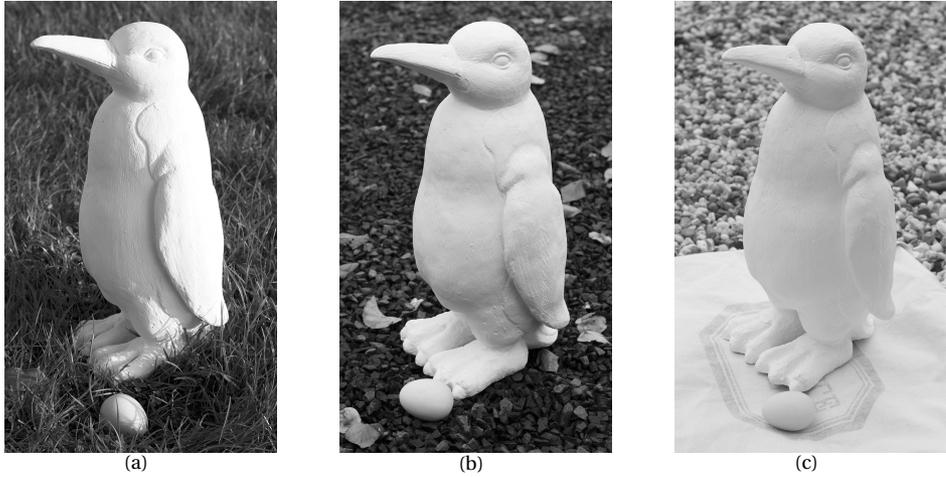
(a)   (b)   (c)

Figure 5.1: The appearance of a penguin statue under light with different diffuseness levels: (a) direct sunlight, (b) overcast sky above a dark ground surface, and (c) overcast sky above a light ground surface.

stance under a cloudy sky. Completely diffuse light is characterized by a totally uniform light distribution and makes three-dimensional shapes appear flat, e.g. as the scenery when skiing in the mist.

The influence of the spatial distribution of light on object shape appearance has been studied through the notion of "modelling index" in interior lighting design. Examples are the "ratio between the cylindrical and horizontal illuminance" by Hewitt [20], the "vector/scalar illumination ratio" (i.e., the strength of flow of light) by Cuttle [6, 30], and the vertical and horizontal modelling indicators (VMI and HMI) by Bean [4]. Since these "modelling indices" are highly correlated with the light diffuseness, they are also considered as diffuseness metrics in our study. But, apart from using these "modelling indices", we focus in the rest of this study on the light distribution, and not its effects on object appearance or how the resulting optical structures are interpreted by the human visual system. Relationships between the light diffuseness and objects' appearance are addressed in detail in other studies [12, 33, 40, 48].

Besides the "modelling indices", other practical ways to quantify diffuseness have been proposed. Frandsen proposed the scale of light to indicate the potential of an illumination distribution to form shadow patterns over 3D opaque objects [15]. Morgenstern et al. [33, 34] proposed the ICE (Illuminance Contrast Energy), a measure of the contrast over a white matte spherical gauge object . Inanici [23] used the directional-to-diffuse ratio to quantify the diffuseness of light by isolating the diffuse and directional components of a rendered luminous environment .

Thus, various practically defined diffuseness metrics exist but they differ from each other by definition and were implemented in different fields. In order to propose a general and principled way to define and measure light diffuseness, we defined criteria for

the diffuseness metric: A. the metric should describe the full range of diffuseness in a smooth and monotonous manner, B. it should be possible to physically measure the metric, C. The metric should describe the light distribution directly instead of via the appearance of some object, D. it should be possible to easily implement the metric in commercially available optical measurement systems as well as in computer simulations and in a manner that relates to human perception.

In the following sections, we give a review of four well-known diffuseness metrics, which are (1) the "scale of light" by Frandsen [15], (2) the "ratio between cylindrical and horizontal illuminance" by Hewitt et al. [20], (3) the "ratio between illumination vector and scalar" by Cuttle [6, 30], and (4) the "ICE" by Morgenstern et al. [33]. We compare each of these four metrics to the criteria proposed above. Next, inspired by Mury's work on the physical SH representation of the light field and by the basic parameterization of diffuseness as the balance between the ambient and directed light, we prove that Cuttle's "ratio between illumination vector and scalar" (hereafter referred to as D_{Cuttle}) is equivalent to the ratio between the strength of the first order (i.e., the light vector) and the zeroth order (i.e., the light density) of the SH representation of the light field (this ratio is hereafter referred to as D_{Xia}). The diffuseness metric D_{Xia} is entirely based on a mathematical description of the physical light distribution and fulfils all the criteria mentioned above.

Since the relationships between these metrics were so far unclear, we examined them via a model named "probe in a sphere". As Figure 5.2 illustrates, this model consists of a probe (usually, a small white sphere with a Lambertian surface) put right in the center of a big spherical light source with a variable subtended angle. The size of the functional light source is defined by the subtended angle α (see the upper arc depicting the spherical light source in Figure 5.2). The diameter of the spherical light source is much larger than the probe inside (i.e. which basically means that it is at infinite). Thus, by varying the subtended angle α from 0° via 180° to 360°, the degree of diffuseness varies from totally collimated light via hemispherical diffuse to completely diffuse light. This model was first implemented by Cuttle to investigate how the surrounding luminous field influenced the vector/scalar ratio [12]. The model "probe in a sphere" should be considered as a physics model (a simplified representation of something that is either too difficult or impossible to display directly) for natural situations (like daylight on a city square, museum lighting and office lighting). It allows systematic theoretical studies and comparisons of metrics. In addition, in our paper "Light diffuseness metrics Part 2" we consider empirically measured light fields.

5.2. Frandsen's scale of light

5.2.1. Theory

Frandsen proposed the scale of light, which is derived from the comparison between the size of a light source and that of an illuminated object. This relationship is reflected by the self-shadows on an object, which indicate the degree of light diffuseness [15]. Yağmur et al. recently found that the harshness-softness attribute of cast-shadows also
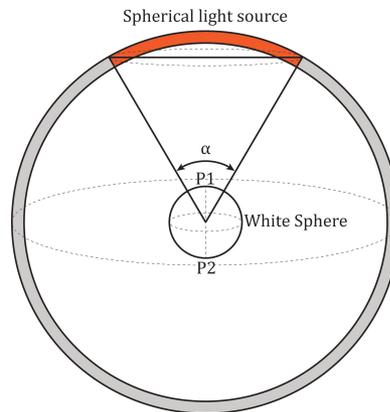
Figure 5.2: Illustration of the computational model "probe in a sphere", a white Lambertian sphere is put right in the center of a large spherical light source. The size of the light source varies with the subtended angle α. The outer spherical light source is assumed to be at infinity.

5

depends on the scale of light; the shadows are softer when the luminaire size increases, or the object size decreases [1].

Frandsen's approach is analogous to our "probe in a sphere" approach. In Frandsen's theory, the solid angle of light source (α in our model) varied from narrow (i.e. 0°, collimated) to hemispherically diffuse (i.e. 180°). As Figure 5.3 (a) shows, when the subtended angle is smaller than 180°, the white sphere can be divided into three zones. The top zone facing the circular light source receives light from the entire source. The bottom zone turned away from the source receives no light. The middle zone receives a varying amount of light from the source, creating a so-called semi-shadow. Frandsen scaled the diffuseness in the range from fully collimated to hemispherical diffuseness based on the ratio of the area of the semi-shadow to the area of the whole sphere. Diffuseness then increases from 0% to 100%, as the subtended angle varies from 0° to 180°. Frandsen scaled this change into 11 steps with an interval of 10%. The left part of Table 5.1 gives detailed information about the scale of light from a fully collimated light to a hemispherical diffuse light as defined by Frandsen ($D_{Frandsen}$).

The scale of light, however, is hard to measure in a real environment. It cannot be judged accurately from the appearance of objects, for instance using a matte sphere as a reference, because small steps in diffuseness are hard to be distinguished in this manner [24, 41, 49, 50]. Moreover, perceived diffuseness is dependent on viewing direction[31, 41]. Furthermore, Frandsen's scale with 11 types of shadows is limited to the range from fully collimated light to hemispherical diffuse light. The other half range from hemispherical diffuse to completely diffuse light is ignored. So, the scale of light does not fulfil criteria A, B, C and D.
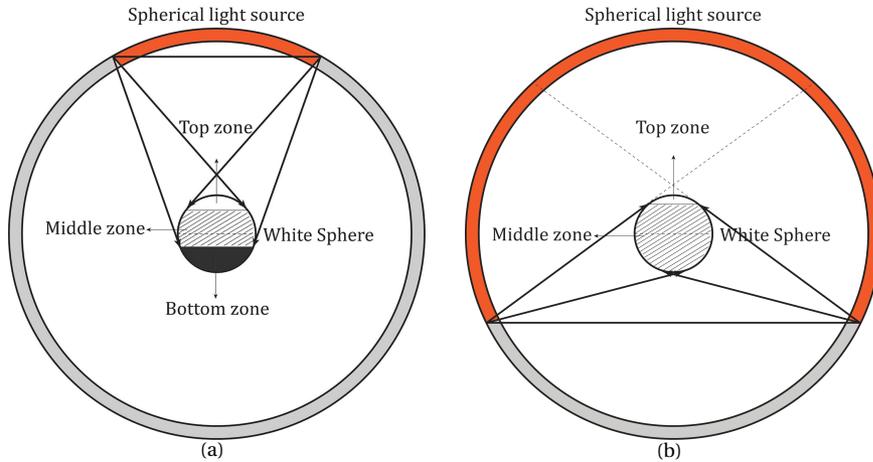
Figure 5.3: Illustration of shadowing zones on a white matte sphere according to Frandsen. In (a): when the subtended angle is smaller than 180°, the white sphere in the center of the spherical light source is divided into three zones: the top zone receives light from the entire source, the middle zone receives a varying amount of light from the source, and the bottom zone receives no light from the source. In (b): when the subtended angle is larger than 180°, the white sphere in the center of the spherical light source is divided into two zones: there's no bottom zone receiving no light.

5.2.2. $D_{Frandsen}$ for the "probe in a sphere" model

In order to be able to compare all metrics, we extended $D_{Frandsen}$ to the full range of possible diffuseness. As Figure 5.3 (b) shows, when the subtended angle is larger than 180°, the white sphere can be divided into two zones. The top zone always receives the same amount of light, as it would from a hemispherical light source. The middle zone receives a varying amount of light from the source. The bottom zone disappears because every part of the sphere is now illuminated. As a consequence, we can extend the scale of light from hemispherical diffuse to totally diffuse by still using the ratio of the area of the semi-shadow to the area of the whole sphere as proposed by Frandsen. As the subtended angle gets larger, the area of the top zone increases and the ratio of the semi-shadow to the area of the whole sphere decreases, but this ratio always remains larger than 50%. We used an interval of 5% in the ratio in order to divide the scale in an equal number of steps for the extended part of the range as for the original range from collimated to hemispherical diffuse. In this manner, we extended Frandsen's scale of light from 0-10 to 0-20. The right part of Table 5.1 gives detailed information about this extended scale, and the appearance of a Lambertian white sphere under the different scale values is illustrated in Figure 5.4. The resulting values are shown in Figure 5.7 (a) and (b).
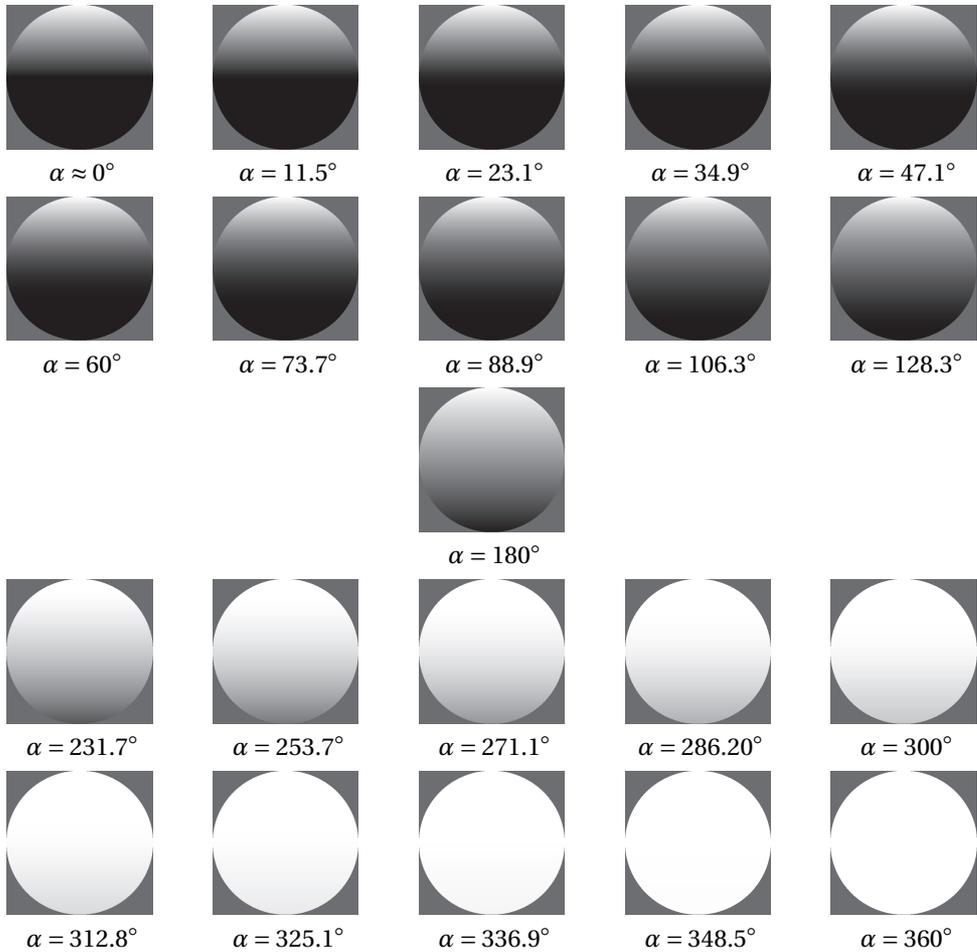
Figure 5.4: The appearance of a rendered Lambertian white sphere in the center of a large spherical light source with variable subtended angle α. The subtended angle varies from 0° via 180° to 360°, and the corresponding diffuseness varied from fully collimated light via hemispherical diffuse to totally diffuse light.

Table 5.1: The left part shows the scale of light as defined by Frandsen, for the range of collimated light to hemispherical diffuse light; the right part shows our extension of the scale of light, for the range from hemispherical diffuse to totally diffuse light.

	$D_{Frandsen}$			$Extended D_{Frandsen}$	
α	Ratio	Scale	α	Ratio	Scale
$\approx 0°$	0%	0	231.7°	95%	11
11.5°	10%	1	253.7°	90%	12
23.1°	20%	2	271.1°	85%	13
34.9°	30%	3	286.2°	80%	14
47.1°	40%	4	300°	75%	15
60.0°	50%	5	312.8°	70%	16
73.7°	60%	6	325.1°	65%	17
88.9°	70%	7	336.9°	60%	18
106.3°	80%	8	348.5°	55%	19
128.3°	90%	9	360°	50%	20
180°	100%	10			

5.3. Hewitt et al.'s cylindrical/horizontal illuminance ratio

5.3.1. Theory

People have noticed that compared to horizontal illumination, which is a provision of task illumination, vertical illumination contributes more to the impression of a space and helps people to recognize shapes and faces. Hewitt et al. have shown that the ratio of horizontal illuminance to mean vertical illuminance gives a reasonable indication of modelling [20]. The average vertical illuminance can be measured using the cylindrical illuminance, which is defined as the total luminous flux falling on the curved surface of a small cylinder at a point of interest, divided by the curved surface area of the cylinder [39]. Instruments exist for the direct measurement of cylindrical illuminance, but their costs are high. An alternative method for obtaining cylindrical illuminance was proposed by Duff et al., i.e. calculating it from the illuminance values measured using a cubic meter [13, 44]. The ratio between the cylindrical illuminance (E_c) and horizontal illuminance (E_h) is proposed as an index of modelling for overhead lighting installations [43] and is hereafter referred to as diffuseness metric D_{Hewitt}. A modelling index between 0.3 and 0.6 is suggested to indicate good modelling [43].

The ratio between cylindrical and horizontal illuminance does fulfil the criteria we have defined for a diffuseness metric. However, it can only indicate the "modelling" properties of an overhead lighting installation. For pure overhead lighting it is assumed to provide a rough assessment of the relationship between the rather diffuse light from (inter-)reflections and the rather directed light from primary light sources. However, the assumptions are violated in many real scenes, for instance if there is also light entering from the side via windows.

5.3.2. D_{Hewitt} for the "probe in a sphere" model

We calculated D_{Hewitt} in the "probe in a sphere" model by replacing the white sphere with a small cylinder. The cylinder was placed with its main axis along the vertical axis in Figure 5.2 so that the average illuminance on the curved surface represents the mean vertical illuminance. D_{Hewitt} varied from "0" for collimated light to "1" for fully diffuse light. The resulting values as a function of subtended angle α are shown in Figure 5.7 (a) and (b).

5.4. Cuttle's vector/scalar illumination ratio

5.4.1. Theory

Hewitt [21] and Lynes et al. [21, 30] proposed the concept of the "flow of light" to de-scribe the potential of light to produce distinct shading patterns. The "flow of light" concept gives information on the direction from which the light comes on average, and on how strongly directed the net light transport is. Cuttle et al. [11] defined the appar-ent strength of the "flow of light" by the illumination vector/scalar ratio (E_{vector}/E_{scalar}), and recommended it as a modelling index . We refer to E_{vector}/E_{scalar} as diffuse-ness metric D_{Cuttle}. The vector component indicates the direction of the "flow of light". The illumination scalar equals the average value of the "illumination solid" over all di-rections, and it is a measure of the ambient light. In general, the "illumination solid" around an illuminated point can be separated into two components: a vector compo-nent and a symmetric component. The vector component is totally asymmetric around the illuminated point, while the symmetric component is totally symmetric around the illuminated point [6, 12]. We refer to Appendix A for the detailed information.

   Though the illumination vector and scalar are defined based on the luminous power distribution in the space, their values and the metric are explained via the appearance of a small matte white sphere. The illumination vector can be reproduced by a distant light source with the illuminance falling on a small sphere as illustrated in Figure 5.5. The magnitude of the vector illuminance can then be approached as the difference between the illuminance on the top point and the bottom point of the matte white sphere:

$$E_{vector} = E_{p1} - E_{p2} \tag{5.1}$$

The scalar illuminance value equals the average illuminance over the whole surface of the sphere and can be calculated as:

$$E_{scalar} = E_{vector}/4 + \bar{E}_{symmetric} \tag{5.2}$$

where $\bar{E}_{symmetric}$ is the average value of the symmetric component over all directions. Thus, the maximum value of D_{Cuttle} is 4, occurring with fully collimated light (i.e., the vector component only) and the minimum value is 0, occurring with completely diffuse light (i.e., the symmetric component only). It has been found that D_{Cuttle} values in the

range of 1.2 to 1.8 are preferred for the appearance of human features in an interview situation [11]. Preference studies also showed that people like the flow of light to be from the top-left/right rather than from the top, with a preference for a vector altitude between 15° and 45° [11].

Later, Cuttle developed a cubic illumination meter to measure the illumination vector, the illumination scalar and the strength of the "flow of light" or D_{Cuttle}[7, 10]. The cubic meter is a small cube with six illuminance meters mounted at its six faces. Thus, Cuttle's method fulfils all our criteria for a diffuseness metric.
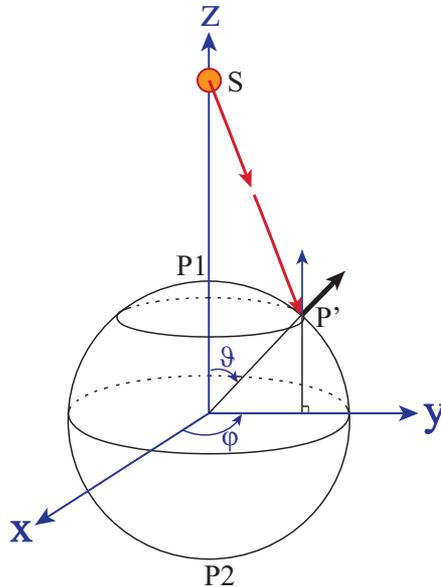
Figure 5.5: Illustration of a unit matte sphere in Figure 5.2 under a fully collimated light with the subtended angle α approaching 0°. P1 is the top point of the white sphere and P2 is the bottom point of the white sphere.

5.4.2. D_{Cuttle} for the "probe in a sphere" model

The illumination scalar proposed by Cuttle in Equation 5.2 represents the average illumination over the sphere surface, derived from the contributions of both the vector and the symmetrical components. The vector component contributes $E_{vector}/4$ to the average illumination over the matte sphere, which can be derived analytically. For instance in Figure 5.5, the bottom hemisphere receives no light ($E_{p2} = 0$) and the illumination falling on the upper hemisphere is directly proportional to the cosine of the angle ϑ between the direction of the light source (i.e., the z axis) and the surface normal. So, the contribution of the vector component to the average illumination over the unit

sphere follows:

$$
\begin{aligned}
(\mathbf{E_{vector}})_{\mathbf{scalar}} &= (E_{p1} - E_{p2})\frac{\int_0^{2\pi}\int_0^{\pi/2}\cos(\vartheta)\sin(\vartheta)\,d\vartheta d\varphi}{4\pi} \\
&= (E_{p1} - E_{p2})/4 \\
&= E_{vector}/4
\end{aligned}
\tag{5.3}
$$

By varying the subtended angle from 0° to 360°, the diffuseness level in our model "probe in a sphere" varies from fully collimated light to fully diffuse light while the vector/scalar illumination ratio varies from 4 to 0 as shown in Figure 5.7(a). The normalized form of D_{Cuttle} is:

$$
(D_{Cuttle})_{Normalized} = 1 - (E_{vector}/E_{scalar})/4
\tag{5.4}
$$

which is shown in Figure 5.7 (b), with "0" corresponding to fully collimated light and "1" corresponding to fully diffuse light.

5.5. Morgenstern et al.'s illuminance contrast energy

5.5.1. Theory

The contrast of a shading pattern over a sphere varies with the degree of light diffuseness. Morgenstern et al. defined a new method, the ICE (Illuminance Contrast Energy) to quantify this variation[33]. If $E(\vartheta, \varphi)$ is the illuminance over the surface of a unit sphere, where ϑ is the altitude from the north pole and φ is the azimuth in a spherical coordinate system, the ICE can be calculated as:

$$
ICE = (\frac{1}{4\pi}\int_0^{2\pi}\int_0^{\pi}(\frac{E(\vartheta,\varphi) - \bar{E}}{\bar{E}})^2 \sin(\vartheta)\,d\vartheta d\varphi)^{1/2}
\tag{5.5}
$$

where $\bar{E}$ is the mean illuminance over the sphere. The value of ICE ranges from 0 for a completely diffuse light to 1.29 for a distant point light source. In order to measure the ICE, Morgenstern et al. used a custom-built multidirectional photometer with 64 evenly spaced photodiodes. These 64 photodiodes made low-resolution but omnidirectional records of the illumination incident from all directions at a point in space at a given time. As such, ICE does not fulfil criterium D, because it cannot be measured in real scenes without the custom-built photometer. It does not literally fulfil criterium C because in order to calculate the ICE the photometer records have to be transformed to values of the illuminance over the gauge sphere. Using their photodiode device, Morgenstern et al. made 570 measurements of the ICE in six natural environments and 53 measurements in a single day from sunrise to sunset [33]. The mean ICE under these circumstances ranged from 0.41 to 0.66.

5.5.2. $D_{Morgenstern}$ **for the "probe in a sphere" model**

We calculated the ICE directly from the illuminance distribution on the small white Lambertian sphere inside the spherical model using Equation 5.5. The resulting values as a function of subtended angle α are shown in Figure 5.7 (a) and (b). The resulting curve is less than 6% higher than the D_{Cuttle} curve in the lower and middle part of the diffuseness range. Overall, the shape of the curve $D_{Morgenstern}$ in this model clearly closely resembles the shape of the D_{Hewitt} and D_{Cuttle} curves.

5.6. D$_{Xia}$: framing "diffuseness" in an integral light field description

From the above review we found that $D_{Morgenstern}$ and $D_{Frandsen}$ did not fulfil all criteria for a diffuseness metric. D_{Hewitt} fulfilled all criteria, but was limited to indicate the light diffuseness properties of overhead lighting. D_{Cuttle} fulfilled all criteria. However, the relationship between D_{Cuttle} and the other properties of the light field (i.e. light density, direction) has not been worked out. In this section, we therefore frame this diffuseness definition in an integral light field description. We call the framed metric D_{Xia}, which is thus conceptually the same as D_{Cuttle} but mathematically framed in a different way. The description of D_{Xia} is based on a mathematical description of the physical light distribution in space instead of on the appearance of an object. D_{Xia} fulfils all criteria and has the advantage that it can be used in a global, integrated description of the light distribution in 3D spaces, in which all modes of the description have a specific physical meaning. The development of D_{Xia} is based on the work of Mury et al. [35–37], i.e., on the physical interpretation of the spherical harmonics representation of the light field in natural scenes, and extends it with a diffuseness metric.

5.6.1. Theory

Locally, the light field is a function of direction and thus a spherical function. We know that any spherical function $f(\vartheta, \varphi)$ can be reconstructed by the sum of its spherical harmonics (SH):

$$f(\vartheta, \varphi) = \sum_{l=0}^{\infty} \sum_{m=-l}^{l} C_l^m Y_l^m(\vartheta, \varphi) \tag{5.6}$$

where C_l^m are the coefficients, $Y_l^m(\vartheta, \varphi)$ are the basis functions, and l represents the order of the angular mode. Each mode consists of $2l + 1$ basis functions ($l \geq 0, -l \leq m \leq l$). Figure 5.6 shows the real-valued spherical harmonic basis functions up to the second order. Any mode l can be represented as a vector of corresponding coefficients $SH_l(f) = \{C_l^{-l}, C_l^{-l+1}, \cdots, C_l^l\}$ and the representation of the entire function is a combination of all the modes, i.e. $SH(f) = \{SH_0(f), SH_1(f), SH_2(f), \cdots\}$. The strength of each mode l can

be calculated using Equation 5.7 [46]:

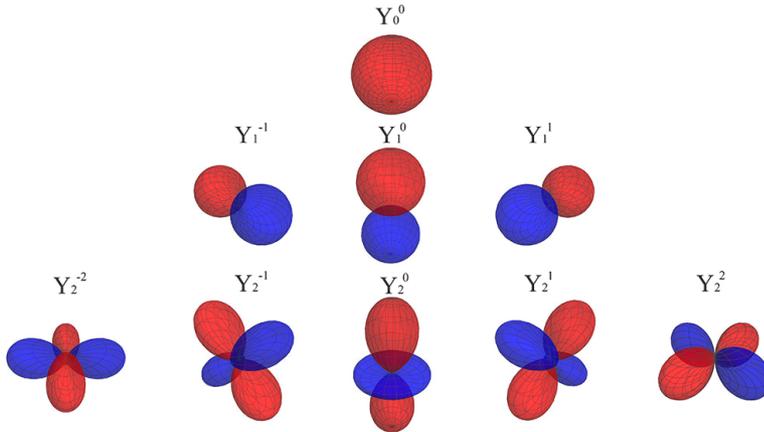$$d(SH_l) = \sqrt{\sum_{m=-l}^{l} (C_l^m)^2}$$ (5.7)

Figure 5.6: Plots of real -valued spherical harmonic basis functions. The first row represents the zeroth order, the second row shows the basis functions of the first order and the third row shows the basis functions of the second order components. Red indicates positive values and blue indicates negative values. For a detailed explanation of the analogy between the SH description and Gershun's theory, see work by Mury et al. [35, 36, 38].

Ramamoorthi et al. proved that for convex Lambertian objects, complex lighting distributions may be successfully replaced by the second order approximation of their SH representation [42]. Mury et al. [35, 36, 38] found that the zeroth order component of a spherical harmonic corresponds to Gershun's "density of light". The zeroth order component is a monopole (see the first row of Figure 5.6), essentially the average radiance over all directions. The first order component corresponds to Gershun's "light vector" and describes the net transport direction of radiant energy. The first order component can be thought of as a dipole and consists of a positive and a negative mode (see the second row of Figure 5.6). We define our diffuseness metric as the ratio between the light vector and the density of light, or in mathematical SH terms:

$$D_{Xia} = d(L_1)/d(L_0)$$ (5.8)

D_{Cuttle} and D_{Xia} are thus conceptually the same, but mathematically they are framed in a different manner. So, how are they mathematically related to each other and what are the (dis)advantages of the two approaches? In order to answer this question, we first express D_{Xia} in terms of the ratio $d(E_1)/d(E_0)$, which is the ratio between the first order and zeroth order SH modes of the irradiance. Ramamoorthi and Hanrahan [42] proved that for convex Lambertian objects, the relation between irradiance and radiance of the

zeroth order SH coefficient is :

$$E_0^0 = \pi \times L_0^0 \qquad (5.9)$$

and of the first order SH is:

$$E_1^m = \frac{2\pi}{3} \times L_1^m, \quad m = -1, 0, 1 \qquad (5.10)$$

Hence:

$$\frac{d(L_1)}{d(L_0)} = \frac{3}{2} \frac{d(E_1)}{d(E_0)} \qquad (5.11)$$

Second, we express D_{Cuttle}, defined as the ratio between E_{vector} and E_{scalar}, in terms of $d(E_1)/d(E_0)$. To do so, we first examine the relationship between $d(E_1)$ and E_{vector}. The E_{vector} was defined as the maximum value of the illuminance difference. However, the SH representation of the illumination distribution accounts for the illumination in all directions. Therefore, we calculated the magnitude of the vector component over the surface of a sphere projected along the direction of the light vector (e.g., the z axis in Figure 5.5) as:

$$E'_{vector} = (E_{p1} - E_{p2}) \int_0^{2\pi} \int_0^{\pi/2} cos(\vartheta) cos(\vartheta) sin(\vartheta) d\vartheta d\varphi$$
$$= \frac{2\pi}{3}(E_{p1} - E_{p2}) \qquad (5.12)$$

Thus, the magnitude of the vector component over the surface of a sphere E'_{vector} is a factor of $2\pi/3$ larger than Cuttle's E_{vector}.

The first order component of the SH approximation of the light field can be transformed into linear functions of the Cartesian coordinates (x, y, z) as follows:

$$\begin{cases} Y_1^{-1}(\vartheta, \varphi) = & -\sqrt{\frac{3}{4\pi}} sin\vartheta sin\varphi = -\sqrt{\frac{3}{4\pi}} y \\ Y_1^0(\vartheta, \varphi) = & \sqrt{\frac{3}{4\pi}} cos\vartheta = \sqrt{\frac{3}{4\pi}} z \\ Y_1^1(\vartheta, \varphi) = & -\sqrt{\frac{3}{4\pi}} sin\vartheta cos\varphi = -\sqrt{\frac{3}{4\pi}} x \end{cases} \qquad (5.13)$$

According to Equation 5.12 and Equation 5.13, the relationship between the magnitude of the light vector E_{vector} and the magnitude of the first order SH component $d(E_1)$ is:

$$E_{vector} = \frac{3}{2\pi} E'_{vector} = \frac{3}{2\pi} \sqrt{\frac{4\pi}{3}} d(E_1) = \sqrt{\frac{3}{\pi}} d(E_1) \qquad (5.14)$$

Subsequently, the relationship between $d(E_0)$ and E_{scalar} is derived. The illumination scalar is the average illuminance over the surface of a unit sphere, so $E_{scalar} = E_o/4\pi$, where E_o is the overall illumination on the sphere. We find:

$$\begin{aligned} \frac{E_{scalar}}{d(E_0)} &= \frac{E_o/4\pi}{C_0^0} \\ &= \frac{1}{4\pi} \frac{\int_{\varphi=0}^{2\pi} \int_{\vartheta=0}^{\pi} f(\vartheta, \varphi) sin\vartheta d\vartheta d\varphi}{\int_{\varphi=0}^{2\pi} \int_{\vartheta=0}^{\pi} f(\vartheta, \varphi) Y_0^0(\vartheta, \varphi) sin\vartheta d\vartheta d\varphi} \\ &= \frac{1}{2\sqrt{\pi}} \end{aligned} \qquad (5.15)$$

Knowing all this, we find the relationship between $d(L_1)/d(L_0)$ (or D_{Xia}) and E_{vector}/E_{scalar} (or D_{Cuttle}) as:

$$\frac{E_{vector}}{E_{scalar}} = \frac{\sqrt{3/\pi}}{1/2\sqrt{\pi}} \frac{d(E_1)}{d(E_0)} = 2\sqrt{3} \frac{2}{3} \frac{d(L_1)}{d(L_0)} = \frac{4}{\sqrt{3}} \frac{d(L_1)}{d(L_0)} \tag{5.16}$$

Hence, the ratio between the illumination vector and scalar is a factor $2\sqrt{3}$ larger than $d(E_1)/d(E_0)$ and $4/\sqrt{3}$ larger than $d(L_1)/d(L_0)$. This result indicates that the diffuseness metric vector/scalar illumination ratio (D_{Cuttle}) is equivalent to the ratio between the strength of the first order and zeroth order of the SH representation of the physical light distribution (i.e., D_{Xia}). The only difference is that D_{Cuttle} is derived from the illuminance and D_{Xia} from the luminance. Since the ratio between E_{vector} and E_{scalar} varies from "4" for fully collimated light to "0" for fully diffuse light, we normalized the metric to a range "0" to "1". The final normalized form of D_{Xia} is:

$$(D_{Xia})_{Normalized} = 1 - d(L_1)/d(L_0)/\sqrt{3} \tag{5.17}$$

The diffuseness metric D_{Xia} fulfils all criteria we proposed before, and it is easily quantified and physically described based on a mathematical representation of the light field in 3D spaces.

5.6.2. D_{Xia} for the "probe in a sphere" model

We fitted SH representations to the luminance maps of our model, varying the subtended angle α from 0° to 360°. Then, the strength of the first and zeroth order components as well as their ratio ($d(L_1)/d(L_0)$) were calculated, and the results of D_{Xia} are shown in Figure 5.7 (a). The normalized curves of D_{Cuttle} and D_{Xia} in Figure 5.7 (b) indeed overlap.

5.7. Results and discussion

Figure 5.7 (a) illustrates the relationships between the five different diffuseness metrics mentioned above. To get a better overview of these relationships, we normalized all diffuseness metrics with "0" corresponding to fully collimated light and "1" corresponding to fully diffuse light in Figure 5.7 (b). In Figure 5.7 (b) we see that the normalized diffuseness metrics D_{Hewitt}, D_{Cuttle}, $D_{Morgenstern}$ and D_{Xia} give very similar results for the "probe in a sphere" model. There is a difference between these normalized diffuseness metrics and $D_{Frandsen}$. It should be noticed that while the other diffuseness metrics concern ratios, the "scale of light" ($D_{Frandsen}$) is an ordinal ranking. Since we want the metric to be perceptually relevant we need psychophysical data to make an argumented choice for the best metric. We are not aware of literature that relates perceptual diffuseness ratings to systematical variations of the physical diffuseness. We are only aware of perceptual matching data for diffuseness [24, 28, 41, 49, 50]. However, since the ratio-based metrics result in curves that resemble typical psychometric curves, we assume that these present the most plausible options for a perceptually relevant metric.
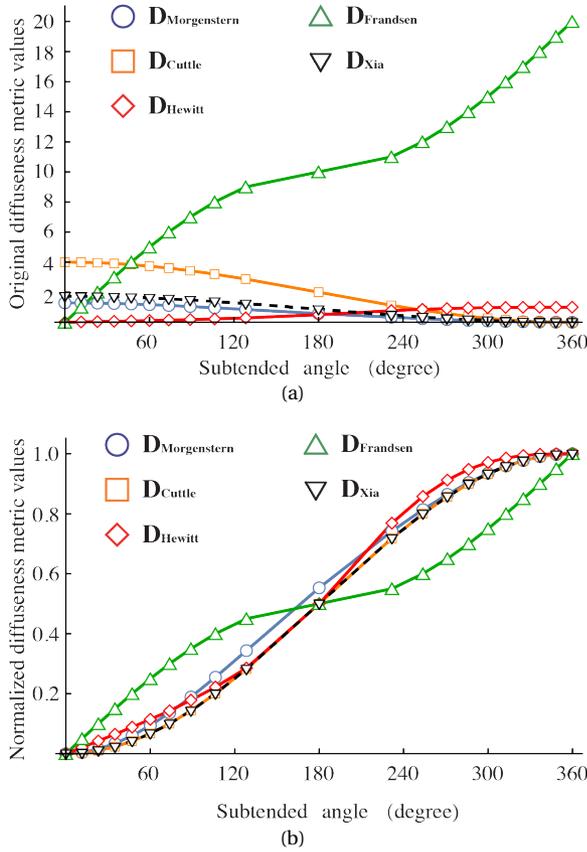
Figure 5.7: The five diffuseness metrics as a function of the subtended angle α in the model "probe in a sphere": (extended) $D_{Frandsen}$, D_{Hewitt}, D_{Cuttle}, $D_{Morgenstern}$ and D_{Xia}. In (a) the original metric values and in (b) all diffuseness metrics normalized to the range [0-1] with 0 corresponding to fully collimated light and 1 corresponding to fully diffuse light.

Morgenstern et al. made 570 measurements of the ICE in natural environments [33]. The results showed that the mean ICE ranged from 0.41 to 0.66 in these environments, which after normalization means a range from 0.5 to 0.7. Cuttle et al. found a preference for the E_{vector}/E_{scalar} ratio in the range from 1.2 to 1.8 for the appearance of human features in an interview situation [11]. This range corresponds to values between 0.55 and 0.7 for the normalized D_{Cuttle}. Thus this range coincides with the diffuseness levels of natural scenes that Morgenstern found and indicates that human features presented in lighting environments with natural diffuseness levels are most preferred by human observers. A D_{Hewitt} index in the range from 0.3 to 0.6 was noted to indicate good modelling [43]. The latter range corresponds to a normalized range from 0.3 to 0.6, and so partly overlaps with natural diffuseness levels, but also is partly extended towards more directed light. The latter guideline for the modelling index, however, was based on tests
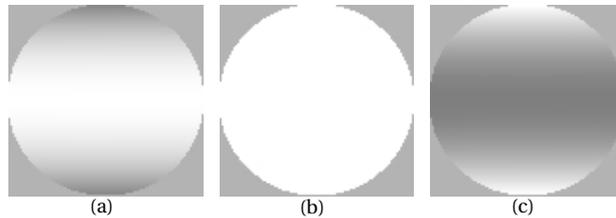
Figure 5.8: Light patterns on a Lambertian sphere with the light vector being zero: (a) a light ring; (b) uniform light field; (c) two opposed point light sources.

using statues of faces instead of real faces. It is probable that for statue illumination or museum lighting the light is preferred to be a bit more directed than natural light. Regarding $D_{Frandsen}$, values between 4 and 6 were noted to be the most common diffuseness levels to be encountered in natural scenes, such as in open scenes with both the sun and clouds in the sky. Translating these values into normalized values results in a range between 0.2 and 0.3, indicating much more directed light than the natural or preferred diffuseness levels mentioned above. Possible reasons for his misestimate might be that Frandsen did not test his statement by experiments and, moreover, neglected half the diffuseness range in his theory.

Although the perception of light diffuseness is based on the appearance of light sources and illuminated objects, neither the vector/scalar illumination ratio nor the first/zeroth order strength of the SH representation, strictly, are an index of object appearance. That is because the formation of the lighting pattern on an object is not only determined by the light diffuseness, but also by the light direction and light density, as well as by the geometric and scattering properties of surfaces and the viewing direction. That is why light diffuseness is different from a "modelling index". "Modelling indices" depend on the light diffuseness, but do not represent the light diffuseness. Instead they (should) represent how well the lighting conditions allow to see 3D shapes in it. Light direction, light density, and other environmental characteristics together with diffuseness determine the appearance of objects, and so the modelling aspect.

The light diffuseness metrics D_{Cuttle} and D_{Xia} describe the relationship between the zeroth order and the first order SH components. Due to effects of second order SH contributions, identical values of D_{Cuttle} or D_{Xia} may result in different lighting patterns on an object. The second order SH component was called "squash tensor" by Mury [35–37] , because of its shape in extreme cases: a light or dark squash. For instance in Figure 5.8, the sphere is illuminated by a light ring (or dark squash) in Figure 5.8 (a), a uniform light field in Figure 5.8(b) and two opposed light sources (or light squash) in Figure 5.8 (c). In all three conditions, both the normalized D_{Cuttle} and D_{Xia} have a value of 1 (since the light vector is 0), but the illumination pattern on the sphere is different. Furthermore, adding an ambient term (zeroth order SH term) to the model "probe in a sphere" simply contributes an additional uniform illumination over the surface of the spherical probe but would not influence the higher order SH components (e.g. the first order). Thus, such change will result in a higher value of the normalized diffuseness.

Morgenstern et al. proved that the ICE is the ratio between the energy in the first to infinite orders and the energy in the zeroth order components of the SH representation of the illumination over a Lambertian sphere. Similar to the effect above, identical values of the ICE may result in different lighting patterns on an object. For example, varying the phase of the SH or shifting energy between harmonics within a single order has no effect on the ICE value, but does change the illumination pattern on an object. A well-known effect in this ballpark concerns variations of the light vector direction with respect to a viewer, which changes the apparent diffuseness [6, 41] but not the physical diffuseness. In future research, we will investigate how to capture such higher order angular variations (so-called light texture [40]) in descriptions, measurements and visualizations.

5.8. Conclusion

In this study, four well-known diffuseness metrics were reviewed and their relationships were examined via a model named "probe in a sphere". We proposed a light diffuseness metric D_{Xia}, which is entirely based on a mathematical description of the physical light distribution in a 3D space (the light field) and fulfils the criteria we defined for diffuseness metrics. Together with the light density and direction it forms a global integral description of the low order properties of the light field structure. It also allows easy extensions to descriptions of the high order components of the light field. Furthermore, the SH representation based method has the advantage that it is clear how the parameters relate and which role they play in the resulting light field. These properties and their variation in 3D space reflect the spatial and form-giving character of light.

References

[1] Ş Aydın-Yağmur and L Dokuzer-Öztürk. Determination of the harshness–softness attribute of shadows. *Lighting Research and Technology*, 0:1–17, 2015.

[2] Ronen Basri and David W Jacobs. Lambertian reflectance and linear subspaces. *Pattern Analysis and Machine Intelligence, IEEE Transactions on*, 25(2):218–233, 2003.

[3] Michael Baxandall. *Shadows and enlightenment*. Yale University Press, 1997.

[4] AR Bean. Modelling indicators for combined side and overhead lighting systems. *Lighting Research and Technology*, 10(4):199–202, 1978.

[5] Peter Boyce. Lighting quality for all. In *SLL and CIBSE Ireland International Lighting Conference Dublin, April*, pages 1–7, 2013.

[6] C Cuttle. Lighting patterns and the flow of light. *Lighting research and Technology*, 3(3):171–189, 1971.

[7] C Cuttle. Cubic illumination. *Lighting Research and Technology*, 29(1):1–14, 1997.

[8] C Cuttle. Perceived adequacy of illumination: A new basis for lighting practice. In *Proceedings of the 3rd Professional Lighting Design Convention, Professional Lighting Designers Association*, pages 27–31, 2011.

[9] C Cuttle. A new direction for general lighting practice. *Lighting Research and Technology*, 45(1):22–39, 2013.

[10] C Cuttle. Research note: A practical approach to cubic illuminance measurement. *Lighting Research and Technology*, 46(1):31–34, 2014.

[11] C Cuttle, WB Valentine, JA Lynes, and W Burt. Beyond the working plane. *Proceedings of the CIE, Washington, DC*, 1967.

[12] Christopher Cuttle. *Lighting by design*. Routledge, Oxford: Architectural Press, 2008.

[13] James Duff. In-field measurment of cylindrical illuminance and the impact of room surface reflectance on the visual environment. In *the SLL and CIBSE Ireland International Lighting Conference, Dublin*, pages 1–11, 2013.

[14] Russell Epstein, Peter W Hallinan, and Alan L Yuille. 5 ± 2 eigenimages suffice: an empirical investigation of low-dimensional lighting models. In *Physics-Based Modeling in Computer Vision, 1995., Proceedings of the Workshop on*, page 108. IEEE, 1995.

[15] Sophus Frandsen. The scale of light–a new concept and its application. In *Paper on 2nd European Conference on Architecture*, pages 4– 8, 1989.

[16] Rüdiger Ganslandt and Harald Hofmann. Handbook of lighting design. *ERCO GmbH*, 1992.

5

[17] Andreī Gershun. The light field (translated by moon, parry hiram and timoshenko, gregory). *Journal of Mathematics and Physics*, 18(1):51–151, 1939.

[18] James Gurney. *Color and light: A guide for the realist painter*. Andrews McMeel Publishing, 2010.

[19] Peter W Hallinan. A low-dimensional representation of human faces for arbitrary lighting conditions. In *Computer Vision and Pattern Recognition, 1994. Proceedings CVPR'94., 1994 IEEE Computer Society Conference on*, pages 995–999. IEEE, 1994.

[20] H Hewitt, DJ Bridgers, and RH Simons. Lighting and the environment some studies in appraisal and design. *Lighting Research and Technology*, 30(4 IEStrans):91–116, 1965.

[21] Harry Hewitt. The study of pleasantness. *Light and lighting*, 56:154–164, 1963.

[22] Fil Hunter, Steven Biver, and Paul Fuqua. *Light–science & Magic: An Introduction to Photographic Lighting*. Taylor & Francis, 2007.

[23] Mehlika Inanici. computational approach for determining the directionality of light: directional-to-diffuse ratio. In *Building Simulation*, pages 1182–1188, 2007.

[24] Tatiana Kartashova, Huib de Ridder, Susan F te Pas, Marga Schoemaker, and Sylvia C Pont. The visual light field in paintings of museum prinsenhof: comparing settings in empty space and on objects. In *IS&T/SPIE Electronic Imaging*, pages 93941M–93941M. International Society for Optics and Photonics, 2015.

[25] Kevin Kelly and James Duff Mr. Lighting design in europe: Aligning the demands for lower energy usage with better quality. *Civil Engineering and Architecture*, 9:283–290, 2015.

[26] Richard Kelly. Lighting as an integral part of architecture. *College Art Journal*, pages 24–30, 1952.

[27] Richard Kelly, Dietrich Neumann, and D Michelle Addington. *The structure of light: Richard Kelly and the illumination of modern architecture*. Yale University Press, 2010.

[28] Jan J Koenderink, Sylvia C Pont, Andrea J van Doorn, Astrid ML Kappers, and James T Todd. The visual light field. *PERCEPTION-LONDON-*, 36(11):1595, 2007.

[29] Jan J Koenderink, Andrea J van Doorn, Astrid ML Kappers, Sylvia C Pont, and James T Todd. The perception of light fields in empty space. *Journal of Vision*, 5(8):558–558, 2005.

[30] JA Lynes, W Burt, GK Jackson, and C Cuttle. The flow of light into buildings. *Lighting Research and Technology*, 31(3 IEStrans):65–91, 1966.

[31] M. Madsen and M Donn. Experiments with a digital'light-flow-meter'in daylight art museum buildings. In *presented at the 5th International Radiance Scientific Workshop, UK: Leicester, Sep 13-14*, 2006.

5

[32] Lou Michel. *Light: the shape of space: designing with space and light.* John Wiley & Sons, 1995.

[33] Yaniv Morgenstern, Wilson S Geisler, and Richard F Murray. Human vision is attuned to the diffuseness of natural light. *Journal of vision*, 14(9):15, 2014.

[34] Yaniv Morgenstern, Wilson S Geisler, and Richard F Murray. The role of natural lighting diffuseness in human visual perception. In *IS&T/SPIE Electronic Imaging*, pages 93940P–93940P. International Society for Optics and Photonics, 2015.

[35] Alexander A Mury, Sylvia C Pont, and Jan J Koenderink. Light field constancy within natural scenes. *Applied Optics*, 46(29):7308–7316, 2007.

[36] Alexander A Mury, Sylvia C Pont, and Jan J Koenderink. Structure of light fields in natural scenes. *Applied Optics*, 48(28):5386–5395, 2009A.

[37] Alexander A Mury, Sylvia C Pont, and Jan J Koenderink. Representing the light field in finite three-dimensional spaces from sparse discrete samples. *Applied Optics*, 48(3):450–457, 2009B.

[38] Alexander Alexeevich Mury. *The light field in natural scenes.* PhD thesis, TU Delft, Delft University of Technology, 2009.

[39] A Nassar, MM El-Ganainy, FA Moktader, SM El-Kareem, and MA Haridi. Cylindrical illuminance and its importance in integrating daylight with artificial light. *Lighting Research and Technology*, 35(3):217–222, 2003.

[40] Sylvia C Pont. Spatial and form-giving qualities of light. *Handbook of Experimental Phenomenology: Visual Perception of Shape, Space and Appearance*, pages 205–222, 2013.

[41] Sylvia C Pont and Jan J Koenderink. Matching illumination of solid objects. *Perception & psychophysics*, 69(3):459–468, 2007.

[42] Ravi Ramamoorthi and Pat Hanrahan. On the relationship between radiance and irradiance: determining the illumination from images of a convex lambertian object. *JOSA A*, 18(10):2448–2459, 2001.

[43] PJ Raynham. *The SLL Code for Lighting*. The Society of Light and Lighting, UK, 2012.

[44] E Rowlands and D Loe. Preferred illuminance distribution in interiors. *Proc 18th CIE Session, London P-75-17*, 1975.

[45] James A Schirillo. We infer light in space. *Psychonomic bulletin & review*, 20(5):905–915, 2013.

[46] Robert D Stock and Melvin W Siegel. Orientation invariant light source parameters. *Optical Engineering*, 35(9):2651–2660, 1996.

5

[47] Susan F te Pas and Sylvia C Pont. A comparison of material and illumination discrimination performance for real rough, real smooth and computer generated smooth spheres. In *Proceedings of the 2nd symposium on Applied perception in graphics and visualization*, pages 75–81. ACM, 2005.

[48] JM Waldram. Studies in interior lighting. *Lighting Research and Technology*, 19(4 IEStrans):95–133, 1954.

[49] Ling Xia, Sylvia C Pont, and Ingrid Heynderickx. The sensitivity of observers to light field in real scenes. In *EXPERIENCING LIGHT*, page 120, 2014.

[50] Ling Xia, Sylvia C Pont, and Ingrid Heynderickx. The visual light field in real scenes. *i-Perception*, 5(7):613–629, 2014.

5

6

OBJECTIVE MEASURES: DESCRIPTION, PRACTICAL MEASUREMENT AND VISUALIZATION

Abstract

We introduce a way to simultaneously measure the light density, light vector and diffuseness of the light field using a cubic illumination meter based on the spherical harmonics representation of the light field. This approach was applied to six light probe images of natural scenes and four real scenes built in our laboratory, and the results were compared to those obtained using Cuttle's method. We also demonstrated a way to simultaneously and intuitively visualize the global structure of the light distribution using light tubes and colour coding for the light density, light flow and diffuseness variations through the space. Together with Mury's work, we will then have a complete way to describe, measure and visualize the local and global low order properties of the light distribution in three-dimensional spaces.

6

6.1. Introduction

The distribution of light in a three-dimensional space strongly influences the appearance of that space and the objects inside it. There is no doubt that the primary purpose of artificial lighting is pure visibility. However, with advances in lighting technology, peoples' expectation of lighting now far exceeds this primary function of lighting. Modern designers prefer to see lighting principally in terms of how it influences the appearance of people's surroundings and makes it possible to create various atmospheres [3, 7, 8, 17–19]. In this line of thought, Cuttle [6] proposed that the lighting profession must move to the third stage. The first stage of the lighting profession focused on providing uniform illumination over a horizontal plane, whereas the second stage provided illumination suited to human needs based on visual performance. Cuttle stated that the third stage should aim at revealing the potential of illumination to interact with its surroundings to create various types of visual experiences. In order to do so, we require methods to describe, measure and visualize the structure of the light distribution throughout the space. These methods provide insights into the spatial and form-giving character of light and allow predictions of how an object would look like in this light. In this paper, we introduce ways to measure the physical (objective) light diffuseness. The (subjective) perception of light diffuseness is influenced by many additional factors such as the illumination direction [4, 30], the shape and material of the illuminated object, and the perspective of the observer [24]. Relating perceptual diffuseness ratings to systematical variations of the physical diffuseness thus encompasses an extensive psychophysical study, which we intend to do in the future.

The light density, the primary illumination direction, and the diffuseness shapes the basic (low-order) properties of a light field, which can be sensed by the human visual system (HVS) [21, 22, 30, 33]. The light density and direction were mathematically and physically defined by Gershun [15] in his 5-dimensional function of the light field and by Mury et al. [29] using a spherical harmonics (SH) representation of the light field. In "Light diffuseness metric, Part 1: Theory" of this work, we gave a review of four well-known diffuseness metrics, namely (1) the "scale of light" by Frandsen ($D_{Frandsen}$) [13], (2) the "ratio between cylindrical and horizontal illuminance" by Hewitt (D_{Hewitt})[16], (3) the "ratio between illumination vector and scalar" by Cuttle (D_{Cuttle}) [4] and Lynes et al. [23] and (4) the "Illuminance Contrast Energy (ICE)" metric of Morgenstern et al. ($D_{Morgenstern}$) [25]. Their relationships were examined via a model named "probe in a sphere" and the results showed that the normalized diffuseness metrics D_{Hewitt}, D_{Cuttle} and $D_{Morgenstern}$ gave very similar results to the "probe in a sphere model". Inspired by Mury's work on the physical SH representation of the light field and by the basic parameterization of diffuseness as the balance between the ambient and directed light, we proved that D_{Cuttle} is equivalent to the ratio between the strength of the first order (i.e., the light vector) and the zeroth order (i.e., the light density) of the SH representation of the light field (D_{Xia}). The diffuseness metric D_{Xia} is entirely based on a mathematical description of the physical light distribution and fulfils the criteria we defined as being relevant for diffuseness metric. Together with the light density and direction it represents the low-order properties of the global structure of the light field. Furthermore, the SH-based method allows all parameters to be described within one integral descrip-

tion/decomposition, in which it is clear how the parameters relate and which role they play in the resulting light field. For instance, Kelly [18, 19], considered one of the pioneers of architectural lighting design, used "ambient luminescence", "focal glow" and "play of brilliants" to describe the light effects in lighting design. In the SH representation of the light field, the zeroth order describes the "ambient luminescence", the first order gives information about "focal glow" and the higher orders are related to the "play of brilliants".

In this study, we demonstrate how the density of light, light direction and diffuseness can be simultaneously measured using a cubic meter and visualized using "light tubes".

6.2. Measuring the light field's light density, direction and diffuseness simultaneously

6.2.1. Cuttle's method

Cuttle proposed a simple solution to measure the illumination vector and scalar, as well as the ratio between illumination vector and scalar (i.e., the inverse of the light diffuseness) [5, 9]. Using a cubic illlumination meter, six illuminance values in three mutually perpendicular directions can be measured, these being $E_{(+x)}$, $E_{(-x)}$, $E_{(+y)}$, $E_{(-y)}$, $E_{(+z)}$, $E_{(-z)}$. The illumination vector component can be calculated as:

$$\mathbf{E_{vector}} = (E_{(+x)} - E_{(-x)}, E_{(+y)} - E_{(-y)}, E_{(+z)} - E_{(-z)}) \tag{6.1}$$

and the scalar component as:

$$\begin{aligned} E_{scalar} &= \frac{|\mathbf{E_{vector}}|}{4} + \bar{E}_{symmetric} \\ &= \frac{|\mathbf{E_{vector}}|}{4} + \frac{min(E_{(+x)}, E_{(-x)}) + min(E_{(+y)}, E_{(-y)}) + min(E_{(+z)}, E_{(-z)})}{3} \end{aligned} \tag{6.2}$$

with "min" denoting the minimum. Consequently, the strength of the flow of light (i.e., the inverse of the light diffuseness) can be easily found as $|\mathbf{E_{vector}}|/E_{scalar}$. The normalized form of the diffuseness is:

$$(D_{Cuttle})_{Normalized} = 1 - (|\mathbf{E_{vector}}|/E_{scalar})/4 \tag{6.3}$$

with "0" corresponding to fully collimated light and "1" corresponding to fully diffuse light. Cuttle's method uses simple calculations and is suitable for quick, local measurements of the diffuseness level of natural scenes.

6.2.2. Xia's method

In this section, we propose a similar but differently framed approach to simultaneously recover these main, low order properties of the light field: using a SH representation of the light field. In "Light diffuseness metric, Part 1: theory" of this work, we proved that the ratio between the strength of the first- and zeroth-order components of the SH

representation (D_{Xia}) gives the diffuseness. Thus, to simultaneously measure the light density, direction and diffuseness, the first two orders of the SH representation of the light field are sufficient.

Mury et al. [28] managed to measure the light field up to the second-order SH representation by using a custom-made device called a "Plenopter". This second-order representation consists of nine coefficients, which could be estimated using a device composed of 12 faces with a light sensor on each. Since we only need the zeroth and first order of the representation, we only need to estimate four coefficients, which can be done with a cubic illumination meter.

The cubic illumination meter comprises six illuminance meters mounted on the faces of a small cube, yielding six values P_j ($j = 1, \cdots, 6$). The illuminance meters have a certain angular sensitivity profile $S_j(\vartheta, \varphi)$ that should be convoluted with the incident light distribution $f_j(\vartheta, \varphi)$ on that illuminance meter. Thus,

$$P_j = \int S_j(\vartheta, \varphi) \cdot f_j(\vartheta, \varphi) d\Omega, \qquad j = 1, \cdots, 6 \tag{6.4}$$

The illumination meter's angular sensitivity profile can be decomposed to SHs and presented as:

$$S_j(\vartheta, \varphi) = \sum_{l=0}^{\infty} \sum_{m=-l}^{l} (s_j)_l^m Y_l^m(\vartheta, \varphi) \tag{6.5}$$

The shape of the sensitivity profile follows the cosine law as a function of the angle between the incident direction of light and the normal to the surface to which the meter is attached. Furthermore, the incident light can be reconstructed by the sum of its harmonics. Combining the above results in:

$$
\begin{aligned}
P_j &= \int \left[\sum_{l=0}^{\infty} \sum_{m=-l}^{l} (s_j)_l^m Y_l^m(\vartheta, \varphi) \right] \left[\sum_{l'=0}^{\infty} \sum_{m'=-l'}^{l'} C_{l'}^{m'} Y_{l'}^{m'}(\vartheta, \varphi) \right] d\Omega \\
&= \sum_{ll'mm'} (s_j)_l^m C_{l'}^{m'} \int Y_l^m(\vartheta, \varphi) Y_{l'}^{m'}(\vartheta, \varphi) d\Omega, \qquad j = 1, \cdots, 6
\end{aligned}
\tag{6.6}
$$

where $C_{l'}^{m'}$ are the coefficients of the SH decomposition of the incident light filed.

Because of the orthonormality of the SHs basis function, we finally get

$$P_j = \sum_{lm} (s_j)_l^m C_l^m, \qquad j = 1, \cdots, 6 \tag{6.7}$$

Thus, we obtain a system of six equations with four unknown coefficients. By using a least squares approach, solutions for the overdetermined system can be fitted. Thus, the zeroth- and first-order modes of the SHs representation of the light field can be recovered and these carry the information about the light density (i.e., the zeroth order), light vector (i.e., the first order) and the normalized diffuseness as:

$$(D_{Xia})_{Normalized} = 1 - d(L_1)/d(L_0)/\sqrt{3} \tag{6.8}$$

where $d(L_0)$ is the strength of the zeroth order and $d(L_1)$ indicates the strength of the first-order SH representation of the light field. In the normalized diffuseness metric,

"0" corresponds to fully collimated light and "1" corresponds to fully diffuse light. The advantages of the SH representation are that all parameters can be described within one integral description/decomposition, in which it is clear how the parameters relate and which role they play in the resulting light field. Moreover, the SH representation can be used as such in, for instance, fast real time computer rendering and can be linked to components of lighting plans for design and architecture.

The cubic illumination meter is easily built with commercially available components, namely the Konica-Minolta T-10MA illuminance meters (as shown in Figure 6.1). Additional materials are provided in Appendix C for laser-cutting and building the cube basis.

Figure 6.1: Our cubic illumination meter, built with commercially available components on the basis of a laser-cut cube basis (see Appendix C for additional materials to build this basis). Note: our cubic meter has 6 large faces and 2 small faces. The small face on the top was cut to place a spirit level and the small face on the bottom was cut to fix the cubic meter on a metal stick.

6.3. Measurement error predictions

6.3.1. Error analysis: Influence of light field orientation and second-order SH contributions

How robust can D_{Xia} and D_{Cuttle} measure the diffuseness of a light field using a cubic illumination meter? To answer this question, we simulated a light field by using a sum of SH functions. According to Ramamoorthi and Hanrahan [31], complex lighting on approximate Lambertian surfaces can be successfully replaced by its second-order approximation. Thus, we simulated a light field in terms of a second-order SH representation:

$$\begin{cases} w_0 = 1 \\ f(\vartheta,\varphi) = \qquad w_0 \cdot Y_0^0(\vartheta,\varphi) + w_1/w_0 \cdot (a_1 Y_1^{-1}(\vartheta,\varphi) + a_2 Y_1^0(\vartheta,\varphi) + a_3 Y_1^1(\vartheta,\varphi)) \\ \qquad + w_2/w_0 \cdot (b_1 Y_2^{-2}(\vartheta,\varphi) + b_2 Y_2^{-1}(\vartheta,\varphi) + b_3 Y_2^0(\vartheta,\varphi) + b_4 Y_2^1(\vartheta,\varphi) + b_5 Y_2^2(\vartheta,\varphi)) \end{cases}$$
$$(6.9)$$

We varied the ratios defining the relative strength of the first three orders (i.e., w_1/w_0, w_2/w_0) and the weights of the components within the first and second order (i.e., $a_1, a_2, a_3; b_1, b_2, b_3, b_4, b_5$). Since the theoretical value of $d(L_1)/d(L_0)$ for the model "probe in a sphere" ranges from 1.73 to 0, we set the range of w_1/w_0 from 0 to 1.7 with an interval of 0.1. We then calculated the theoretical illumination falling on the six faces of the cubic meter under the simulated light field. With these six values we calculated D_{Cuttle}. Next, we used the least squares approach to fit the four coefficients of the zeroth- and first-order SH representation and determined D_{Xia}. The results are shown in Figure 6.2 and Figure 6.3.
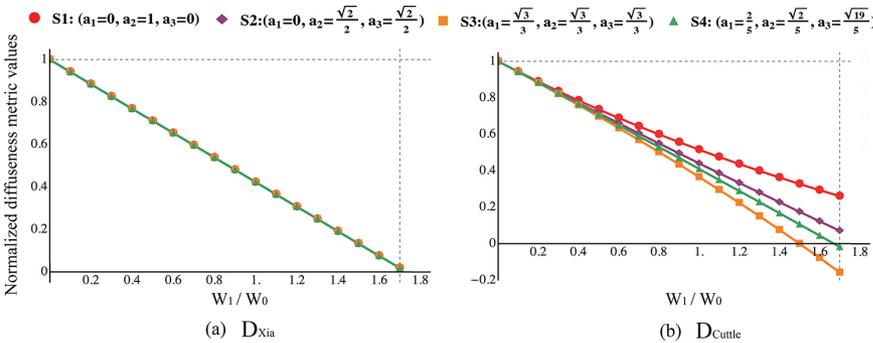

Figure 6.2: Simulated diffuseness values as a function of the theoretical diffuseness for four different weight distributions within the first order component.

Figure 6.2 shows the normalized D_{Xia} and D_{Cuttle} values calculated as a function of the relative strength w_1/w_0 for different weights of the first-order components (i.e., a_1, a_2, a_3), representing different orientations of the light field while its structure remains the same. Clearly, the straight line shows that the original D_{Xia} value (before normalized) is exactly the same as w_1/w_0. D_{Cuttle} deviates from w_1/w_0 with a slope being dependent on the weights of the first-order components, or the orientation of the light field.

Figure 6.3 shows the normalized D_{Xia} and D_{Cuttle} values as a function of w_1/w_0 for different relative strengths w_2/w_0 and weights of the second-order components (i.e., b_1, b_2, b_3, b_4, b_5). Both the calculated D_{Xia} and D_{Cuttle} are independent of w_2/w_0 and of the weights of the second order components (the three curves in each plot overlap).

6.3.2. Error analysis: Effect of attitude of the cubic illumination meter

In Section 6.3.1, we found that D_{Cuttle} depended on the orientation of the light field. This implies that D_{Cuttle} will vary with the cubic illumination meter's attitude in the
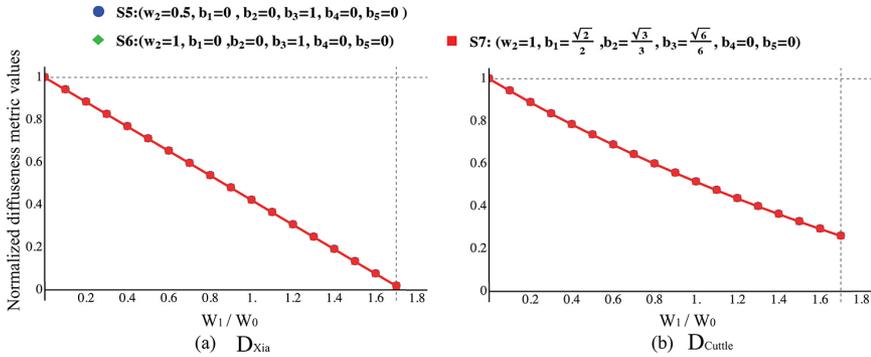
Figure 6.3: Simulated diffuseness values as a function of the theoretical diffuseness for two relative strengths of the second order SH component w_2/w_0 (0.5 or 1). For w_2/w_0 is 1, two different weights distributions within the second order components were adopted. The first order components were set as $a_1 = 0, a_2 = 1, a_3 = 0$.

light field. Here we analyze this variation and evaluate whether optimizing the meter's attitude can reduce measurement errors.

In order to answer the question above, the model "probe in a sphere" was used. We chose four different attitudes for the cubic illumination meter; their bird's eye views are illustrated in Figure 6.4. In Figure 6.4(a), the cubic illumination meter was positioned symmetrically with respect to the light source with four faces parallel to the light vector along the z-axis. As a consequence, these four faces always received the same illumination (Attitude 1). Figure 6.4 (b) shows Attitude 2, for which we rotated the cubic illumination meter 20° around the x-axis, so that it had two faces parallel to the light vector, receiving the same illumination. For Attitude 3, illustrated in Figure 6.4(c), we did an additional rotation of 15° around the y-axis, so that no faces were parallel to the light vector and all received a different amount of illumination. Finally, for Attitude 4, shown in Figure 6.4 (d), the cubic illumination meter was firstly rotated 45° around the x-axis and then rotated 35° around the y-axis, so that one of the diagonals was parallel to the z-axis. As a consequence, it had no face parallel to the light vector, but the three faces turned upwards all received the same illumination, and the other three faces turned downwards did likewise. We then calculated the illumination falling on the six faces of the cubic illumination meter for the four attitudes and for subtended angles of the spherical light source ranging from 0° to 360°. For each situation, we fitted the four coefficients of the SH representation of the light field, and used them to determine D_{Xia}. In Figure 6.5 (a), we show the simulated and normalized D_{Xia} values together with the theoretical diffuseness values for the different subtended angles. The theoretical diffuseness values were obtained by fitting the SH representations to the luminance maps of our model instead of to the simulated cubic illumination meter readings.

When the subtended angle α was bigger than 180°, all six faces of the cubic meter were illuminated and the recovered D_{Xia} was exactly the same as the theoretical one. When α was larger than 90° but smaller than 180°, at least five faces of the cubic meter were illuminated, and then the recovered D_{Xia} was quite close to the theoretical one.
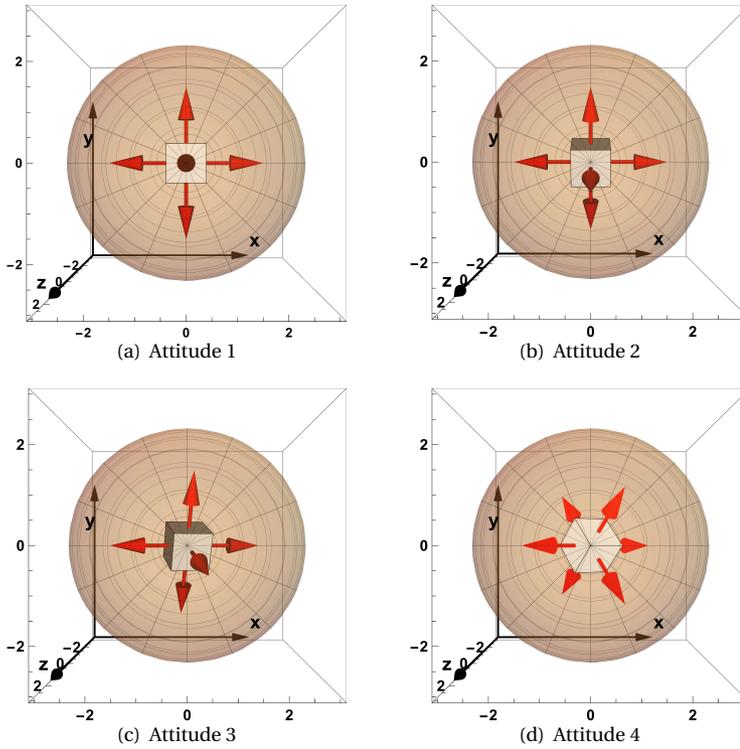
(a) Attitude 1

(b) Attitude 2

(c) Attitude 3

(d) Attitude 4

Figure 6.4: The simulated attitudes of the cubic meter in the center of the large spherical light source, with the light vector along the z-axis: (a) Attitude 1: the cubic meter was symmetrically positioned with respect to the light source with 4 faces parallel to the z-axis, (b) Attitude 2: rotated 20° around the x-axis, (c) Attitude 3: with an additional rotation of 15° around the y-axis, and (d) Attitude 4: firstly rotated 45° around the x-axis and then rotated 35° around the y-axis.

When α was smaller than 90°, however, the recovered D_{Xia} was different between the four attitudes, and only the curve for Attitude 3 was close to the theoretical value. So, D_{Xia} approached the theoretical values best when the number of illuminated faces was maximized and diversified and is a logical result of the SH fitting procedure. This effect implies that D_{Xia} is not robust for extremely collimated light if we put the cubic meter symmetrically with respect to the light source. In such cases, the normalized D_{Xia} may generate negative values (see Figure 6.5(a)). This happens because of the least squares fitting approach of the SH functions. When the light source is rather collimated (subtended angle <90°), some of the faces of the cubic illumination meter (e.g. the bottom face) may not be illuminated and set to zero in our fitting approach. However, the first-order SHs representation of the light field varies rather symmetrically and smoothly over all directions. Consequently, a small part of the energy will be in the higher order terms of the SH fit, which is excluded from our analysis (analogous to what happens for a block wave or called "Ringing" effects in Fourier decompositions). Fortunately, this situation is
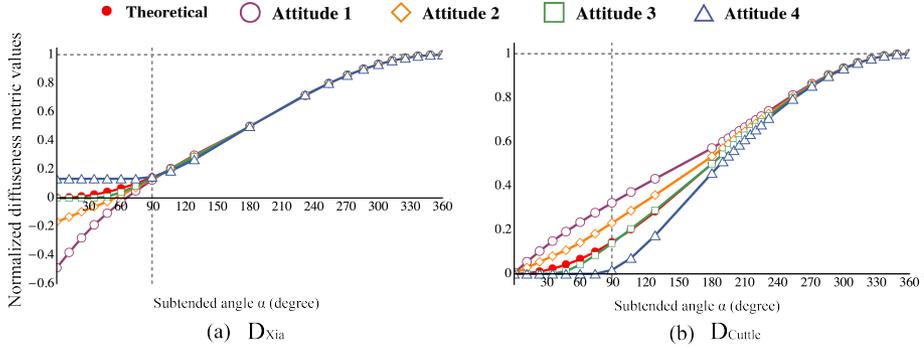
Figure 6.5: (a) Simulated D_{Xia} values and (b) simulated D_{Cuttle} values, as a function of the subtended angle α of the spherical light source for four cubic meter attitudes.

quite uncommon in natural scenes because there are always reflections from surroundings in real lighting environments.

In Figure 6.5(b), we show the simulated and normalized D_{Cuttle} values together with the theoretical diffuseness. Consistent with the findings in Section 6.3.1, D_{Cuttle} varied with the attitude of the cubic illumination meter, though all curves originate in zero. Furthermore, the optimization guidelines that apply to D_{Xia} also apply to D_{Cuttle}.

6.4. Simulated cubic illumination measurements

In order to investigate the robustness of D_{Xia} and D_{Cuttle} in real complicated lighting environments, we first simulated cubic meter measurements. To do so, we employed six HDR Panoramic light probe images from Debevec's High-Resolution Light Probe Image Gallery [11, 12]. The images used were named "Dining room", "Uffizi Gallery", "Grace Cathedral", "Doge's palace", "Sunset" and "Glacier" and their gray-scale tone maps are shown in Figure B.2.

We assumed a cubic illumination meter right in the center of each scene. Since the values recovered from this meter may be influenced by the cube orientation, we simulated one hundred attitudes of the meter for each light probe image, by systematically varying the latitude and longitude of the cube with 20° intervals. We then calculated the illuminance on the six faces of the cubic meter for each attitude in each light probe image. From these illuminances, the normalized D_{Xia} and D_{Cuttle} were calculated and plotted in Figure 6.7. The boxes with dashed frames in Figure 6.7 indicate the distribution of normalized D_{Cuttle} values, while the boxes with solid frames show the distribution of normalized D_{Xia} values. The median value of all boxes is consistent with the value $d(L_1)/d(L_0)$ that was calculated from the complete SH representation of each light probe image.

The recovered D_{Cuttle} values seem less sensitive to the cubic meter's orientation than the recovered D_{Xia} values for the scenes "Dining room" and "Grace Cathedral", while the opposite is true for the other scenes. In Section 6.3.1, we prove that in theory, the recovered D_{Xia} reflects $d(L_1)/d(L_0)$ well, while the recovered D_{Cuttle} is expected to vary

(a) Dining room

(b) Uffizi Gallery

(c) Grace Cathedral
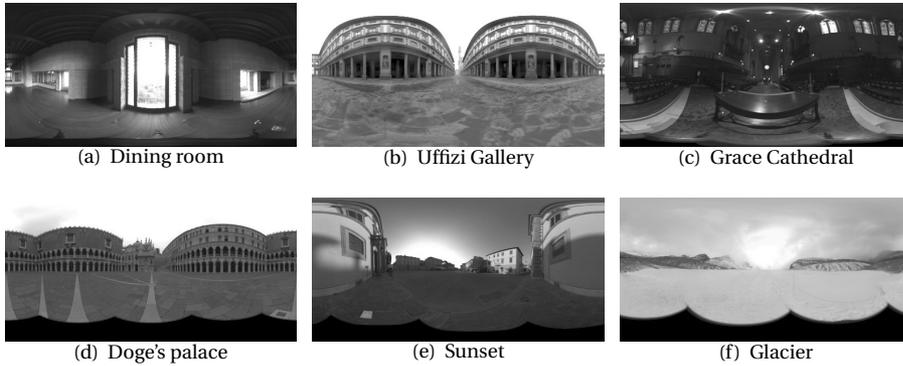

(d) Doge's palace

(e) Sunset

(f) Glacier

Figure 6.6: The grayscale tonemaps for HDR Panorama photographs of six natural scenes (a) Dining room (b) Uffizi Gallery (c) Grace Cathedral (d) Doge's palace (e) Sunset (f) Glacier

with the orientation of the cubic meter in the light field. However, in Section 6.3.2, we show that D_{Xia} estimates are expected to vary somewhat in collimated light. In such light, the faces of the cube away from the collimated light source are not illuminated, and so, their values are set to zero; this hinders robust SH fitting. The scenes "Dining room" and "Grace Cathedral" have more small bright, collimated light sources than the other scenes, and so were expected to yield less robust results for D_{Xia}. Based on these findings we conclude that the recovered D_{Cuttle} value is somewhat better at measuring light fields with a high contrast, such as in dark interior scenes with small bright windows or lamps, while the recovered D_{Xia} metric is somewhat more suitable for light fields with low contrast, such as for open outside environments. However, overall, the D_{Cuttle} and D_{Xia} simulations show only a small spread over the 100 different attitudes of the cubic meter, which indicates that both of them can well be used to measure the diffuseness for any random orientation of the cubic meter.

In a former study by Pont and Koenderink [30], observers matched levels of diffuseness on spheres using a visual probe. These results showed that perceived diffuseness correlated well with physical changes in the stimuli, but the variance was quite large . In another study by Xia et al. [34], observers were asked to judge whether a probe fitted a scene in terms of lighting for different settings of diffuseness on probe and scene. These results showed that the observers could not perceive a mismatch in diffuseness for small differences between probe and scene (i.e., for differences in scale of light between 24% and 43%, and between 43% and 59%). The latter values correspond to 0.01, 0.05 and 0.1 in normalized D_{Xia} or D_{Cuttle} units, respectively. Thus, the errors in our simulated measurements are relatively small compared to typical spread in perceived diffuseness.

6.5. Real cubic illumination measurements

In order to systematically vary the diffuseness in a real scene we built a box space of two walls forming a corner, in which we varied the reflectance of the walls and the primary
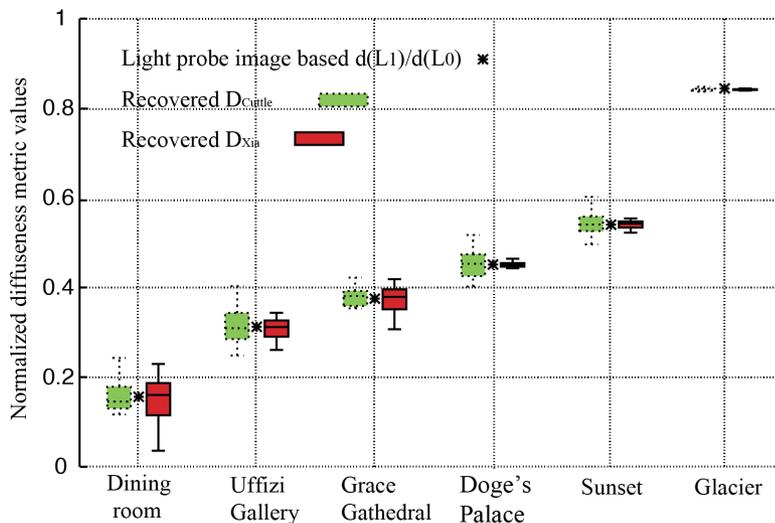
Figure 6.7: Box plot for normalized D_{Cuttle} and D_{Xia} values obtained from 100 different simulated attitudes of the cubic illumination meter in six light probe images. The black "*" indicate the normalized $d(L_1)/d(L_0)$ estimated from the full SH representation of each image.

6

illumination source. The reflectance was changed by putting either white or black paper (i.e., photography background paper rolls, all 2 m wide and room-height) in front of these walls. The white matte environment was used to generate secondary reflections by diffuse scattering, and thus showed an increase in light density or ambient illumination, in comparison to the black environment. We illuminated the corner with a spotlight (i.e., collimated light) or by indirect illumination via the ceiling with two large diffuse lamps (i.e., semi-diffuse light from above). Thus, the two environments and two types of luminaires resulted in four different light fields in total (i.e., LF I: semi-diffuse light plus white background; LF II: collimated light plus white background; LF III: semi-diffuse light plus black background; LF IV: collimated light plus black background). The cubic meter was put in the center of the corner. Table 6.1, showing the resulting measurements, illustrates that the results were quite similar for the two approaches for all light fields. The diffuseness varied systematically for the light fields; the values for the spotlight were indeed lower than for the semi-diffuse light from above. Note that the environment reflectance had a much bigger impact on the light qualities than the luminaires; the diffuseness increased with about 0.6 if the black walls were changed into white ones.

6.6. Visualization of the global structure of a light field

The measurements in the last two sections concerned local measurements of the light field. However, the light field is also a function of position. If we take into account its dependency on direction and position we get a five-dimensional function. So how can we derive and picture the global structure of a light field? Mury et al. [28] managed to

Table 6.1: The average illumination, light vector in Cartesian coordinates, and normalized diffuseness level at the location of the meter in four different light fields for both Cuttle's and Xia's approach. LF I: semi-diffuse light plus white background; LF II: collimated light plus white background; LF III: semi-diffuse light plus black background; LF IV: collimated light plus black background.

Method	Light Field	$E_{average}$ (lm/m^2)	Light vector		Normalized Diffuseness
			Unit light vector	Magnitude	
Cuttle	I	240.3	(-0.36, 0.58, 0.73)	113.32	0.88
	II	950.7	(0.38, 0.77, 0.51)	669.58	0.82
	III	68.5	(0.56, 0.73, 0.38)	199.15	0.27
	IV	356.2	(0.68, 0.68, 0.25)	1221.20	0.14
Xia	I	235.9	(-0.36, 0.58, 0.73)	113.30	0.88
	II	972.9	(0.38, 0.77, 0.51)	669.49	0.83
	III	75.7	(0.56, 0.73, 0.38)	199.12	0.34
	IV	391.2	(0.68, 0.68, 0.25)	1221.02	0.22

visualize the structure of a light field globally over an entire space by using light tubes. The tube's direction is locally tangential to the light vector (i.e., the direction of net energy transfer) and its width is locally inversely related to the magnitude of that vector (i.e., the larger the net light transport, the smaller the tube). The tubes usually start at light sources, where they are quite narrow, and they end at light absorbing surfaces, where they tend to be quite wide.

The light tubes representation actually shows what lighting architects call the "light flow" [4, 23]. However, Mury et al.'s light tubes did not carry any information about the diffuseness, which is an essential characteristic of the complete radiant structure of the light field that has great impact on the appearance of objects inside the room. We suggest using the colour saturation of the light tubes to visualize the diffuseness and the colour brightness to visualize the "light density" of the light field. In this manner, all lower order variables of the global structure of the light distribution in 3D space can be visualized simultaneously and intuitively.

Figure 6.8 (a) and (b) (based on measurements by Mury et al.) shows, as examples, side views of the light tubes in a Light Lab visualized using our method. The Light Lab (i.e., a laboratory space at Philips Research Eindhoven) was a typical empty office room of 4 by 6 by 3 meters. Figure 6.8 (a) shows the lab illuminated by three diffuse area light sources (indicated by the yellow squares) mounted in the ceiling along one of the long walls (hereafter referred to as Light Lab condition A). Figure 6.8 (b) shows the lab illuminated by the same sources but now in a triangular configuration (hereinafter referred to as Light Lab condition B). Figure 6.9 (a) and (b) illustrate the arrangements of the light sources in a generic view. Figure 6.8 (c) and (d) are interactive 3D figures showing the same "light flow" as Figure 6.8 (a) and (b) but allowing interactive manipulation of the view and dynamic change. Figure 6.8 (e) illustrates the colour coded legend used in Figure 6.8 (a), (b),(c) and (d). The colour saturation from left to right represents the normalized light diffuseness, i.e., the less saturated the colour is, the more diffuse the local light field is. We only show normalized diffuseness values from 0.3 to 1, since they actually

range from 0.35 to 0.86 in the measurements. The brightness of the colour indicates the "light density"; the brighter the colour, the higher the "light density". The "light density" was normalized to the range from 0 to 1.

Building on the idea of using "light probes" to visualize light qualities, we also made a legend showing in Figure 6.8 (f) the appearance of a sphere for the conditions shown in the legend of Figure 6.8 (e). For these renderings we used a combination of collimated and diffuse illumination. The altitude ϑ and azimuth φ for the point light source were set at 70° and 20° respectively, just as an example.

In previous research, a family of flow lines on a plane is used to characterise the illuminance field in a lighted room [10, 15]. The direction of flow lines coincides with the directions of the illuminance vectors and the concentration of the flow lines is directly proportional to the illuminance vector strength. For light fields that are constant along one dimension, drawing the flow lines on one plane is sufficient to visualize the light flow directions. However, this method does not work for most natural light fields since the three-dimensional structure of natural light fields is often not symmetric and in many cases quite complicated. For instance, Figure 6.9 (c) to (h) shows the flow lines on different planes parallel to the x-z plane in Light Lab condition A and Light Lab condition B. The selected planes are illustrated in Figure 6.9 (a) and Figure 6.9 (b). Figure 6.9 (i) shows the legends; the brighter the colour of the flow lines, the higher the "light density". The normalized light diffuseness is represented by the gray level of the "wash", i.e., the darker the wash, the more diffuse the local light field is. It is clear that the structure of flow lines is quite similar on the different planes in Light Lab condition A but not in Light Lab condition B. Thus, compared to illustrating flow lines on planes, the light tubes are a more inclusive and intuitive method to visualize the 3D structure of natural light fields. Moreover, the light tubes also show the variations in the strength of the flow.

6.7. Discussion and conclusions

We introduced a way to simultaneously measure the light density, light vector and diffuseness (variations) of the light field using a cubic illumination meter. Both with our method and Cuttle's method using a cubic meter we can measure the magnitude and direction of the illumination vector quite well but the scalar illumination less accurately. This result agrees with former results, e.g. Ashdown and Eng [1] state that: *"One difficulty with cubic illumination meters is that they are sensitive to orientation in the presence of strongly directional lighting, with a maximum possible variance of 33 percent for the scalar illuminance. This is not usually a concern with most office lighting designs, but it can be important for exhibit and theatre lighting."* We applied our method to six light probe images of natural scenes and four real scenes built in our laboratory, and compared the results to those calculated using Cuttle's method. This comparison showed that both methods could measure the diffuseness accurately and robustly in natural scenes using a cubic illumination meter. We found that care should be taken to maximize the number of lighted cubic meter faces and ensure the illumination diversity on six faces.

Finally, we demonstrated a way to simultaneously and intuitively visualize the global structure of a light field up to its first order properties or spatial variations of the light
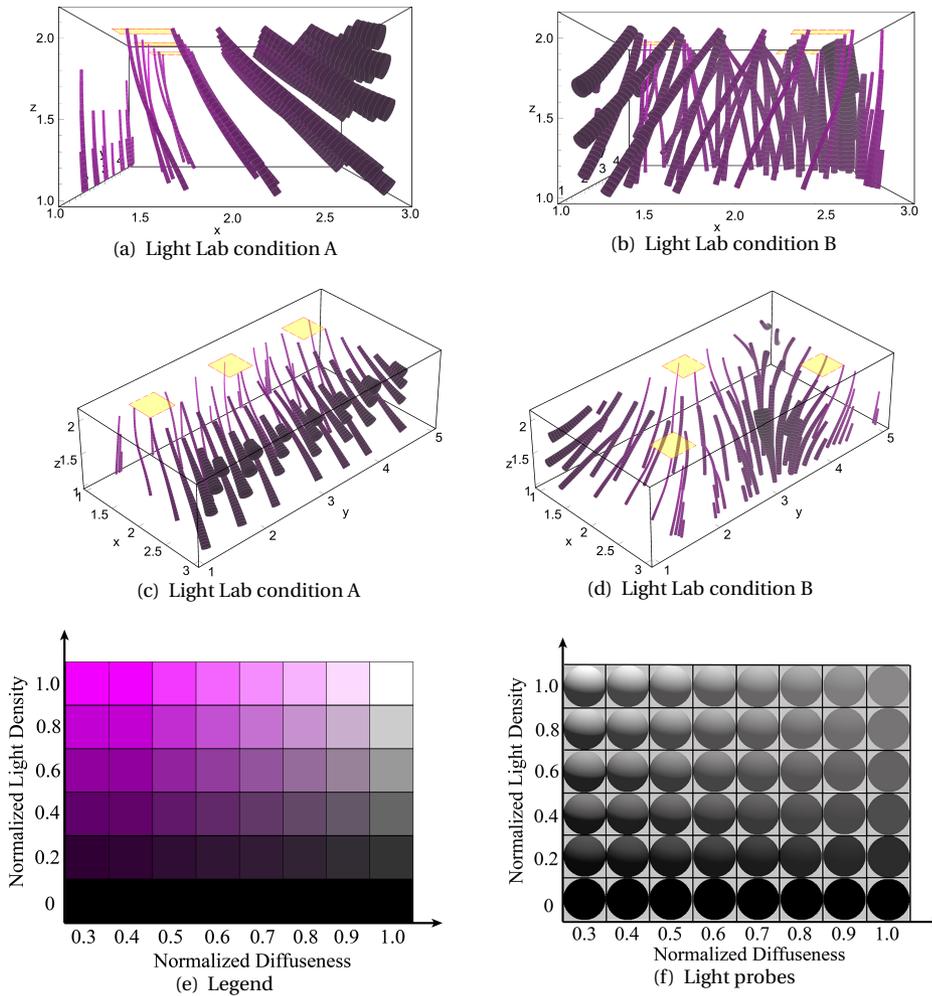
(a) Light Lab condition A

(b) Light Lab condition B

(c) Light Lab condition A

(d) Light Lab condition B

(e) Legend

(f) Light probes

Figure 6.8: (colour printed). A side view of the "light flow" in a room with three diffuse area light sources mounted in the ceiling (a) along one of the long walls (Light lab condition A) and (b) in a triangular configuration (Light Lab condition B). The light sources are indicated by yellow squares. A tube's direction is locally tangential to the light vector, the tube's width is inversely proportional to the magnitude of the light vector, the saturation of tube's colour indicates the light diffuseness and the colour brightness is proportional to the light density. Different perspectives of the "light flow" are shown in (c) and (d) (various perspectives of the "light flow" can be achieved by interacting real-time with the digital versions of the 3D models in (c) and (d) (we used a 3D canvas in the digital pdf versions of this thesis). The legend is shown in (e): the more saturated the colour is, the more directed the local light field, and the brighter the colour is, the higher the light density. The appearance of a white matte sphere for the conditions shown in the legend in (e) is given in (f) (for a light direction: $\vartheta = 20°$, $\varphi = 70°$).

(a) Light Lab condition A

(b) Light Lab condition B

(c) Light Lab condition A (y=1.7)

(d) Light Lab condition A (y=3.0)

(e) Light Lab condition A (y=4.3)

(f) Light Lab condition B (y=1.7)

(g) Light Lab condition B (y=3.0)

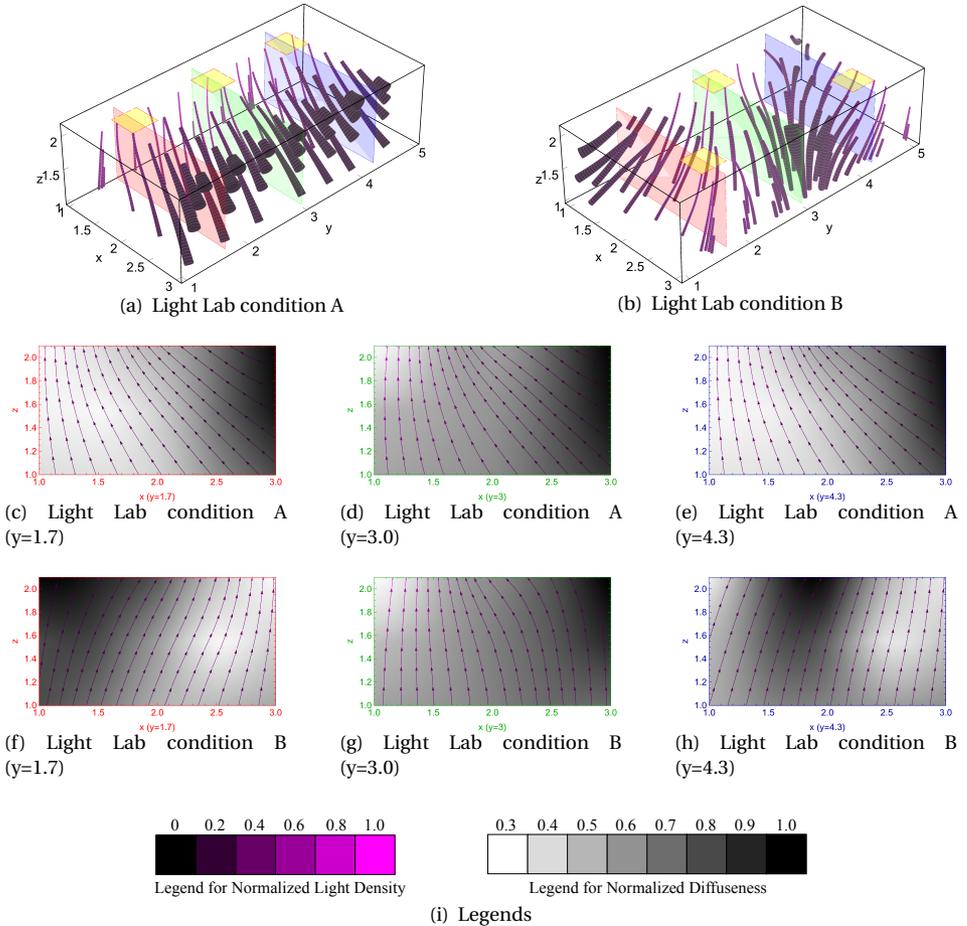(h) Light Lab condition B (y=4.3)

(i) Legends

Figure 6.9: (colour printed). The planes that were selected to show the "flow lines" in (a) Light Lab condition A and in (b) Light Lab condition B. "Flow lines" on planes parallel to the x-z plane when (c) y=1.7, (d) y=3.0 and (e) y=4.3 in Light Lab condition A and (f) y=1.7, (g) y=3.0 and (h) y=4.3 in Light Lab condition B. (i) The legends used: the brighter the colour of the "flow lines", the higher the light density, and the darker the "wash", the more diffuse the local light field.

density, vector and diffuseness using light tubes. Furthermore, via a legend we visual-ized the light effects on the appearance of a spherical "light probe". It might seem a good idea to directly render such probes within a space to visualize the light field. How-ever, we think the light tubes approach works better, because judgments of light direc-tion and diffuseness from the appearance of a white sphere are confounded due to basic image ambiguities [2, 20]. For example, observers confused more frontal illumination with higher levels of diffuseness [30]. This was also found in a practical test [24].

Besides using a cubic illumination meter, other methods can be used to measure the light scalar and vector. One example is a half table-tennis ball photosensor mounted on a two-axis mechanical stage proposed by Fuller et al [14] (or its modern version using a light meter app on a smart phone plus a hemispherical diffuse cap). Dale et al. [10] proposed another simple way to infer the light vector using a grease-spot device. Both methods are intuitive in providing information about the light vector. In Fuller et al.'s setup the light vector lies along the direction where the photosensor reaches the max-imum value. In Dale's setup the light vector lies in the plane of the grease-spot device when the difference between grease-spot and its surround paper vanishes because both sides have the same illumination. In Fuller's setup, taking another reading by rotating the tennis ball photosensor by 180° to the opposite direction of the light vector, the light scalar can be calculated as half of the sum of both readings. In Dale's setup, however, there is no direct way to get the light scalar. Nevertheless, rotating the mechanical stage and the grease-spot both need a lot of effort. Apart from the two experimental setups mentioned above, it is known that the average of the illuminance on the four sides of a regular tetrahedron is close to the scalar illuminance [32]. However, the light vector can't be measured robustly by the illuminance on the tetrahedron faces (we have also verified this point using our SH approach in Appendix B).

The novel diffuseness metric D_{Xia} is conceptually equivalent with D_{Cuttle} but with different methods to recover their values. Nevertheless, each of these two methods has its advantages and disadvantages. Cuttle's method requires simple calculations that can be done with a pen and a piece of paper. Thus, Cuttle's method is most suitable for a quick, local estimation of the diffuseness level in a natural scene. In contrast, our SH representation based method needs computation software on a computer in order to fit the SH representation to the data. The SH representation based D_{Xia}, together with the light flow and light density forms a global, integrated description of the lower order properties of the light field distribution in a three-dimensional space. This method fits all parameters being described within one integral description / decomposition, in which it is clear how the parameters relate and which role they play in the resulting light field. With the development of lighting modelling and rendering software, the SH method will have more and more advantages in fast, real-time rendering. Furthermore, in lighting design, software tends to be used more and more as an assisting tool. HDR environment maps were already used widely in computer graphics. Currently lighting design software can also export such maps easily. We suggest to provide the light density, light vector and D_{Xia}, together with the HDR environmental maps in order to give lighting and graphics designers a reference of the ambient, direction and diffuseness levels. Moreover, next to this local description for a single HDR map our method allows to give insights into the global structure of the light field in three-dimensional spaces. Light distributions in nat-

ural spaces show spatial variations of the ambient, vector and diffuseness, which can be captured using simple cubic illumination meter measurements and visualizations of interpolated data, e.g. the light flow representation using light tubes, as we demonstrated.

Mury et al. [26–28] described the light field in terms of the lower order SH approximation and successfully measured its components in natural scenes. The main contribution of this study is that we extended the work of Mury et al. by adding description, measurement and visualization methods for the diffuseness characteristic or, in other words, we re-framed the diffuseness metric of Cuttle in an integral description of the light field. This approach makes it possible to progress towards the third stage of the lighting profession as Cuttle described the innovative step lighting science should take towards dealing with light instead of lamps [6].

6

References

[1] Ian Ashdown and P Eng. The virtual photometer: modeling the flow of light. In *IESNA 1998 Annual Conference Technical Papers*, 1998.

[2] Peter N Belhumeur, David J Kriegman, and Alan L Yuille. The bas-relief ambiguity. *International journal of computer vision*, 35(1):33–44, 1999.

[3] Peter Boyce. Lighting quality for all. In *SLL and CIBSE Ireland International Lighting Conference Dublin, April*, pages 1–7, 2013.

[4] C Cuttle. Lighting patterns and the flow of light. *Lighting research and Technology*, 3(3):171–189, 1971.

[5] C Cuttle. Cubic illumination. *Lighting Research and Technology*, 29(1):1–14, 1997.

[6] C Cuttle. Towards the third stage of the lighting profession. *Lighting Research and Technology*, 42(1):73–93, 2009.

[7] C Cuttle. Perceived adequacy of illumination: A new basis for lighting practice. In *Proceedings of the 3rd Professional Lighting Design Convention, Professional Lighting Designers Association*, pages 27–31, 2011.

[8] C Cuttle. A new direction for general lighting practice. *Lighting Research and Technology*, 45(1):22–39, 2013.

[9] C Cuttle. Research note: A practical approach to cubic illuminance measurement. *Lighting Research and Technology*, 46(1):31–34, 2014.

[10] NPG Dale, JN Broadbridge, and PM Crowther. Measuring the direction of the flow of light. *Lighting Research and Technology*, 4(1):43–44, 1972.

[11] Paul Debevec. Rendering synthetic objects into real scenes: Bridging traditional and image-based graphics with global illumination and high dynamic range photography. In *ACM SIGGRAPH 2008 classes*, page 32. ACM, 2008.

[12] Paul Debevec. High-resolution light probe image gallery. website, 2008-2015.

[13] Sophus Frandsen. The scale of light–a new concept and its application. In *Paper on 2nd European Conference on Architecture*, pages 4– 8, 1989.

[14] M Fuller, MBD Upton, and J Whalen. The photometry of the flow of light. *Lighting Research and Technology*, 3(4):282–284, 1971.

[15] Andreī Gershun. The light field (translated by moon, parry hiram and timoshenko, gregory). *Journal of Mathematics and Physics*, 18(1):51–151, 1939.

[16] H Hewitt, DJ Bridgers, and RH Simons. Lighting and the environment some studies in appraisal and design. *Lighting Research and Technology*, 30(4 IEStrans):91–116, 1965.

6

[17] Kevin Kelly and James Duff Mr. Lighting design in europe: Aligning the demands for lower energy usage with better quality. *Civil Engineering and Architecture*, 9:283–290, 2015.

[18] Richard Kelly. Lighting as an integral part of architecture. *College Art Journal*, pages 24–30, 1952.

[19] Richard Kelly, Dietrich Neumann, and D Michelle Addington. *The structure of light: Richard Kelly and the illumination of modern architecture*. Yale University Press, 2010.

[20] Jan J Koenderink and Sylvia C Pont. Irradiation direction from texture. *JOSA A*, 20(10):1875–1882, 2003.

[21] Jan J Koenderink, Sylvia C Pont, Andrea J van Doorn, Astrid ML Kappers, and James T Todd. The visual light field. *PERCEPTION-LONDON-*, 36(11):1595, 2007.

[22] Jan J Koenderink, Andrea J van Doorn, Astrid ML Kappers, Sylvia C Pont, and James T Todd. The perception of light fields in empty space. *Journal of Vision*, 5(8):558–558, 2005.

[23] JA Lynes, W Burt, GK Jackson, and C Cuttle. The flow of light into buildings. *Lighting Research and Technology*, 31(3 IEStrans):65–91, 1966.

[24] M. Madsen and M Donn. Experiments with a digital'light-flow-meter'in daylight art museum buildings. In *presented at the 5th International Radiance Scientific Workshop, UK: Leicester, Sep 13-14*, 2006.

[25] Yaniv Morgenstern, Wilson S Geisler, and Richard F Murray. Human vision is attuned to the diffuseness of natural light. *Journal of vision*, 14(9):15, 2014.

[26] Alexander A Mury, Sylvia C Pont, and Jan J Koenderink. Light field constancy within natural scenes. *Applied Optics*, 46(29):7308–7316, 2007.

[27] Alexander A Mury, Sylvia C Pont, and Jan J Koenderink. Structure of light fields in natural scenes. *Applied Optics*, 48(28):5386–5395, 2009A.

[28] Alexander A Mury, Sylvia C Pont, and Jan J Koenderink. Representing the light field in finite three-dimensional spaces from sparse discrete samples. *Applied Optics*, 48(3):450–457, 2009B.

[29] Alexander Alexeevich Mury. *The light field in natural scenes*. PhD thesis, TU Delft, Delft University of Technology, 2009.

[30] Sylvia C Pont and Jan J Koenderink. Matching illumination of solid objects. *Perception & psychophysics*, 69(3):459–468, 2007.

[31] Ravi Ramamoorthi and Pat Hanrahan. On the relationship between radiance and irradiance: determining the illumination from images of a convex lambertian object. *JOSA A*, 18(10):2448–2459, 2001.

[32] William Thomas Singleton. *The body at work: Biological ergonomics.* Cambridge University Press, 1982.

[33] Susan F te Pas and Sylvia C Pont. A comparison of material and illumination discrimination performance for real rough, real smooth and computer generated smooth spheres. In *Proceedings of the 2nd symposium on Applied perception in graphics and visualization,* pages 75–81. ACM, 2005.

[34] Ling Xia, Sylvia C Pont, and Ingrid Heynderickx. The visual light field in real scenes. *i-Perception*, 5(7):613–629, 2014.

6

7
CONCLUSIONS

Abstract

This chapter outlines the main contributions of this thesis and answers the research questions posed in Chapter 1. Limitations and interesting directions for future work are also discussed in this chapter.

7

7.1. Main findings and contributions

This thesis aims to bridge the gap between the second stage and third stage of the lighting profession by investigating human perception and metrics of light fields. The study was set out to answer the following main research questions:

1. Are human beings sensitive to variations of light field properties in real scenes and in what way can their perception be measured intuitively?

2. How well can human beings infer light field properties and how can we measure their sensitivity using our real experimental setup?

3. Can observers' perception of light direction be influenced by scene content and layout in real scenes?

4. Can we find a mathematical way to describe the light diffuseness based on the physical light distribution of light fields?

5. Can we describe, measure and visualize the complete first order structure of the light field in an integral way?

These research questions have been answered in Chapters 2-6, and the main findings and contributions of this thesis are enumerated below in the order of the research questions:

-1.- **We developed a novel experimental setup based on the generic notion of a "gauge object" to investigate human sensitivity to variations of light field properties in real scenes (see Chapter 2).**

In this setup, a probe and a scene were optically mixed together using a semitransparent mirror, and the probe and the scene were illuminated separately. Experiments conducted using this setup showed that observers were also sensitive to the lower order properties of the light field (i.e. light density, direction and diffuseness) for real scenes. Furthermore, the results showed that the use of a rough instead of smooth probe significantly improved observers' abilities to detect mismatches in lighting diffuseness and directions. Thus, "illumination flow" over 3D objects may enable the judgment of light field properties. The experimental setup proposed and the results discussed in Chapter 2 answered the first research question.

Practical contributions: The introduction of a light probe in a scene can serve as a purely visual "yardstick", which allows quantifying what light qualities the observers perceive. Before I developed this novel experimental setup, this method could only be used on a computer screen by rendering the appearance of a probe. This setup can also be used in research into human perception of material, color, and lightness [3].

Cuttle used a smooth matte Lambertian sphere to examine the light flow (i.e. strength and transfer directions of the light). Our results showed that a rough sphere (e.g. a

matte golf ball) is a less ambiguous probe comparing with a smooth sphere to reveal the direction and diffuseness properties of the light field. Consequently, we recommend the rough sphere to lighting professionals to visualize the light flow and diffuseness (variations) in a space.

-2.- **We implemented a method of adjustment to measure observers' abilities to infer the three basic lighting properties, i.e., light density, light direction and light diffuseness, independently and simultaneously (see Chapter 3).**

Two experiments were performed using the experimental setup proposed in Chapter 2 with one investigating independent estimation and the other simultaneous estimation of the three basic lighting properties (i.e. light density, direction and diffuseness). The results of the two experiments were compared and showed that the observers were well able to do both tasks. Furthermore, it was found that the simultaneous adjustment method using an optically mixed scene and probe is an efficient way to measure observers' sensitivity for light field characteristics in real scenes. The use of the adjustment method and the results discussed in Chapter 3 answered the second research question.

Practical contributions: The sensitivity of observers to the light density, direction and diffuseness in real scenes confirms that lighting designers and engineers should consider these lighting properties in order to achieve good light quality.

This study showed that simultaneous adjustment of light density, direction and diffuseness of light is feasible in lighting design or lighting perception research, in which the designers/observers can use these properties as "buttons". Meanwhile, we should also be aware of the perceptual interactions between these lighting properties, that happen due to basic image ambiguities in the retinal image.

-3.- **We presented a first systematic exploration of effects of scene content and layout on light direction perception in real scenes (see Chapter 4).**

Two experiments were performed using the experimental setup proposed in Chapter 2 and the adjustment method tested in Chapter 3. The first experiment was designed to investigate whether scene layout and content influences light direction perception in real scenes. In the second experiment, we investigated how shape properties influenced the light direction estimation. The results showed that scene layout and content indeed influenced light direction perception, and in a systematic way. Furthermore, we found that increasing the number of the visible faces of an object and using globally spherical shapes in the scene both increased the veridicality of the estimation of the light direction on our spherical probe. The results discussed in Chapter 4 answered the third research question.

Practical contributions: The results indicate that the perception of the flow of light can be influenced by shapes and their arrangement in space. It confirms that light, material, shape and space perception should be studied in an integrated manner because they are confounded, a fact that was acknowledged in computer sci-

ence already a long time ago [4, 10, 13] and recently also in perception research [1, 5–7, 11].

The conclusions of this research are conceptually important in interior design, computer rendering and scene selection for psychophysical experiments. For instance, when selecting the scene content for computer renderings or psychophysical experiments, the properties of shape, material and lighting should all be considered as influential on the "theme" to be expressed.

-4.- **We did a theoretical and empirical review of four diffuseness metrics leading to a newly proposed diffuseness metric D_{xia}, which is based on a description of the physical light field (see Chapter 5).**

Four well-known diffuseness metrics were reviewed, being (1) the "scale of light" (i.e. $D_{Frandsen}$), (2). the ratio between cylindrical and horizontal illuminance (i.e. D_{Hewitt}), (3). the ratio between illumination vector and scalar (i.e. D_{Cuttle}) and (4). ICE (i.e. $D_{Morgenstern}$, Illuminance Contrast Energy). The relationships between these four diffuseness metrics were examined using a model named "probe in a sphere" and we found that the metrics, except for DFrandsen, gave similar results in this model. Examining each of these four diffuseness metrics against our criteria proposed for a general purpose diffuseness metric, it was found that D_{Cuttle} fulfilled all criteria. Extending Mury's work on spherical harmonics (SH) representations of light fields, we re-framed D_{Cuttle} in an integral SH description of the light field and this metric was named D_{Xia}. The newly proposed D_{Xia} in Chapter 5 answered the fourth research question.

Practical contributions: Examining the relationships between four well-known diffuseness metrics allows comparing the work on these four diffuseness metrics in different fields (e.g. lighting design, architecture, computer graphics). In other words, this work helps the experts in different fields to communicate with each other about their light diffuseness related work.

The newly proposed diffuseness metric D_{Xia}, together with the light density and direction, form a global integrated description of the lower order properties of the light field structure. The SH representation based method makes clear how the parameters relate and which role they play in the resulting light field or actual light in a space. This can provide insights for lighting designers and engineers.

-5.- **We introduced a way to simultaneously describe, measure and visualize the light density, light vector and diffuseness (variations) of the light field based on its spherical harmonics (SH) representation of light field (see Chapter 6).**

Based on the work in Chapter 5, we proposed a method to measure the local light density, light vector and diffuseness of the light field using a cubic meter by recovering the first order SH representation of the light field. This method was tested using six light probe images and four real scenes and the results were compared to the results using Cuttle's method. Furthermore, we demonstrated a way to simultaneously and intuitively visualize the global structure of the light distribution

(which can be interpolated from a matrix of local measurements) using light tubes and color coding for the light density, light flow and diffuseness variations through the space. The measurement and visualization method proposed in Chapter 6, together with Mury's work, answered the fifth research question.

Practical contributions: The comparison between our method and Cuttle's method shows that both methods give measurements of light density, light direction and diffuseness with a robustness similar to human sensitivities for these parameters. We found that Cuttle's method is most suitable for a quick, local estimation of the basic structure of the light field in a natural scene. In contrast, our method needs computation software on a computer to fit the SH representation to the data but it can easily provide insights in A. how parameters hang together and B. the global structure of the light field and the spatial and form-giving character of light. Furthermore, our method has advantages in computer assisted lighting design schemes and computer graphics, because of its mathematical basis. Thus, our work in Chapter 6 can serve as methodological guidance for lighting professionals and experts in computer science who want to describe, measure and visualize light.

Based on our SH method, it is quite easy to compute the light density, light direction and diffuseness from cubic light meter measurements or HDR environmental maps. The HDR maps are used more and more widely in lighting rendering software and computer graphics. We suggest providing these parameters standardly with these maps in order to give lighting and graphics designers a reference of the ambient (light density), focus and diffuseness levels.

7

7.2. Limitations and future work

We conclude this thesis by reflecting on limitations of our work, and discuss interesting directions for future work.

First, this study successfully introduced an intuitive way to measure human being's sensitivities for basic light field properties in real scenes. However, this research was performed using a viewing box, which is a limited representation of real scenes. First of all, the content in the viewing box is far more simple than general content in the real word. Secondly, the viewing box only allows the observers to look at the scene instead of being part of it. Thermal effects of infrared radiation or intraocular light scattering [12] might give extra information about lighting properties if the observers are present in the scene. For instance, when standing on a beach on a sunny day one can be aware of the direction of the sun without opening one's eyes either by the heat or the light from eyelid transmittance. Thus observers might be even more sensitive to the low order lighting properties when they are presented in the scenes than when looking at the scenes. It would be interesting to investigate observers' sensitivities for light field properties while they are present in the scenes. Moreover, developing a method to quantify lighting perception of observers being in real scenes would be interesting in itself, not just for research purposes but also for its possible applications in lighting design and engineering.

Second, we found that the "illumination flow" over the golf ball compared to the

smooth sphere served as an additional cue to estimate for the light direction and diffuseness. However, "illumination flow" can be generated via various types of mesorelief. For instance, Figure 7.1 (a) shows a rough probe with dimples, with shadows and inter-reflections within each dimple (similar, but with more and deeper dimples, to our golf ball). In Figure 7.1 (b), the "illumination flow" is generated by small bumps over the sphere and the light inter-reflects and generates shadows between bumps. Figure 7.1 (c) shows a sphere with a faceted surface, which causes no light inter-reflections over the surface, but gives distinct brightness contrast steps when compared to the smooth sphere. It still needs to be investigated which kind of mesorelief can provide information about the light field properties in the least ambiguous manner, meaning with the smallest perceptual interactions for "reading" the different light properties from its appearance. In lighting design, Cuttle proposed the "effective vector to scalar ratio", which accounts for the viewing direction in the diffuseness readings from a smooth spherical probe. It will be interesting to empirically investigate this concept and to investigate the influence of probe properties on the perceptual interactions of the observed light properties. This topic is connected to the next issue.

(a)	(b)	(c)
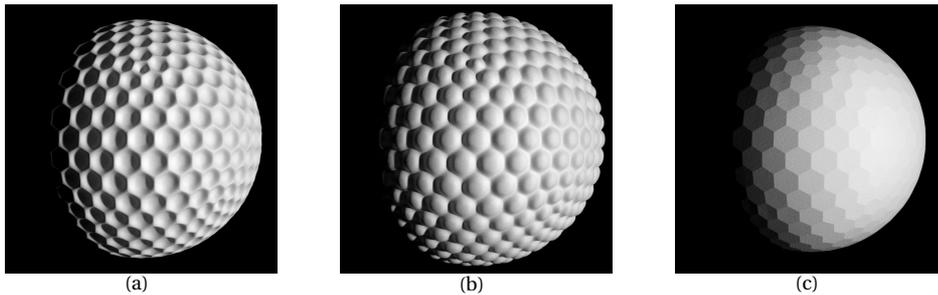
Figure 7.1: Examples of spherical probes with various types of mesorelief over the surfaces: (a) with dimples (b) with bumps (c) with facets.

Third, we proposed a diffuseness metric based on a mathematical description of the physical light field and introduced a way to measure it. However, this study was restricted to physical analysis and measurement. How the measured diffuseness levels relate to observers' assessments of diffuseness in natural scenes still needs to be investigated.

Fourth, we demonstrated a way to simultaneously and intuitively visualize the global structure of the light field using light tubes and color coding for the light density, light flow and diffuseness variations through a space. If this method can be implemented into lighting design software, it will give intuitive insights into the global light qualities in the designed space. It is exciting to witness how one of my colleagues, Tatiana Kartashova, is now taking this step in collaboration with Maxwell Render company.

Fifth, our descriptions addressed the light up to the mathematical first order of the SH representation. Mury addressed the physical meaning of its second order component and called it the squash tensor [8], but we are not aware of research into the perception of this component (e.g. a light ring or two punctate sources in opposite directions [2]).

Mury and Pont both addressed the intuition that the perception of the higher order SH components might be described by a statistical summary [9]. Such a summary might well correspond to what lighting designers summarize as "play of brilliants". However, these higher order components need further study into perception as well as ecological optics. Together with the first order properties they would form a complete framework to describe the light distribution in a 3D space in a perception-based or human-centered way. The next steps would be incorporating color and temporal dynamics.

7

References

[1] Peter N Belhumeur, David J Kriegman, and Alan L Yuille. The bas-relief ambiguity. *International journal of computer vision*, 35(1):33–44, 1999.

[2] K Doerschner, H Boyaci, and LT Maloney. Testing limits on matte surface color perception in three-dimensional scenes with complex light fields. *Vision research*, 47(28):3409–3423, 2007.

[3] Alan Gilchrist, Christos Kossyfidis, Frederick Bonato, Tiziano Agostini, Joseph Cataliotti, Xiaojun Li, Branka Spehar, Vidal Annan, and Elias Economou. An anchoring theory of lightness perception. *Psychological review*, 106(4):795, 1999.

[4] Darrell R Hougen and Narendra Ahuja. Estimation of the light source distribution and its use in integrated shape recovery from stereo and shading. In *Computer Vision, 1993. Proceedings., Fourth International Conference on*, pages 148–155. IEEE, 1993.

[5] Byung-Geun Khang, Jan J Koenderink, and Astrid ML Kappers. Perception of illumination direction in images of 3-d convex objects: Influence of surface materials and light fields. *Perception*, 35(5):625–645, 2006.

[6] Byung-Geun Khang, Jan J Koenderink, and Astrid ML Kappers. Shape from shading from images rendered with various surface types and light fields. *Perception*, 36(8):1191–1213, 2007.

[7] Michael S Langer and Heinrich H Bülthoff. A prior for global convexity in local shape-from-shading. *Perception*, 30(4):403–410, 2001.

[8] Alexander A Mury, Sylvia C Pont, and Jan J Koenderink. Light field constancy within natural scenes. *Applied Optics*, 46(29):7308–7316, 2007.

[9] Alexander A Mury, Sylvia C Pont, and Jan J Koenderink. Structure of light fields in natural scenes. *Applied Optics*, 48(28):5386–5395, 2009A.

[10] Shree K Nayar, Katsushi Ikeuchi, and Takeo Kanade. Surface reflection: physical and geometrical perspectives. *IEEE Transactions on Pattern Analysis & Machine Intelligence*, (7):611–634, 1991.

[11] Pierre Poulin. Shading and inverse shading from direct illumination. 1994.

[12] TJTP Van den Berg. Importance of pathological intraocular light scatter for visual disability. *Documenta Ophthalmologica*, 61(3-4):327–333, 1986.

[13] Qinfen Zheng and Rama Chellappa. Estimation of illuminant direction, albedo, and shape from shading. In *Computer Vision and Pattern Recognition, 1991. Proceedings CVPR'91., IEEE Computer Society Conference on*, pages 540–545. IEEE, 1991.

7
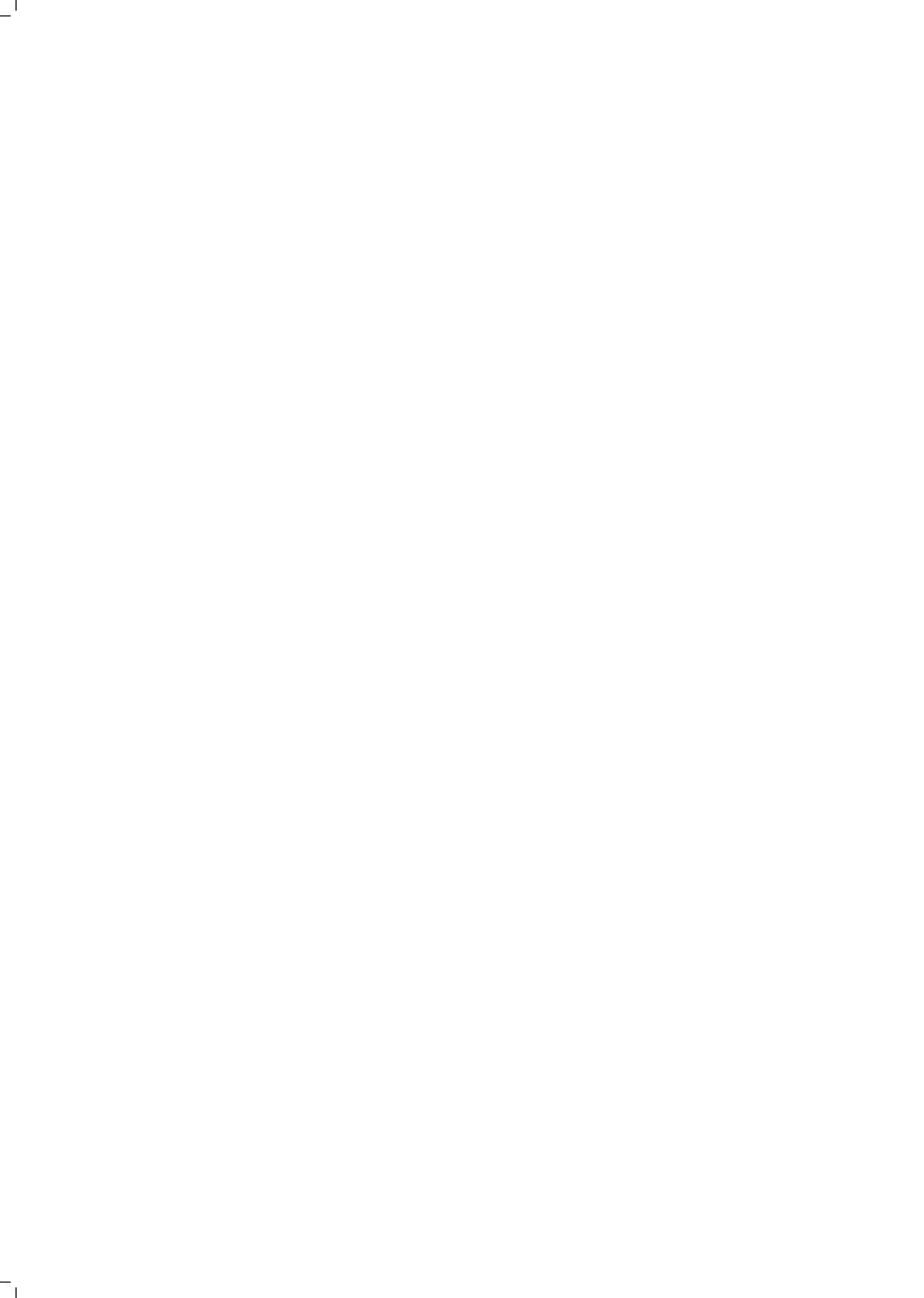
APPENDIX A - LIGHT DISTRIBUTION SOLIDS

The concept of light distribution solids has been proposed by L. Weber [7] a long time ago. Later, both Gershun [4] and Cuttle [2] used this concept to describe the distribution of light about a point in that space. The concept helps to understand the spatial and form-giving lighting effects on objects' appearances and the relationship between D_{Cuttle} and D_{Xia}. We distinguish luminance distribution solids and illuminace distribution solids.

.1. Luminance distribution solid

The luminance distribution solid describes the spatial distribution of the luminance around a point. A 360-degree panoramic environmental map forms a nice example of a measurement of the luminance solid. Figure A.1 (a) gives an example of the luminance solid in point "O" developed from a single point light source "S1" in a dark environment (the light solid distribution is a three-dimensional concept, but to simplify it we just show the projections on the x-y plane). The distance from the point "O" is in direct proportion to the luminance value in that direction. In the case of Figure A.1 (a), the luminance is zero in all directions except the direction of the point light source "S1".

Usually, it is the luminance solid that is observable. Adelson called the luminance distribution including its spectral and temporal characteristics, the "plenoptic function" [1] and described how the human visual system can extract meaningful information about the outside world from it. If the range of luminance in the field of view is too high for the visual system to cope with, it causes glare (i.e. discomfort glare and disability glare), such as from the headlamps of a car at night. Recent research showed that light sources outside the field of view can also cause glare if its luminance is extremely high, which is called overhead glare [5, 8].

.2. Illuminance solid

The luminance solid uniquely determines the form of the illuminance solid. The illuminance solid describes the spatial illuminance distribution about a point and it describes how the illuminance at a point varies according to the direction of the measuring surface. Figure A.1 (b) shows the illuminance solid in point "O" determined by the luminance solid in Figure A.1 (a). The distance between the origin of the axes "O" and each point on the circumference of the circle is proportional to the illuminance measured at the origin of the axes on a plane normal to that direction. According to the cosine law,
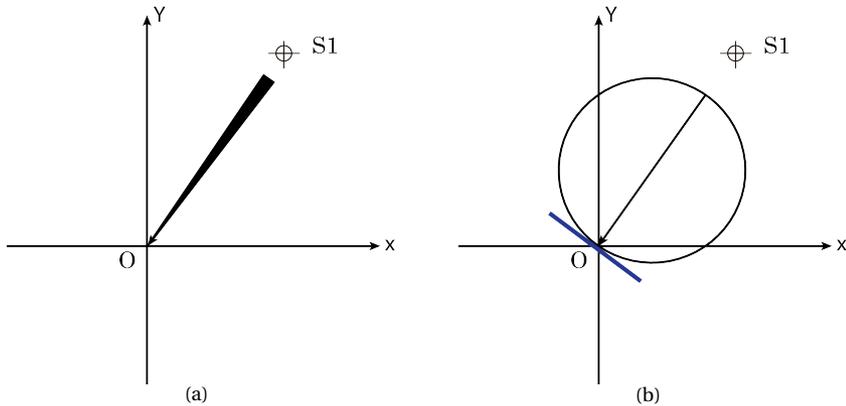
Figure A.1: Light distribution solids around point "O" due to a single light source in a dark environment: (a) luminance distribution solid and (b) illuminance solid.

the maximum illuminance occurs in the direction of the source and it declines in accordance with the cosine of the angle of incidence.

The illuminance solid is completely specified by the luminance solid. The inverse problem of finding the luminance solid when the illuminance solid is given has no unique solution. The appearances of three-dimensional objects are influenced by the lighting patterns that are generated through optical interactions between those objects and the distribution of illumination [3]. Three types of object lighting patterns are shading, highlight and shadow patterns. These patterns are superimposed over objects' surfaces. The illuminance solid determines the shading pattern for Lambertian surfaces, while the luminance solid should be also considered for the highlight and shadow patterns. Thus, if different light fields result in the same illuminance solid they will generate identical shading patterns on convex Lambertian shapes.

.3. Optical mixing of illuminance solids and the resultant diffuseness level of the mixed light field

Figure A.2 (a) shows the luminance solids around point "O" due to two point light sources "S1" and "S2" in a dark environment. Figure A.2 (b) shows the corresponding illuminance solids, which both follow the cosine law. These two illuminance solid distributions can be superposed, resulting in the dark blue shape in Figure A.2 (c). The superposition of two illuminance solid vector distributions can be described by its average direction and strength of the light vector, and the cosine distribution or illuminance solid that would have been generated by a corresponding point light source, namely the light blue shape in Figure A.2 (d). This resultant vector or light vector indicates the direction of the "flow of light". Subtracting the vector component from the conjunct illumination solid in Figure A.2 (c) results in a symmetric shape around the point "O", which is

called the symmetric component of the illuminance solid distribution and is illustrated in Figure A.2(e) in red. Its magnitude in any direction is equal to its magnitude in the opposite direction. This mixing rule also applies for superposing the illumination solids of multiple light sources. Consequently, the illumination solid at any illuminated point in a space can be separated into two components: the vector and symmetric components. The illumination scalar is equal to the average value of the illuminance solid over all directions.

(a)

(b)　　　(c)　　　(d)　　　(e)
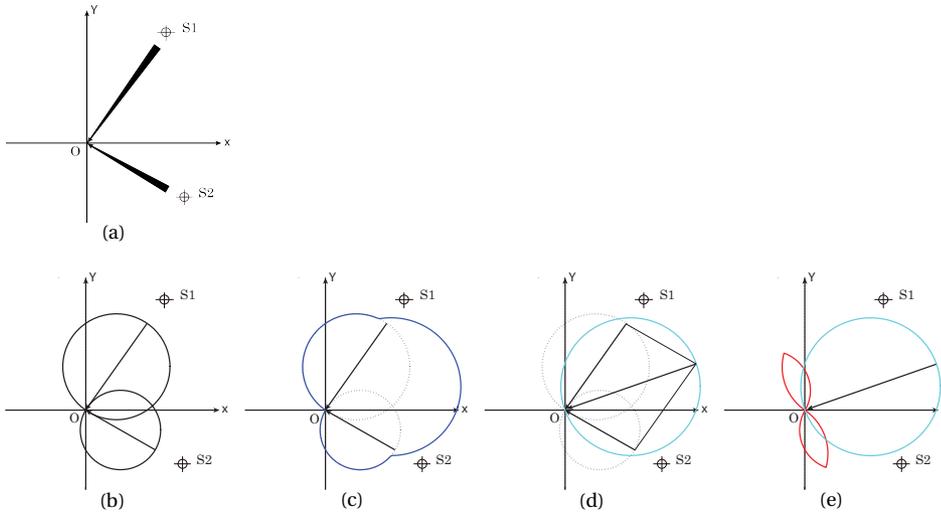
Figure A.2: The light solid distributions around point "O" due to two point light sources "S1" and "S2" in a dark environment: (a) the luminance distribution solid for source "S1" and "S2", (b) the illuminance solids for source "S1" and "S2", (c) the dark blue shape illustrates the superposed illuminance solid distribution due to "S1" and "S2", (d) the light blue circle illustrates the equivalent illuminace distribution of the resultant vector component and (e) the red shape illustrates the symmetric component of the illumination solid.

In Chapter 5 and Chapter 6, we showed that the luminance distribution solid (i.e. the HDR panoramic photographs of natural scenes) can be reconstructed by the sum of its spherical harmonics (SH). The zeroth order component of the SH representation represents the scalar component of the illumination solid. The first order component corresponds to the vector component of the illumination solid.

The relationship between the zeroth order component of the SH representation of the luminance distribution solid and the illumination scalar is:

$$E_{scalar} = \frac{1}{2\sqrt{\pi}}d(E_0) = \frac{1}{2\sqrt{\pi}} \cdot \pi \cdot d(L_0) = \frac{\sqrt{\pi}}{2}d(L_0) \tag{A.1}$$

Meanwhile, the relationship between the strength of the first order component of the SH representation of the luminance distribution solid and the magnitude of the light

vector is:

$$E_{vector} = \sqrt{\frac{3}{\pi}} d(E_1) = \sqrt{\frac{3}{\pi}} \cdot \frac{2\pi}{3} d(L_1) = 2\sqrt{\frac{\pi}{3}} d(L_1) \tag{A.2}$$

Similarly, the illuminance solid can also be reconstructed using the sum of its spherical harmonics components. As Figure A.3 shows, the shapes of the SH basis functions of the first order are asymmetric around their axes, while the other orders are symmetric around the origin. Thus, the zeroth order component together with the higher order components (higher than first order) determine the shape of the illuminance solid for the symmetric component. Ramamoorthi et al. [6] has proved that, theoretically, the appearance of a convex Lambertian surface was largely determined by up to the second order spherical harmonics approximation of the light field. We usually judge the light from the appearance of objects. Since appearance of many objects is largely determined by their diffuse reflectance, we hypothesize that light perception is primarily determined by a 2nd order SH approach of the light field. The rest ("brilliance") can only be seen via highlights and shadows through the object's appearance or directly by human eyes as "sparks".

Since light can't be negative, it should be noted that the non-negativity poses a restriction on the combinations of SH basis functions both for the luminance solid and illuminance solid. Thus, it is not possible to produce the luminance solid or illuminance solid from any arbitrary combination of SH basis functions.
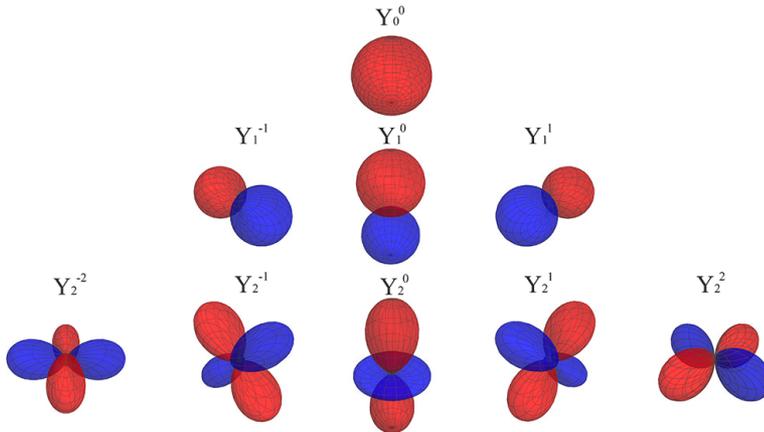
Figure A.3: Plots of real-valued spherical harmonic basis functions. The first row represents the zeroth order, the second row shows the basis functions of the first order and the third row show the basis functions of the second order components (The coloured version is shown in Figure 5.6, where red indicates positive values and blue indicates negative values).

In Chapter 5, we found that Cuttle's diffuseness metric (i.e. the "strength of the light flow") measured using the vector/scalar ratio can be re-framed as the ratio between the strength of the first order and zeroth order components in the SH representation of the light field. That raises the question of how to calculate the diffuseness level of a superposition of two illuminance solids? As shown in Figure A.2, any illuminance solid can

be separated into two components: the vector and symmetric components. Thus, the resultant diffuseness levels D_{Cuttle} (unnormalized) can be calculated using the ratio between the strength of the resultant vector and scalar, as the following equations show:

$$E_{vector}{}^{mixed} = (E_{vector(x)}{}^{S1} + E_{vector(x)}{}^{S2}, E_{vector(y)}{}^{S1} + E_{vector(y)}{}^{S2}, E_{vector(z)}{}^{S1} + E_{vector(z)}{}^{S2})$$
(A.3)

$$D_{Cuttle} = \frac{\left| E_{vector}{}^{mixed} \right|}{E_{scalar}{}^{S1} + E_{scalar}{}^{S2}}$$
(A.4)

Similarly, if two light fields are represented as spherical harmonics of the luminance solids, the resultant diffuseness level of the superposed light field (DXia, unnormalized) can be calculated as:

$$D_{Xia} = \frac{\left| (-C_1^{1\,S1} - C_1^{1\,S2}, -C_1^{-1\,S1} - C_1^{-1\,S2}, C_1^{0\,S1} + C_1^{0\,S2}) \right|}{C_0{}^{S1} + C_0{}^{S2}}$$
(A.5)

where C_l^m are the coefficients of the basic SH basis functions. Thus, the diffuseness level of a mixed light field is not a simple summation of the diffuseness levels of its source light fields, but instead the ratio between the superposed light vectors and summed light densities.

References

[1] Edward H Adelson and James R Bergen. The plenoptic function and the elements of early vision, chapter 1, 1991.

[2] C Cuttle. Lighting patterns and the flow of light. *Lighting research and Technology*, 3(3):171–189, 1971.

[3] Christopher Cuttle. *Lighting Design: A Perception-Based Approach*. Routledge, 2015.

[4] Andreī Gershun. The light field (translated by moon, parry hiram and timoshenko, gregory). *Journal of Mathematics and Physics*, 18(1):51–151, 1939.

[5] P Ngai and P Boyce. The effect of overhead glare on visual discomfort. *Journal of the Illuminating Engineering Society*, 29(2):29–38, 2000.

[6] Ravi Ramamoorthi and Pat Hanrahan. On the relationship between radiance and irradiance: determining the illumination from images of a convex lambertian object. *JOSA A*, 18(10):2448–2459, 2001.

[7] Leonhard Weber. Intensitätsmessungen des diffusen tageslichtes. *Annalen der Physik*, 262(11):374–389, 1885.

[8] Ling Xia, Yan Tu, Lu Liu, Yin Wang, Sheng Peng, Martine Knoop, and Ingrid Heynderickx. A study on overhead glare in office lighting conditions. *Journal of the Society for Information Display*, 19(12):888–898, 2011.

APPENDIX B-MEASURING THE LIGHT FIELD, USING A CUBIC ILLUMINANCE METER OR A TETRAHEDRON SHAPED ILLUMINANCE METER

In Chapter 6 we found that both Cuttle's and our newly proposed method can recover the light density, light vector and diffuseness based on measurements with a cubic meter. The theory behind Cuttle's method estimates the illumination solid and the theory behind our method fits the first order approximation of the SH representation of the luminance distribution. Besides using the cubic meter, it is known that the average of the illuminance on the four sides of a regular tetrahedron is close to the scalar illuminance [2]. Furthermore, the first four coefficients of the first order SH representation can be fitted approximately based on the four measurements on a tetrahedron. Thus, one can wonder whether a regular tetrahedron shaped illuminance meter covers enough directions to measure the first order SH properties of the light field? In order to answer this question, we systematically investigated the robustness of our metrics using a cubic meter and a tetrahedron meter in recovering the light density, direction and diffuseness. The bases of the cubic and the tetrahedron illuminance meters are shown in Figure B.1.

(a)

(b)
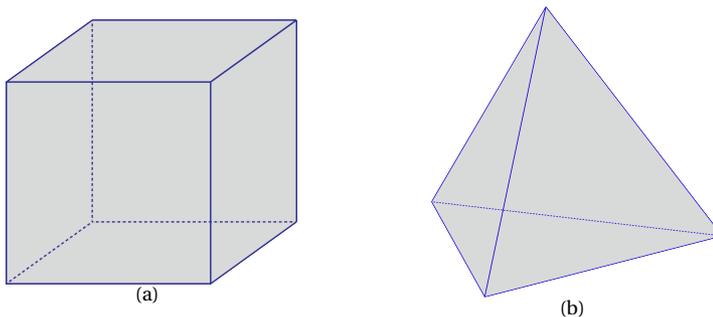
Figure B.1: A cube and a regular tetrahedron. The cubic illumination meter can be built by attaching an illuminance meter on each of the six faces of the cube and the tetrahedron illuminance meter can be built by attaching illuminance meter on each of its four faces.

In order to simulate measurements in real complicated lighting environments, again, the six HDR Panoramic photographs of the natural scenes in Chapter 6 were used (see Figure B.2). The cubic and the tetrahedron meter were assumed to be right in the center of each scene and we simulated 100 postures for each meter by systematically varying the latitude and longitude of the meter with 20° intervals. The illuminance values were calculated for each of the faces of the cubic and tetrahedron meter faces for each posture in each light probe image. In terms of the cubic meter measurements, we recovered the light density, direction and diffuseness based on the illuminance of the six faces using both Cuttle's method and our SH based method as introduced in Chapter 5. As for the tetrahedron meter, the low order properties of light field were also recovered in two ways. In one way, we calculated the scalar component by averaging the illuminance of the four faces and the vector component by projecting the four measurements in a Cartesian coordinate system and then extracting the direction information. In the other way, we fitted the first order SH representation of the light field using the four illuminance values. A detailed comparison of the results of these four methods is given below.

(a) Dining room	(b) Uffizi Gallery	(c) Grace Cathedral
(d) Doge's palace	(e) Sunset	(f) Glacier
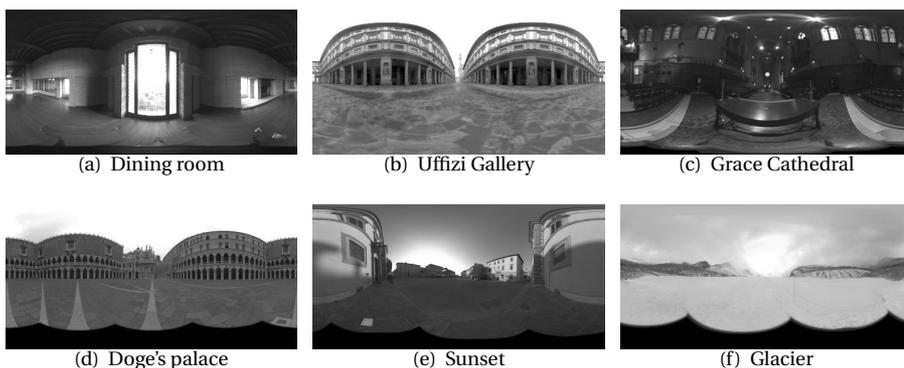
Figure B.2: The grayscale tonemaps for HDR Panorama photographs of six natural scenes (a) Dining room (b) Uffizi Gallery (c) Grace Cathedral (d) Doge's palace (e) Sunset (f) Glacier (available from:http://gl.ict.usc.edu/Data/HighResProbes/)

Figure B.3 shows the box plot for the recovered light density obtained from 100 different simulated postures of the cubic meter and the tetrahedron meter. A and B represent the light density estimates based on the cubic meter measurements, with A using Cuttle's method (i.e., illuminance scalar component) and B using our SH based method (i.e. $\sqrt{\pi}/2$ times of the zeroth order component of the SH representation of the light field as shown in Equation A.1). C and D represent the light density estimates based on the tetrahedron meter measurements, with C using the average of the four illuminance values and D using the SH fitting method. In Figure B.4, we show histograms of the signed light density differences between the meter estimates and the estimate from the full SH representation of each probe image.

In general, for the cubic meter, the SH based method is less sensitive to the meter's posture than Cuttle's method expect for the "Dining room" and "Grace Gathedral" maps. Surprisingly, for the tetrahedron meter, the performance of the two methods is similar,

and they both are a little more robust than the methods using the cubic illumination meter. Nevertheless, the recovered light densities are all quite close to the theoretical ones.
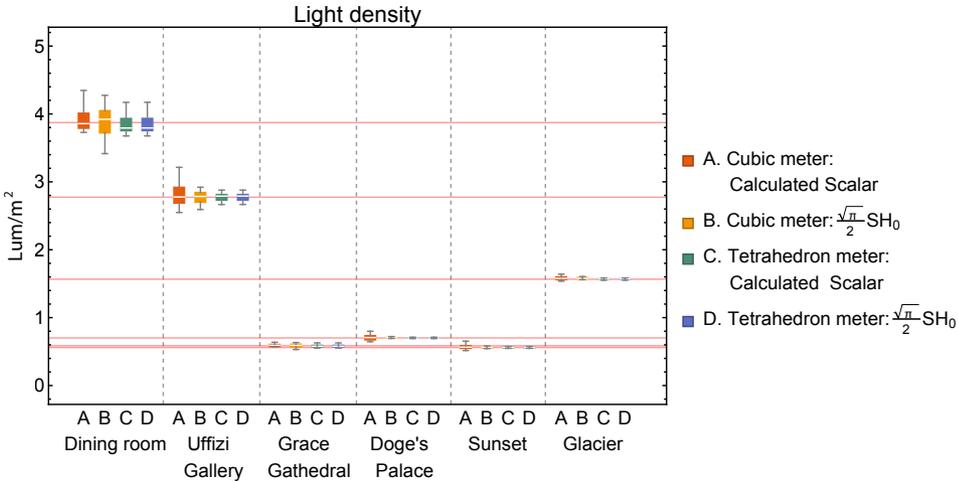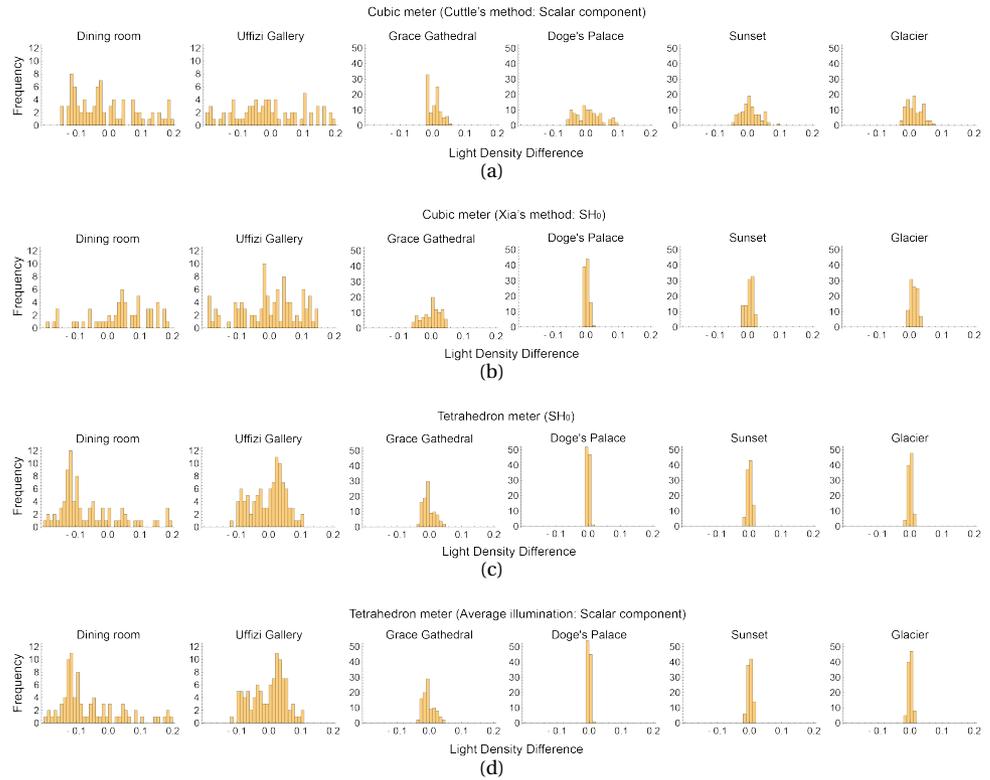

Figure B.3: Box plot for the recovered light density obtained from 100 different simulated postures of the cubic and the tetrahedron illuminance meters in six light probe images. The horizontal red lines indicate the light density estimated from the full SH representation of each image.

.1. Measurement of the light vector

Figure B.5 shows the box plot for the estimated light vector strength and Figure B.6 reveals the estimated directions of the light vectors. Based on the measurements using the cubic illumination meter, both Cuttle's and our SH methods estimate the light vector strength and light vector directions precisely and the results are independent of the posture of the cubic meter. However, the results based on the measurements with the tetrahedron meter show big variances in the estimated light vector strength and direction. The results indicate that, although the tetrahedron meter allows measuring the illumination scalar quite well, it cannot be used to estimate the light vector robustly.

.2. Measurement of the light diffuseness

Since the cubic meter allows measuring the light vector accurately but not so the illumination scalar, the variance in the estimates of the light diffuseness are primarily determined by the error in the scalar component. The tetrahedron meter allows measuring the scalar component more robustly than the cubic meter and thus a combination of a cubic meter to measure the light vector and a tetrahedron meter to measure the light density is expected to optimize the diffuseness estimates. In Figure B.7 we plot this optimized estimate besides D_{Cuttle} and D_{Xia} ("0" represents fully collimated light and "1"

Figure B.4: Histograms of the signed difference in light density between the meter estimates and the estimate from the full SH representation of each image when using (a) a cubic meter with Cuttle's method, (b) a cubic meter with Xia's method, (c) a tetrahedron meter by averaging the illuminance on the four faces and (d) a tetrahedron meter using the SH fitting method.
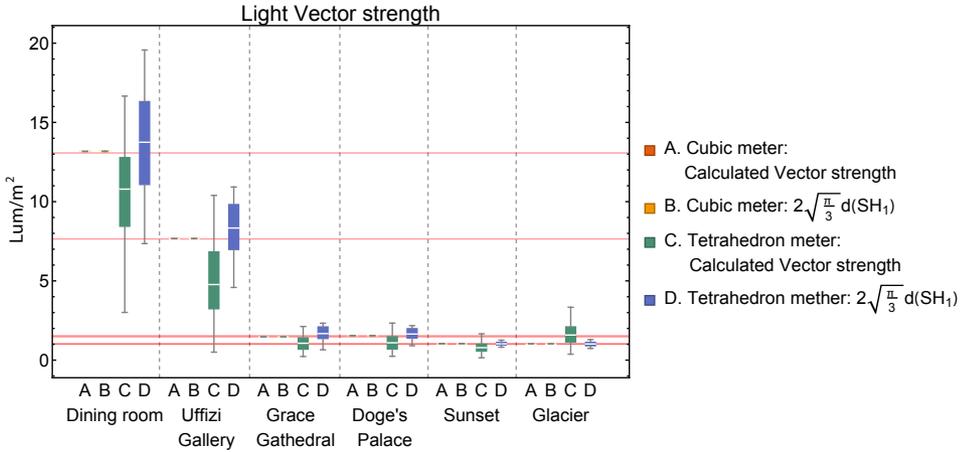
Figure B.5: Box plot for the recovered light vector strength obtained from 100 different simulated postures of the cubic and the tetrahedron illuminatnce meters in six light probe images. The horizontal red lines indicate the light vector strength estimates from the full SH representation of each image.

represents fully diffuse light). As expected, the results show that the ratio between the vector strength estimated with the cubic meter and the scalar measured with the tetrahedron meter is somewhat less sensitive to the posture of the illumination meters. Overall, the spread over the 100 different postures is small and the results indicate that all methods can well be used to measure the diffuseness.

.3. Measurement of the global light field structure using a smartphone

Concluding, we did a systematical investigation into the performance of a cubic meter and a tetrahedron meter in measuring the local light density, direction and diffuseness. Besides the local description of light field, the light distribution in natural spaces shows spatial variations of the ambient, vector and diffuseness (i.e., the so-called global structure of the light field). This kind of variation can be captured using simple cubic measurements and interpolation of these measurements over the space.

Nowadays, smart phones can function as light meters either by using their built-in cameras plus a diffusing dome such as the Luxi (fits over the phone's camera) or by using a plug-in device (e.g. Lumu, a built-in sensor and diffusion dome that plugs in the headphones jack and measures the light level directly) [1]. With the help of the phone's position and orientation sensors, a smart phone based cubic meter or tetrahedron meter can be easily built. The global structure of the light field can then be obtained by measuring the cubic illumination at several points of the space and visualizing the interpolated data. We believe that the development of such an app for smart phones could serve as a tool to provide insights into the spatial and form-giving character of light in 3D space
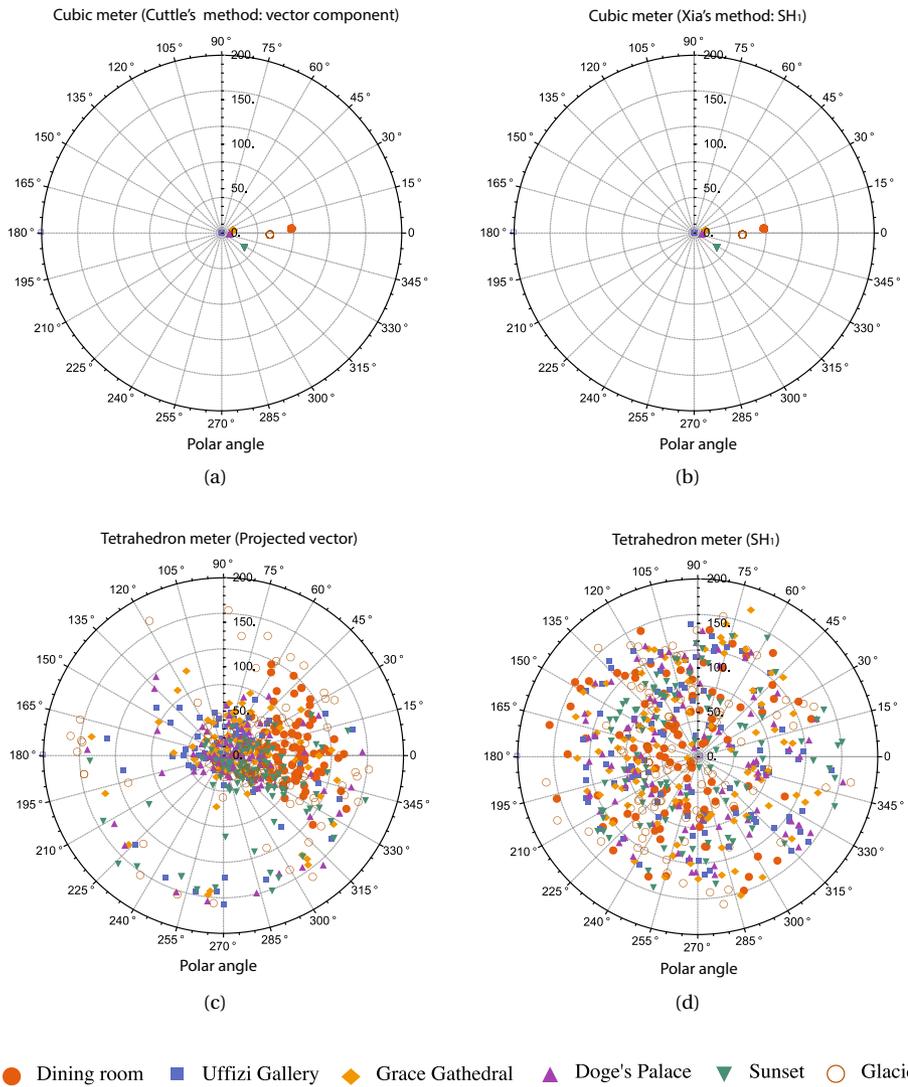
Figure B.6: Polar plots for the recovered light direction obtained from 100 simulated postures of the cubic and the tetrahedron illuminance meters in six light probe images, when using (a) a cubic meter and Cuttle's method, (b) a cubic meter and Xia's method, (c) a tetrahedron meter and projection method and (d) a tetrahedron meter and the SH fitting method.
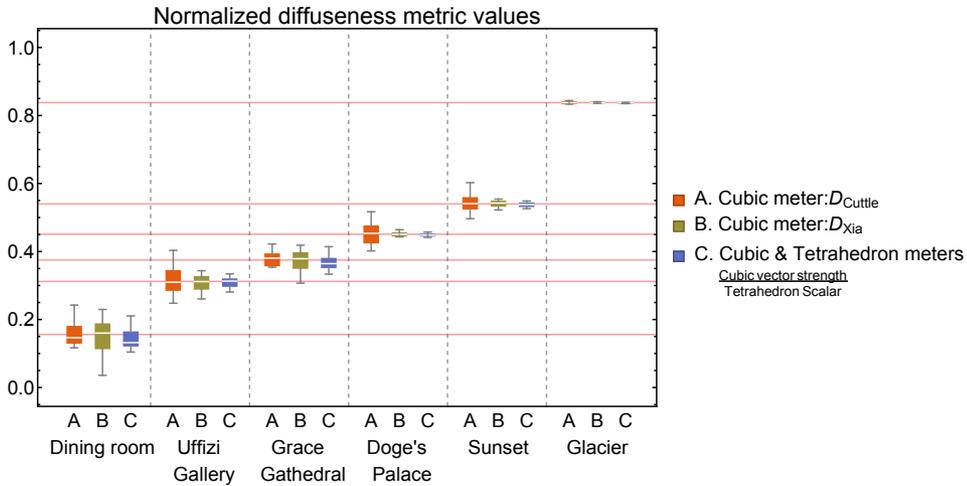
Figure B.7: Box plot for the normalized light diffuseness obtained from 100 different simulated postures of the cubic and the tetrahedron illumination meters in six light probe images. The horizontal red lines indicate the normalized light diffuseness estimated from the full SH representation of the images.

for people who are interested in lighting.

References

[1] Joan Manel Berenguer. Is it possible use an iphone as a lightmeter? website, 11 October 2013.

[2] William Thomas Singleton. *The body at work: Biological ergonomics.* Cambridge University Press, 1982.
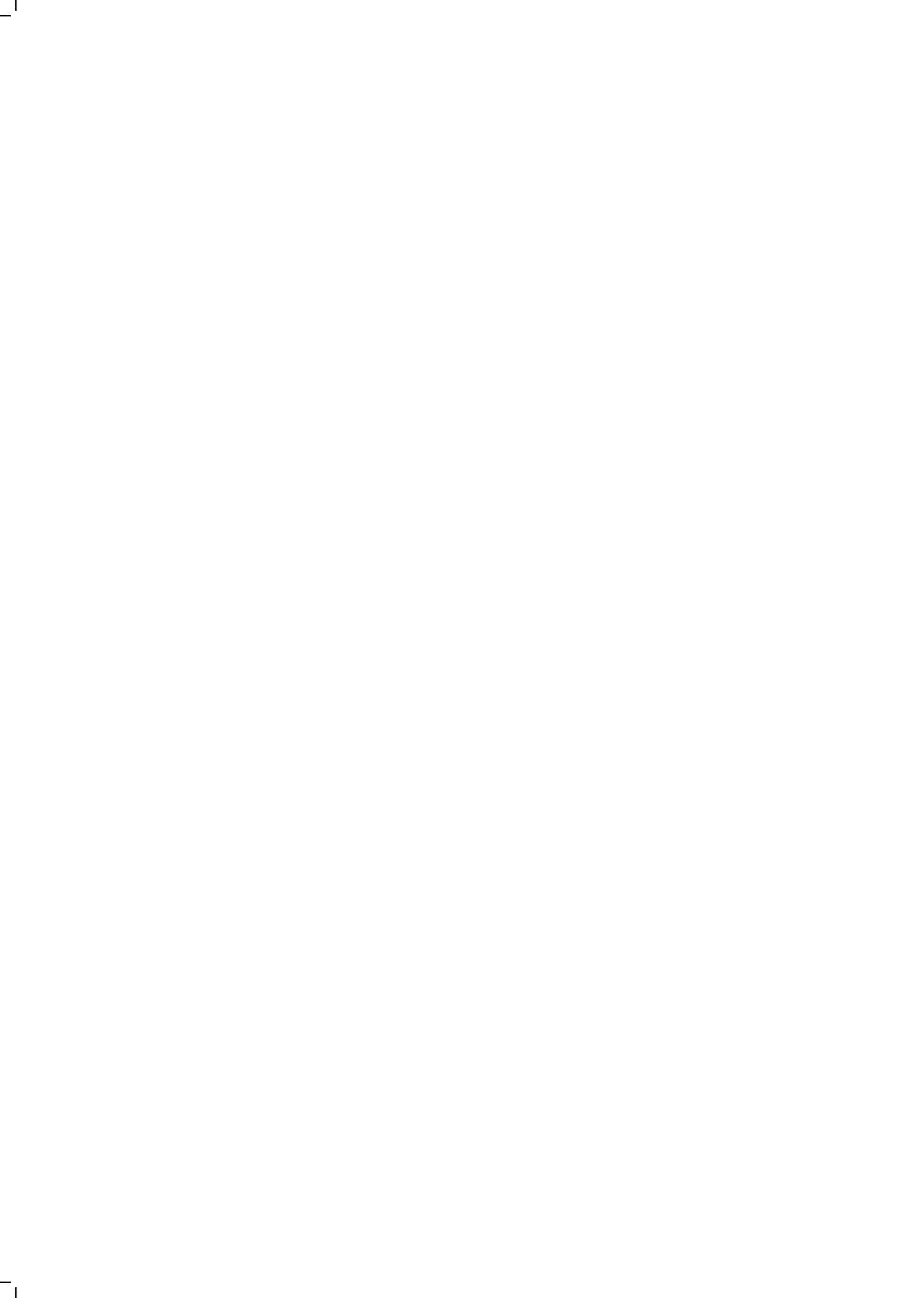
APPENDIX C-MATERIALS FOR MAKING A CUBIC ILLUMINANCE METER

.1. Materials

We designed a cubic illumination meter, which can be easily built with commercially available components. The basis of the cubic meter was assembled using laser-cut MDF boards of 6 mm thickness. Figure C.1 illustrates the blue print of the laser-cut MDF board for making a cube of $10cm \times 10cm \times 10cm$. It consists of 2 layers, an outer and an inner cube. Six small illuminance meters (T-10MA from KONICA MINOLTA) were installed inside the 6 holes that were cut in the outer cube and the inner cube provided flat ground surfaces for the meters. A spirit level can be fixed to the horizontally cut top of the cubic meter to level it. A metal bar can be fit through the inner cube from the bottom to the top, to stabilize the cubic meter. The stick can then be fixed on a tripod. Finally, the outer cube was covered with light absorbing black-out material (black flocked paper, from Edmund Optics) to avoid scattering from the surfaces of the cubic meter.
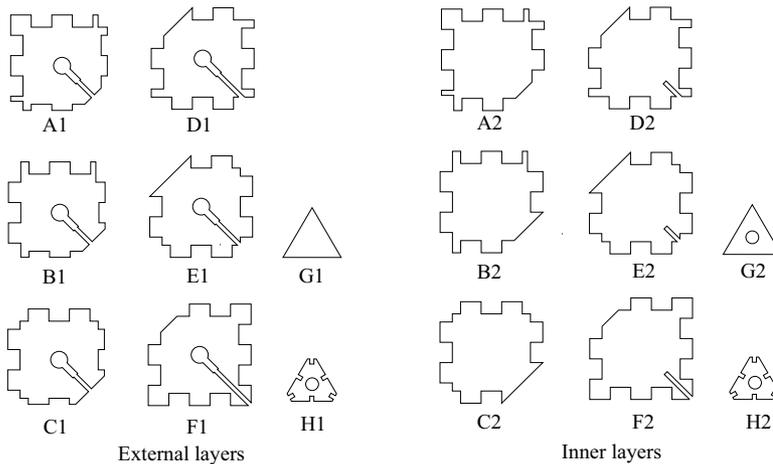
Figure C.1: The blueprint for laser-cutting the 6mm MDF board for making the cubic basis of the cubic illumination meter.
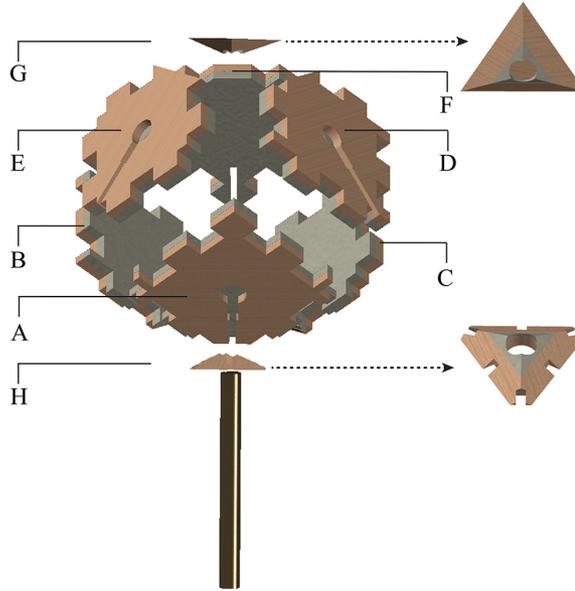
Figure C.2: The scheme for assembling the cubic basis of the cubic illumination meter from the parts in Figure C.1. Here we labeled the parts with just the letters denoting the parts. They all consist of two layers, the parts numbered 2 on the inside and the parts numbered 1 on the outside. The assembled meter can be seen in Figure 5.1.

.2. Assembly

After the 16 forms in Figure C.1 were cut out, G1 and G2 were glued together as G, and so were H1 and H2 glued together as H. Note that all parts numbered 1 concern parts of the outer cube and all parts numbered 2 the inner cube. We cut the angles of the three edges of G and H to $35.26°$ ($arctan(\sqrt{2}/2)$) to let them fit the top and bottom side of the assembled cube, as Figure C.2 shows. The inner and outer cubes were not glued together, because they were stable when assembled.

ACKNOWLEDGMENTS

Writing this last part of my thesis, reminds me of the four years I enjoyed working as a PhD student at TU Delft. At this moment, my heart is full of appreciations for all the help I have received and these appreciations will always be with me. I would like to thank all the people who involved in my PhD research, without their support, writing this dissertation would be impossible. Many thanks to all my friends involved in my four-year PhD life. You have made this period the most precious experience in my life so far.

First and foremost, I would like to thank my promoter Prof. Sylvia C.Pont. Dear Sylvia, it is not possible for me to express my appreciations for your supervision within several sentences. When I first arrived the Netherlands, I was exciting but also nervous and shy because everything was new to me. You introduced me to every member of the group and ask me to join you in the EEMCS Pi-lab meeting. I felt less stressed after seeing people here are so friendly and wiling to help. You invited me to your home and introduced your family to me, which made me feel so warm and was really helpful to ease my homesick. At the beginning of my PhD research, I had no clue what I was going to do. Perceptual metrics of light field is such a broad and abstract field for me. You helped me to quickly be familiar with this field through doing, from building my experimental setup to doing the first pilot experiment. You also gave me the opportunity to go to Computational Vision Summer School, where I got the change to communicate with peers and it inspired me a lot. I want to thank you for your great encouragement, thoughtful guidance and giving me your knowledgeable and valuable insights on my research during the four years and especially for your patience on my English. In addition, thank you for being so patient and dedicated for every discussion, spending countless time to modify my papers, putting your trust in me. I have learned so much from you about how to do research and also how to live a happy life.

My sincere gratitude goes to my promotor Prof. Ingrid Heynderickx. Dear Ingrid, thank you for giving me an opportunity to start my PhD study in Netherlands. You are also the person who guided me into lighting perception area before I came to the Netherlands. Thank you for all the suggestions on my research and so much of time spent on revising my papers. Thank you for your encouragement, support during all these years and keeping me on the right track. Your trust in me gave me the strength to continue with my studies.

I also want to thank Prof. Huib. de Ridder who gave me a great support for my PhD research. As the head of the group and the leader of our weekly discussion group, you were always patient to listen to the ideas from PhD students and willing to give us advice. In addition, you were so good at inspiring us and encouraging us to put ideas into actions.

I would like to give my thanks to Maarten Wijntjes. You are always full of enthusiasm and cool ideas about doing research, which I admire so much. Thank you for giving me

so many great feedbacks from experimental design to data analysis during our weekly discussion meetings. Also, thank you for lending me the vision lab to do my experiments.

I want to give my special thanks to my officemates Tatiana kartashova, Qian Liu, Fan Zhang, Jie Li, Qiong Peng, Xueliang Li and so on. I had a lot of fun with you and shared happiness and sadness during my PhD life. Tatiana, thank you for all the discussions we had on the light field and all the help you provided in my research. I was also grateful to the English speaking environment you have made in our office and this was quite helpful in improving my oral English. In addition, special thanks for all the sweets you shared with us. Qian, thank you for introducing me to the wonderland of crafts and letting me know how well the habits, work and family can be balanced. Fan Zhang, thank you for all the humour sense you have brought to the office. Jie Li, I was so deeply impressed by your elegance and capability of doing everything so well. I like your cakes so much, from smell, taste to decorations. Qiong, thanks so much for letting me know it is never too late to pursue one's dreams. Xueliang, thank you for the pencil drawings and the time shared together when I was writing my thesis.

I want to express my acknowledgement to all the members of the Pi-lab. Besides the people already mentioned, I want to give my thanks to Judith Redi, Harold Nefs, Tingting Zhang, Yi Zhu, Ernestasia Siahaan, thank you for broadening my view on the area of image quality perception, video quality perception and depth perception. Reinier Jansen and Rene van Egmond, thanks for sharing the knowledge on sound research. Dear Willemijn Elkhuizen, thank you for letting me know how material appearance reproduction of paints can benefit from perception research and thank you for helping me with the Dutch translation of my Summary. I really appreciate all the discussion and presentations we had in the these meetings and enjoyed lunch with cultural difference so much.

In addition, I would like to thank all my colleagues in my group. Every month, we got an opportunity sitting together to report our progress in research and discuss other work plans, which looks like a big family to me. Besides the "family time" we spent together, you also gave me different kinds of support in my research such as giving advice on building my experimental setups, being the participants of my experiments. Bertus Naagen, thank you for helping me with all kinds of computer problems and the 3D printing of my probes.

I would like to thank the ID department secretaries: Daphne van der Does, Amanda Klumpers Nieuwpoort, Denise Keislair, Joost Niermeijer, Charleyne van zijl and Franca Post from CICAT. I can always find help from you whenever I encounter any kinds of problems.

I would like to give my appreciations to all the participants who took part in my experiment.

I want to express my sincere thanks to my friends. My PhD life would not have went so smoothly without you. Special thanks are given to Tingting Zhang, with two years living inside the same apartment, eating together, going to work and getting off work together, I can't imagine how the life would be without you. Yun Ling, Chao Qu, Ni Kang, Junchao Xu, Yue Ding, Changyun Wei, Yangyang Shi, Dongjuan Xiao, Wei Liu, Wenxin Wang and so on, thank you for being the pioneers in exploring the beauty of the Netherlands and sharing those precious experiences with me. Qian Liu, Yi Zhu, Jie Li, Haozheng

ABOUT THE AUTHOR

Ling Xia was born on February 16, 1987 in Changzhou, Jiangsu Province, China.

After finishing the middle school in 2002 and the high school in 2015 in Changzhou, she studied Electronic Science and Technology in Southeast University in China for her bachelor's degree from 2005 to 2009. She continued her education in Physical Electronics Engineering at the same university and received her master's degree in 2012. Her master's thesis was conducted in collaboration with Philips lighting and focused on the effect of overhead glare on visual discomfort with the LED office lighting.

From Feb. 2012 to Feb. 2016, she was a PhD researcher at the Human Information Communication Design group, department of Industrial Design Engineering, Delft University of Technology, the Netherlands, supervised by Prof. dr. S.C. Pont and Prof. dr. I.E.J. Heyndeickx. Her research interest is on investigating observers' subjective perception of light in real scenes and the objective description, measurement and visualization of the light field.